

Decomposition of Anomalous Diffusion in Various Stochastic Processes

by
Vidushi Adlakha

A dissertation submitted to the Department of Physics,
College of Natural Sciences and Mathematics
in partial fulfillment of the requirements for the degree of

Doctor of Philosophy
in Physics

Chair of Committee: Kevin E. Bassler

Committee Member: Gemunu Gunaratne

Committee Member: Greg Morrison

Committee Member: Joseph McCauley

Committee Member: Ilya Timofeyev

University of Houston
May 2021

Copyright 2021, Vidushi Adlakha

DEDICATION/EPIGRAPH

Dedicated to Ritu Adlakha and Rajesh Adlakha.

ACKNOWLEDGMENTS

There are many who helped me along the way on this journey. I want to take a moment to thank them. I would first like to express my heartfelt gratitude to my advisor Prof. Kevin E. Bassler, for his unwavering support of my Ph.D. studies and related research, for his patience, motivation, and immense knowledge. His guidance helped me in all the time of research and writing of this thesis. I could not have imagined having a better advisor and mentor for my Ph.D.

I would like to thank my thesis committee members, Prof. Gemunu Gunaratne, Prof. Joseph McCauley, Prof. Greg Morrison, and Prof. Ilya Timofeyev, for their insightful comments and encouragement, which motivated me to broaden my research from various perspectives.

My sincere thanks also go to Prof. Holger Kantz, Dr. Erez Aghion, and Dr. Phillip Meyer for stimulating discussions and research conducted in collaboration with the Max Planck Institute of Complex Systems, Dresden, Germany. Also, I would like to thank my friends Raquel Quishpe, Geethal Amila Gamage, Rauf Giwa, Yu-li Chang, and Fei Wang for their support and for all the fun we have had in the last five years.

A special thanks go to my family, parents, brother, and in-laws for their unconditional love and support throughout my graduate life. I am forever grateful for their patience and understanding.

Finally, I could not have completed this dissertation without the support of my fiance, Samarth, who provided stimulating discussions as well as mental and emotional support throughout my research.

ABSTRACT

This dissertation presents three research projects on the decomposition of anomalous diffusion in various stochastic processes.

Stochastic processes that scale anomalously with time, such that the Mean-Squared Displacement (MSD) of the expanding particle is $\langle x^2(t) \rangle \sim t^{2H}$ where H is the *Hurst exponent* and $H \neq 1/2$. Anomalous diffusion is known to occur in such processes due to auto-correlations, the *Joseph effect*, the infinite variance of individual events, the *Noah effect*, or the non-stationarity of increments, the *Moses effect* quantified as the *Joseph*, *Latent* and *Moses* exponents, respectively.

The first project focuses on the Pomeau-Manneville map, a chaotic dynamical system an example of an aging system. The model can have either sub- or super-diffusive behavior due to a combination of the three effects stated above. Scaling exponents quantifying each of the three constitutive effects are calculated analytically and confirmed numerically. Finally, the importance of the Moses effect in the anomalous diffusion of experimental systems is discussed.

The second project studies the origins of anomalous diffusion in an ensemble of time series. The increment distribution converges at increasing times to a time-invariant asymptotic shape after appropriate rescaling based on the quantification of the three effects. This asymptotic limit can be an equilibrium state, an infinite-invariant density, or an infinite-covariant density for different processes. The three effects in a non-linearly coupled Lévy walk model are quantified using time-series analysis methods, and the results are compared to theoretical predictions.

The third project considers diffusion processes with spatially varying diffusivity, which can result in anomalous diffusion. Heterogeneous diffusion processes are analyzed for the cases of exponential, power-law, and logarithmic dependencies of the diffusion coefficient on the particle position. The model exhibits sub- and super-diffusive behavior depending on the value of the space-dependent diffusion coefficient. The numerical methods of time-series analysis quantify the three effects in a heterogeneous diffusion model and compare the results to theoretical predictions. A heterogeneous diffusion model is an alternative approach to non-ergodic, anomalous diffusion that may be especially useful for diffusion in heterogeneous media.

TABLE OF CONTENTS

	DEDICATION	iii
	ACKNOWLEDGMENTS	iv
	ABSTRACT	v
	LIST OF FIGURES	viii
	LIST OF TABLES	ix
1	Introduction	1
1.1	Stochastic Processes	4
1.2	Scaling of Stochastic Processes	4
1.3	Anomalous Diffusion and the Central Limit Theorem	5
1.4	History and State of the Exponents	5
1.4.1	Hurst Exponent H	5
1.4.2	Joseph Exponent J	6
1.4.3	Latent exponent L	6
1.4.4	Moses exponent M	7
1.5	Notion of Aging	7
1.6	Lévy Walks	8
1.7	Heterogeneous Diffusion Processes	8
2	Anomalous Diffusion and the Moses effect in a Model of Aging	10
2.1	Model and its Diffusive Behavior	12
2.2	Joseph, Noah and Moses effects	15
2.2.1	Definitions	15
2.2.2	Values in the Pomeau-Manneville map	17
2.3	Simulation Results	20
2.4	Discussion	22
3	Time Series Analysis of Lévy Walks	26
3.1	Story of Three Exponents: M , L And J	29
3.1.1	Relation between M , L , J and H	34
3.1.2	Scaling Shapes of the Increment Distribution	35
3.2	The Lévy Walk Model	38
3.3	Summary of Main Results	41
3.4	Calculation of Latent exponent L and Moses exponent M	44
3.4.1	Three Regimes for M and L	45
3.4.2	The Integrable Regime, $1/2 + \gamma/2 < \nu < 1$	48
3.4.3	Middle Regime, $\gamma < \nu < 1/2 + \gamma/2$	48
3.4.4	The Non-Integrable Regime, $\nu < \gamma$	49
3.5	Calculation of Joseph exponent J	50
3.6	A Generalized Model	52

3.7	Discussion	54
4	Anomalous Diffusion in Heterogeneous Diffusion Processes	64
4.1	Model and its Diffusive Behavior	66
4.2	Calculation of Exponents	68
4.3	Simulation Results	71
4.4	Discussion	72
5	Conclusion	77
	Appendices	80
A	Proofs for Time Series Analysis of Lévy Walks	80
A.1	Generality of $H = L + J + M - 1$	80
A.2	The ensemble-time averaged MSD and the correlation function	81
A.3	The Joseph effect via DFA	85
A.4	Calculation of $r_0(s)$ and $r_2(s)$	86
A.5	The “ ∞ ” regime, $\nu > \gamma/2 + 1$	87
	BIBLIOGRAPHY	88

LIST OF FIGURES

1	Scaling function of the distribution of the process X	13
2	Log-log plot of the width of X , median of Y and of Z , and mean of R/S as a function of time t	21
3	Values of the scaling exponents quantifying diffusion and the constitutive effects that cause anomalous diffusion in the PM map as a function of parameter z	22
4	Verification of the scaling relation (Eq. 4) for the exponents quantifying diffusion in the PM map as a function of parameter z	23
5	An example of a Lévy walk path $x(t')$ (blue) versus time, generated by the model in subsection 3.2.	31
6	Log-log plots for probability distribution as defined in eq. (66) versus $ v $	57
7	Phase diagram of the scaling exponents describing the decomposition of the anomalous diffusion.	58
8	Log-log plots for the averages of $ v $ and v^2 , as function of time.	59
9	Phase diagrams of the scaling exponents describing the decomposition of the anomalous diffusion of Lévy walks into three constitutive effects, and their various magnitudes.	60
10	Numerical examination of the convergence of the increment PDF $P_t(v)$ to a time-invariant shape, here we used $\gamma = 0.5$, $\nu = 0.875$, leading to $L = 0.5$, and $M = 0.375$	61
11	Numerical examination of the convergence of the increment PDF $P_t(v)$ to a time-invariant shape, here we used $\gamma = 0.5$, $\nu = 0.625$, leading to $L = 0.625$, $M = 0.125$	62
12	Numerical examination of the convergence of the increment PDF $P_t(v)$ to a time-invariant shape, here we used $\gamma = 0.5$, $\nu = 0.375$, leading to $L = 0.75$, $M = 0$	63
13	Functional dependencies on the position variable x of the diffusion coefficients.	74
14	The PDF for sub- and superdiffusive HDPs with power-law diffusivity (98), computed for the parameters $a = 0.01$ and $D_0 = 1$	75
15	Log-log plot of the width of X , median of Y and of Z , and mean of R/S as a function of time t	76

LIST OF TABLES

1	The main notations used in this chapter, by order of their appearance in the main text.	29
2	Summary of the different scaling limit of $P_t(v)$, that can be found from the Moses M and Latent L exponents.	38

1 Introduction

Diffusion is a fundamental process that defines a test particle's stochastic motion and the broadening of its distribution function over time. Following Robert Brown's seminal experiments a year earlier on micron-sized granules' erratic movement in *Clarkia pulchella* pollen grains [44], the diffusive-like motion was first reported in 1828.

Diffusion theory is a well-established and fundamental field of study that is still very active today [154]. An extensive range of stochastic phenomena exhibits deviations from normal diffusive behavior, commonly referred to as anomalous diffusion. Many complex systems exhibit anomalous transport, including electronic transport in solid-state disordered systems [36], molecule motion inside living cells [189] and on their membranes [171], telomere motion inside mammalian cells' nuclei [43], soil transport [149], heat transport in low-dimensional systems [126], and certain classes of billiards [19], among a variety of other phenotypes.

From a statistical viewpoint, all these diverse phenomena share a common description depending on how the broadening of the distribution function of the process $x(t)$ grows in time [154]. This is measured by the variance of the second moment, the so-called mean squared displacement (MSD) $\langle x^2(t) \rangle \simeq t^\gamma$. Normal diffusion corresponds to an MSD that grows linearly in time $\gamma = 1$, while anomalous diffusion is classified as subdiffusive for $\gamma < 1$ and superdiffusive $\gamma > 1$. Stochastic processes have been used to model a range of phenomenon from diffusion of macro-molecules in biological cells to animal and human locomotion [41, 81, 221].

From rather complex but objective systems of physics, we are shifting to the field of biology and biophysics where effects and phenomena are much more difficult to quantify due to their inherent diversity and variability. The anomalous diffusive motion of macromolecules and organelles is a common observation in cell biology [99], and a simple description based on the conventional diffusion equation with diffusion constants measured in dilute solution fails. Anomalous diffusion can be caused by molecular crowding and confinement. In the crowded world of biological cells, anomalous transport is a critical process to investigate because it leads to a better understanding

of living cells' underlying mechanisms. In the broader context of cell biology, living cells contain a plethora of active, non-equilibrium processes, and their link to anomalous diffusion will need to be investigated further in the future.

The densely packed and heterogeneous structures of cells' interiors and cellular membranes are summarized by macromolecular crowding. The most well-known phenomenon is a sub-linear, power-law increase of the mean-square displacement as a function of the lag time, but there are other manifestations like strongly reduced and time-dependent diffusion coefficients, persistent correlations in time, non-Gaussian distributions of spatial displacements, heterogeneous diffusion, and a fraction of immobile particles [99]. Gaussian models such as fractional Brownian motion and Langevin equations for visco-elastic media, the continuous-time random walk (CTRW) model, and the Lorentz model for obstructed transport in a heterogeneous environment are some of the most widely used theoretical models. The spatio-temporal properties of transportation are highlighted in terms of two-point correlation functions and the mean-square displacements' dynamic scaling behavior.

The biggest challenge is determining the physiological implications of anomalous transport in living cells, mainly whether it is merely a peculiarity or provides a biological benefit. More broadly, macromolecular crowding may significantly impact essential components of systems biology such as biochemical reaction kinetics, protein folding, and unfolding dynamics, and intracellular signaling pathways. Over the next decade, at the very least, an enormous amount of interdisciplinary research will be required to develop a unified picture of anomalous transport and its physiological consequences.

Lévy walks are mathematical models used to describe anomalous diffusion. Recent studies in single-particle Hamiltonian systems [112], biophysics [220, 221], and cold atom dynamics [20, 120, 148] demonstrate that this particular type of random walk provides significant insight into complex transport phenomena. The topic of Lévy walks has sparked interest in research communities concerned with the motility of living organisms and their foraging and search strategies [237]. Motility is a multifaceted problem on many levels. Motility can be found at many different scales,

from swimming micron-sized bacteria to albatrosses that can travel hundreds of kilometers at a time. Motility refers to the interactions of moving animals with their surroundings and habitats, which are often difficult to quantify or predict. In a very fascinating twist, Lévy walks are involved in a particular topic of effectiveness of search and foraging strategies. Lévy walks are argued to be the most efficient search strategy under certain conditions imposed on the distribution and properties of targets. There is an ever-increasing number of accounts in which Lévy statistics for animal trajectories are reported.

Levandowsky's work [127, 237] on crawling amoeba was the first to mention the Lévy walk model in a biological context. Amoebae are unicellular organisms that move on surfaces and in three-dimensional media by extending cell protrusions known as pseudopodia. The experiment was carried out by tracking 17 amoeba isolates using a microscope and a video recorder. Various traces lasting 15 to 60 minutes were recorded with a time step of 1 or 2 minutes. The species studied had sizes ranging from 10 to 100 microns and average speeds ranging from 0.16 to 1.3 $\mu\text{m/s}$. The authors measured turning angles, velocity distribution, and mean-squared displacement after each step. The MSD scaled as $\langle x^2(t) \rangle \propto t^\mu$ with $\mu \sim 1.5 - 1.9$ for all observed cells, leading the authors to conclude that the Lévy walk could be a good candidate for a model.

Humans are the most sophisticated organisms, with complex environmental, sociological, technological, and urban factors governing their movement. Human mobility is an active area of study due to its evident relevance to real-world applications. The field of human mobility is linked to the development of transportation systems, mobile networks, and the prevention of contagious disease spread. From dollar bill tracking [41] to mobile phone tracking [81] to a recent study of influenza virus spreading [40], works on this topic have received a lot of attention, both in the public domain and in academia.

Lévy walks are still in active development, and we are seeing them used in robotics and mobile communication technologies [122]. As a result, a better understanding of the model's underlying mechanism would aid in the advancement of Lévy walk models into new unexplored territories.

1.1 Stochastic Processes

A stochastic process is a sequence of random variables indexed either continuously or discretely through a parameter often interpreted as time. The movement of ants in a labyrinth [210], the growth of a bacterial population, or the movement of a gas molecule are examples of such processes [62, 74, 77, 176]. They are ubiquitously used as mathematical models of systems and phenomena that vary randomly. These processes seek applications in a wide range of fields such as biology [38], chemistry [219], ecology [119], neuroscience [117], physics [231], image processing, signal processing [63], control theory [33], computer science [25], and financial markets [169, 200, 208]. They are analyzed using continuous or discrete-time measurements from an ensemble of realizations.

1.2 Scaling of Stochastic Processes

A discrete version of a stochastic process X is the sum of increments δ_s , e.g.

$$X_t = \sum_{s=0}^{t-1} \delta_s \quad (1)$$

The distribution of X_t can be denoted as a function $f(x, t)$. The scaling of a stochastic process is then defined as the measure of how $f(x, t)$ varies with t . A stochastic process is said to be self-similar if for any $a > 0$, there exists an exponent $H \geq 0$ such that

$$X_{at} \stackrel{d}{=} a^H X_t \quad (2)$$

where “ $\stackrel{d}{=}$ ” means equality “in distribution” and H is the *Hurst exponent* which quantifies the scaling of the distribution.

The scaling of a time series helps in understanding the underlying dynamics of a stochastic process. These measurements are dependent on whether the increments of a process are stationary or non-stationary. If the probability distribution of the increments of a stochastic process is independent of t , then the process is a *stationary increment process (SIP)* and if the probability

distribution of the increments is dependent on t , then it is a *non-stationary increment process (NIP)*.

1.3 Anomalous Diffusion and the Central Limit Theorem

A stochastic process is said to diffuse normally if the Mean-Squared Displacement (MSD) of the distribution scales with time as $t^{\frac{1}{2}}$. Most processes are found that scale as t^H where H is called as the *self-affine exponent* or *Hurst exponent* [66]. The MSD of the distribution is given as:

$$\langle x^2(t) \rangle \sim t^{2H} \quad (3)$$

When $H \neq 1/2$, a process is said to diffuse anomalously with time. This behavior is found both in theoretical models and in many experiments; see references [94, 157, 158, 173, 185]. The challenge is to understand the system's underlying dynamics so that H can be precisely determined. Additionally, there is a need to understand the various system features that cause the MSD to deviate from the standard linear scaling predicted by the Central Limit Theorem (CLT). The CLT states that if the increment probability distributions are

- a. uncorrelated,
- b. have finite variance, and
- c. identical, independent of time,

then the processes scale with $H = \frac{1}{2}$. The stochastic processes scale with $H \neq \frac{1}{2}$ may be due to the failure of any one or a combination of the three conditions of the CLT.

1.4 History and State of the Exponents

1.4.1 Hurst Exponent H

In 1968, Mandelbrot [17, 139] introduced the self-similarity exponent H to represent the overall scaling exponents for SIPs. The *Hurst exponent* was a remarkable discovery by hydrologist Harold

Edwin Hurst and he calculated the exponent using the R/S statistic [98]. Mandelbrot decomposed anomalous diffusion ($H \neq 1/2$) into two effects namely the *Joseph effect* quantified by the Joseph exponent J [136] and the *Noah effect* quantified by the Latent exponent L . These exponents are calculated using moment-based estimations. The moment-based estimations of the width cannot be used for fat-tailed distributions as their variances diverge. We use the quantile difference method proposed by Fama and Roll [69] to calculate the overall scaling exponent of the processes. This method is robust and can also be used for processes displaying Noah effect.

1.4.2 Joseph Exponent J

Joseph effect derives its name from the old testament prophet who foretold seven years of prosperity followed by seven years of famine [1]. Mandelbrot introduced the *Joseph exponent* to describe long-range dependence between increments of a time series in SIPs and calculated it using the R/S statistic [17, 139]. This method has been used to estimate the exponent for processes with non-Gaussian increments [140, 141]. Mandelbrot also argued that the R/S statistic is superior to auto-correlation and variance analysis since it can be applied to increments with infinite variance [31, 137]. This method can also be used to calculate the Joseph exponent for some NIPs [54].

Other methods such as the detrended fluctuation analysis (DFA) [177], detrended moving averages [16], and scaling analysis based on the wavelet transform [4] are also used for calculating the Joseph exponent.

1.4.3 Latent exponent L

Mandelbrot first introduced the term *Noah effect* to describe “the observations that extreme precipitation can be very extreme indeed” [139]. He later quantified the effect with *Latent exponent L* and asserted that “ S_t diffuse with exponent $L - 1/2$ ” for SIPs, where S_t is the denominator of R/S statistic [136]. However, he did not clearly state what statistic (mean, variance or median) of S_t scales with $L - 1/2$ for SIPs. With further developments for calculation of L , Fama and McCulloch developed a method to measure the tail index of α -stable distribution which can be used to calculate

L as $L = \frac{1}{\alpha}$ [68, 69, 153]. This method, however, cannot be applied to heavy-tailed distributions that are not α -stable. Inspired by Mandelbrot’s method, it was found that the median of S_t scales with $L - 1/2$ for SIPs and NIPs [54].

1.4.4 Moses exponent M

Moses effect was first introduced in 2018 and derived its name from the biblical reference which reads “Moses led the Israelites after their Exodus from Egypt as they wandered through the wilderness, having no stationary settlements” [54]. The effect is quantified as the *Moses exponent* M , which is used to determine whether or not the increments of a stochastic process are stationary. Common examples of processes with non-stationary increments are intraday prices of financial markets [27, 58, 166], the abundance of solar flares [125, 180, 181], and temperature fluctuations in turbulence [50, 180, 181].

1.5 Notion of Aging

Anomalous diffusion processes may exhibit aging [70, 118, 121, 147, 202]. This means that the age of the process controls the statistical properties of the process. Aging in diffusion processes yields an interesting, insightful perspective on dynamics in a disordered medium, and more generally, is used as a tool to probe complex systems [22].

The functional dependence on time is generally more involved in NIPs, and the origin of time can no longer be chosen arbitrarily. As a result, a new concept of aging emerges. The explicit dependence of a physical observable on the time span t_a between the original preparation of the system and the start of data recording is defined as aging of a system [187]. In some experiments, the aging time t_a is defined differently. Some common examples include the time of flight measurements of charge carriers in polymeric semiconductors in which the system is prepared by knocking out the charge carriers by a light flash [191], the initiation time in blinking quantum dot systems is given by the first exposure of the quantum dot to the laser light source [187] and the spin glass systems [61, 87]. In some other systems like the motion of tracers in living biological cells, the

aging time is not precisely defined.

1.6 Lévy Walks

The random walk is a fundamental concept that has applications ranging from quantum physics to finance. Remarkably, one random walk model appears to be widely used in many fields as a tool for analyzing transport phenomena where the dispersal process is faster than Brownian diffusion [237]. This random walk model is called the Lévy walk model. The term Lévy walk was coined by Shlesinger *et al.* (1982). A Lévy walk model is defined as a model with the ability to generate anomalously fast diffusion and have a finite velocity of a random walker. These models have rich statistical behaviors which can be found by tuning a few well-defined handles. They have found a number of applications in classical chaos, nonlinear hydrodynamics [110, 111, 198, 199], single-particle Hamiltonian systems [112, 238], blinking quantum dots [144, 146, 209], cold atom optics [192], motility of living organisms, their foraging, and search strategies [221, 170], robotics, and mobile communication technologies [122]. This wide range of applications demonstrates that Lévy walk models provide significant insight into complex transport phenomena.

1.7 Heterogeneous Diffusion Processes

Heterogeneous diffusion processes are defined as processes with deterministic power-law space-dependent diffusivities [56]. Space-dependent diffusivity appears to be a natural description for diffusion in heterogeneous systems from a physical standpoint. Examples include Richardson diffusion in turbulence [182] and mesoscopic approaches to transport in heterogeneous porous media [60, 88] and on random fractals [130, 174]. Recent studies show that the maps of the local cytoplasmic diffusivities in bacterial and eukaryotic cells showed a highly heterogeneous landscape [67, 116], recalling the strongly time-varying diffusion coefficients of tracers in cells [223].

In what follows, this dissertation first concentrates on Pomeau-Manneville Map: application of an aging system in Chapter 2, starting from the basic definition and understanding of the process and then turning to discuss the importance of *Moses effect* in an aging system. Chapter 3 focuses

on the decomposition of anomalous diffusion found in Lévy walks. This work uses simulations and time-series analysis of single Lévy walk trajectories to investigate the emergence of the three effects in different parameter regimes of the model and compare the findings with analytical results based on the well-developed theory for this process. Chapter 4 is devoted to the decomposition of anomalous diffusion for heterogeneous diffusion processes. Chapter 5 discusses the generalization of the exponents in different dimensions for various random processes.

2 Anomalous Diffusion and the Moses effect in a Model of Aging

This chapter has been published [163].

According to the Central Limit Theorem, the distribution of a process that is the sum of many random increments will have a variance that grows linearly in time. Such processes are said to diffuse normally. Many experimental systems, however, are known to diffuse anomalously. Examples include cold atoms in dissipative optical lattices [52, 109], motion in a crowded environment such as the cytoplasm of biological cells [76, 229, 228], blinking quantum dots [103, 143, 186], and intra-day trades in financial markets [27, 54, 194]. Understanding the nature of the dynamics of these systems that leads to anomalous diffusion is a topic of intense interest.

For stochastic processes with stationary increments, that is, increments with a time-independent distribution, Mandelbrot [139] decomposed the nature of anomalous diffusion into two root causes or effects. He recognized that it could be caused either by long-time increment correlations or by increment distributions that have sufficiently fat tails so that their variance is infinite. He called the effect due to increment correlations the *Joseph effect*, and the effect due to fat-tailed increment distributions the *Noah effect*. Both effects violate the premises of the Central Limit Theorem.

A third way that the Central Limit Theorem premises can be violated is if a stochastic process has non-stationary increments. Chen, *et al.*, in keeping with the biblically themed names of the other effects, recently named this root cause of anomalous diffusion the *Moses effect* [54]. With the Moses effect, the nature of anomalous diffusion in processes with non-stationary increments can now be decomposed as Mandelbrot did for processes with stationary increments. Any one of the Joseph, Noah, or Moses effects, or a combination of them, can cause anomalous diffusion.

For self-affine processes, which have a distribution that scales with a power law of time t^H , where H is what Mandelbrot called the *Hurst exponent*, scaling exponents can be defined to quantify each of the three effects that can cause anomalous scaling. The *Joseph exponent* J quantifies the increment correlations in the Joseph effect. When $J \neq 1/2$ increment correlations exist and can cause anomalous scaling. If $J > 1/2$ the increments are positively correlated, while if $J < 1/2$

they are anti-correlated. The *latent exponent* L quantifies the effect of increment distribution fat-tails in the Noah effect. When $L > 1/2$, the increment distribution has “fat tails” and anomalous scaling can result. The *Moses exponent* M quantifies the effect of non-stationarity of the increment distributions in the Moses effect. When $M > 1/2$ the increment distribution widens with time, and for $M < 1/2$ it shrinks with time. The exponents J , L and M are related to H through the scaling relation

$$H = J + L + M - 1 . \tag{4}$$

If $H \neq 1/2$ the diffusion is anomalous. If $H < 1/2$ the process is sub-diffusive, and if $H > 1/2$ it is super-diffusive. Robust statistical methods that analyze ensembles of realizations of a stochastic process can be used to determine each of the four exponents [54] independently.

Physical systems with aging behavior can have non-stationary, time-dependent behavior and diffuse anomalously. Aging systems can also be non-Markovian, having long-time increment correlations, which also can contribute to the anomalous behavior [22, 187, 192]. In this paper, we decompose the anomalous diffusion found in a simple model of aging behavior [21, 75] and discover that it is due to a rich combination of the Joseph, Noah, and Moses effects. The Moses effect arises from an intrinsic non-stationarity that leads to aging even though the increments do not explicitly depend on time. The model process consists of increments that are generated by a nonlinear map. Although the map is a deterministic system, it is intermittently chaotic, and the increments it generates model stochastic, noise-driven increments in physical systems.

The chapter is organized as follows. In the first subsection, we introduce our model system and describe its anomalous diffusive behavior. Then, in the second subsection, we quantitatively decompose the anomalous diffusion into its root causes using analytic scaling arguments for each of the different constitutive effects. In the third subsection, we confirm our analytical results with numerical simulations. In the final subsection, we discuss our results and the importance of the Moses effect for anomalous diffusive behavior observed in experimental systems.

2.1 Model and its Diffusive Behavior

Consider a one-dimensional, discrete-time process X_t , defined for integer time $t \in [0, \infty)$. The process is the sum of increments $\{\delta_t\}$

$$X_t = \sum_{s=0}^{t-1} \delta_s; X_0 = 0 \quad (5)$$

that are iterates of the modified Pomeau-Manneville (PM) map [178]

$$\delta_{t+1} = \begin{cases} -4\delta_t + 3 & \text{if } 0.5 < \delta_t \leq 1.0 \\ \delta_t \left(1 + |2\delta_t|^{z-1}\right) & \text{if } |\delta_t| \leq 0.5 \\ -4\delta_t - 3 & \text{if } -1 \leq \delta_t < -0.5 \end{cases}, \quad (6)$$

with $z > 1$. This map has been studied extensively in the past. It has been linked to anomalous diffusion [75] aging [21] and weak ergodicity breaking [29]. The initial increment δ_0 is chosen randomly from a uniform distribution in the interval $[-1, 1]$. Since there is aging in the system, this initial distribution is important. The distribution changes over time as we present in subsection 3. The dependence on the initial distribution is similar to aging continuous time random walks [22].

The distribution of the process $P(X_t)$ scales with time

$$P(X_t) = t^{-H} P^*(X_t/t^H) \quad (7)$$

where H is the *Hurst exponent* and P^* is the *scaling function* shown in Fig. 8. In the figure, the scaling parameter is $u = X_t/t^H$. The function is shown at four different times t , spanning 3 decades from 10^3 to 10^6 . Here the PM map parameter is $z = 2.5$ and the Hurst exponent is $H = 0.38$. Lines connecting the data points are shown as guides to the eye. The scaling functions converge for large t , but corrections to scaling are noticeable at smaller t . To measure H empirically, one

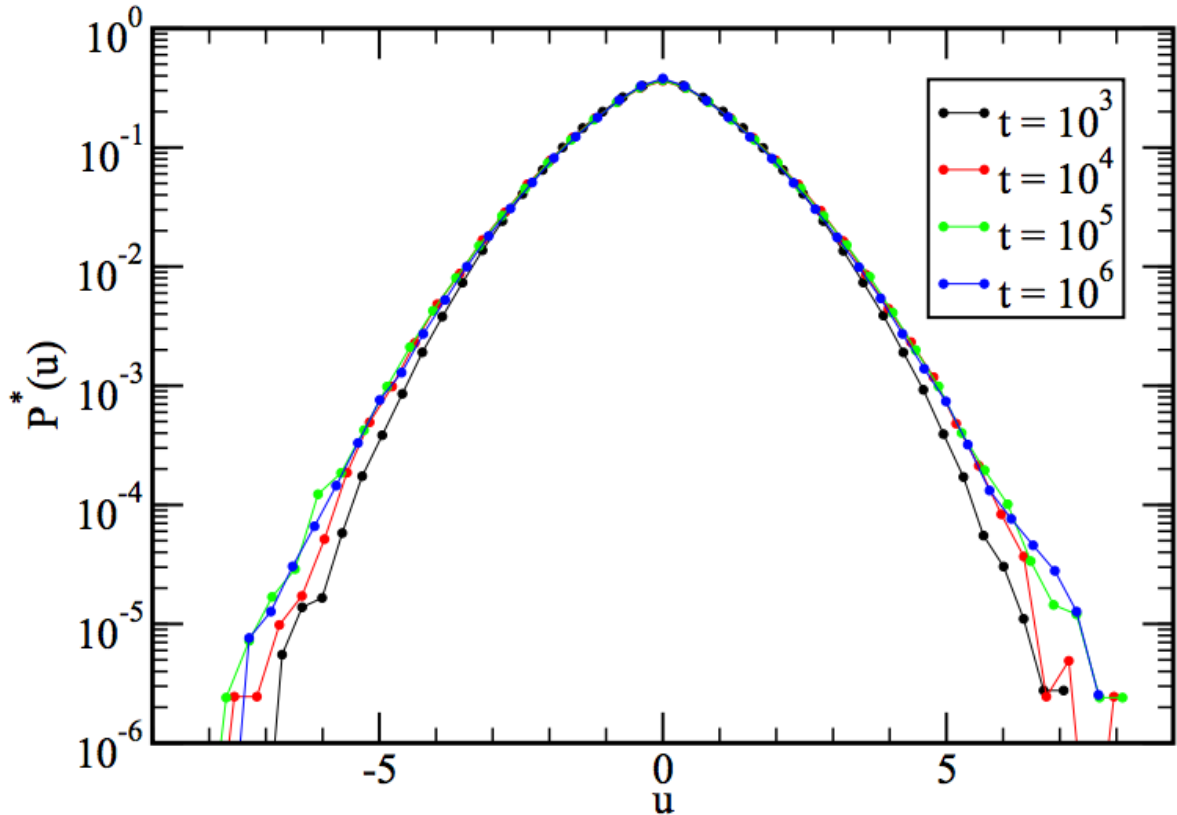


Figure 1: Scaling function of the distribution of the process X .

can simply measure the scaling of the width of distribution

$$w[X_t] \sim t^H, \quad (8)$$

which can be defined as, say, the distance between the 75th quantile and the 25th quantile of $P(X_t)$, or, as the standard deviation of the distribution $\sqrt{\langle X_t^2 \rangle}$, if it is finite. Here $\langle X_t \rangle = 0$ for all t .

The value of H can be calculated from the theory of stochastic renewal processes. A more rigorous calculation was presented in [172]. Here we recall the salient points. Stochastic renewal processes have a well-defined waiting time distribution. In our case, a waiting period is defined as the time that the system spends in the interval $|\delta| \leq 0.5$. In this region, the dynamics of the system are regular with δ monotonically increasing (or decreasing if it's negative), while it escapes from

the unstable fixed point at $\delta = 0$. The dynamics can be approximated by a continuous differential equation

$$\frac{d\delta}{dt} = \delta (2\delta)^{z-1} \quad \text{when } \delta \rightarrow 0. \quad (9)$$

Once δ reaches the outer part $|\delta| > 0.5$, the dynamics is chaotic until a “reinjection” into the regular region occurs. Hence, this type of system is intermittently chaotic. Generally, the chaotic motion is very short, thus it is sufficient to consider only the waiting periods.

Integrating Eq. (9) and assuming a uniform distribution for reinjected δ , the distribution of waiting times τ can be calculated [75, 13]

$$P(\tau) \propto \tau^{\frac{z}{1-z}}. \quad (10)$$

For $z > 2$ the mean waiting time diverges, which gives rise to all the effects we discuss in this article. During each waiting period the process X_t performs a “jump” due to many small steps δ in the same direction. We define the displacement χ during jumps that start at renewal (reinjection) times $t = t_r$ as

$$\chi = X_{t_r+\tau} - X_{t_r}. \quad (11)$$

It can be calculated from Eqs. (9,10) to be [161]

$$\chi \sim \frac{1}{2}(z-1)^{\frac{2-z}{1-z}} \frac{1}{z-2} \tau^{\frac{2-z}{1-z}}, \quad (12)$$

thus giving a relation between χ and the waiting times. The joint probability density function (PDF) for χ and τ then is

$$P(\chi, \tau) \propto \tau^{\frac{z}{1-z}} \frac{1}{2} \left[\delta(\chi - \tau^{\frac{2-z}{1-z}}) + \delta(\chi + \tau^{\frac{2-z}{1-z}}) \right], \quad (13)$$

where δ here is the Dirac δ -function. Eq. (13) is well known in stochastic renewal processes [6, 159].

From here, the value of the Hurst exponent can be calculated from the scaling of the ensemble-averaged mean squared displacement of the process $\langle X_t^2 \rangle \propto t^{2H}$. As for continuous-time random walks [12], the calculation can be performed in Fourier-Laplace space. There the mean squared displacement is equal to the second derivative of the spatial distribution of the process. Results are known for processes of with PDFs of the form of Eq. (13) for Levy flights [12] and Levy walks [15]. The results in both cases are the same and therefore independent of the exact path the system takes during each waiting time. They thus apply to our system as well [161, 162, 172]

$$H = \begin{cases} 0.5 & \text{if } z < 2 \\ 0.5/(z-1) & \text{if } 2 < z < \frac{5}{2} \\ (z-2)/(z-1) & \text{if } \frac{5}{2} < z \end{cases} . \quad (14)$$

At the crossover points, logarithmic corrections appear [13], which make numerical calculations more difficult. For $2 < z < 3$, $H < \frac{1}{2}$ and the system is sub-diffusive, while for $z > 3$, $H > \frac{1}{2}$ and the system is super-diffusive.

2.2 Joseph, Noah and Moses effects

2.2.1 Definitions

Anomalous diffusion can be decomposed into effects that are root causes for the violation of the premises of the Central Limit Theorem (CLT). For a process X_t that is the sum of random increments $\{\delta_t\}$, if the increments: (1) are independent, (2) have a distribution with finite variance, and (3) are identically distributed, the CLT holds. Violation of these premises does not necessarily lead to anomalous diffusion, e.g., CLT can still hold for systems with exponential decay of correlations. However, if it does, it is referred to as the (1) Joseph, (2) Noah, and (3) Moses effects, respectively. Each of these constitutive effects, or a combination of them, can cause anomalous diffusion. For self-affine processes, they can be quantified by scaling exponents, which are related to each other and the Hurst exponent by Eq. 4. These exponents are defined as follows.

To define the exponents, first define the following random variables: the sum of the absolute values of increments

$$Y_t = \sum_{s=0}^{t-1} |\delta_s|, \quad (15)$$

and the sum of increment squares

$$Z_t = \sum_{s=0}^{t-1} \delta_s^2. \quad (16)$$

Then, the Moses exponent M and the Latent exponent L , which quantify the Moses effect and Noah effect, respectively, are defined by the scaling of ensemble-averaged median of these variables

$$m[Y_t] \sim t^{M+1/2} \quad (17)$$

$$m[Z_t] \sim t^{2L+2M-1}, \quad (18)$$

or, similarly, of their means, if they are finite.

The Joseph exponent J , which quantifies the Joseph effect, is defined by the scaling of the ensemble-averaged rescaled range statistic (R/S) [98]

$$E[R_t/S_t] \sim t^J, \quad (19)$$

where R_t is the range of the process

$$R_t = \max_{1 \leq s \leq t} \left[X_s - \frac{s}{t} X_t \right] - \min_{1 \leq s \leq t} \left[X_s - \frac{s}{t} X_t \right] \quad (20)$$

and S_t is the standard deviation of increments up to time t

$$S_t^2 = \frac{1}{t} Z_t - \left[\frac{1}{t} X_t \right]^2. \quad (21)$$

It should be noted that there is some confusion in the literature with exponents J and H . The J defined in Eq. 19 is the exponent originally defined by Hurst and is the exponent that is found

through detrended fluctuation analysis (DFA) [92, 177]. In papers utilizing DFA, it is often referred to as the Hurst exponent, e.g., in [106]. Mandelbrot first called this exponent J and distinguished it from the H defined in Eq. 8 [139]. Of course, in processes with no Noah or Moses effects, J and H become equivalent.

2.2.2 Values in the Pomeau-Manneville map

To calculate the values of the scaling exponents for the PM map, we utilize the concept of infinite invariant densities in infinite ergodic theory. Such densities have well-defined shapes that scale with time. The increment density $P(\delta_t)$ is an excellent example of this. It does not satisfy the central limit theorem. However, it does satisfy two other limit theorems.

First, it can be shown [113], that there exists an infinite invariant density $P_{\text{inf}}(|\delta|) \propto |\delta|^{1-z}$ that is related to the actual density by

$$P(|\delta_t|) \sim t^{\frac{2-z}{z-1}} P_{\text{inf}}(|\delta|) \quad (22)$$

for $|\delta_t|$ not close to zero. The density $P(|\delta_t|)$ must be normalizable since it is a physical density. Therefore, it is truncated for small values of δ . For longer aging times t , the location of the cutoff of the density moves closer and closer towards zero. Thus, the infinite invariant density in the limit of large t has a well-defined power law shape but is not integrable.

There is a second way to obtain an invariant expression related to the increment density. It was derived by Dynkin [64] in the context of renewal theory, while Thaler [214] established the connection to the underlying transformations. The application to the PM map was shown in [9]. It can be shown that by transforming the increment δ according to

$$\gamma = 2|\delta| (t(z-1))^{\frac{1}{z-1}}, \quad (23)$$

one obtains an invariant distribution

$$P(\gamma) = \frac{z-1}{\pi} \sin\left(\frac{\pi}{z-1}\right) \frac{1}{1+\gamma^{z-1}} \quad (24)$$

for γ .

Both of these limit theorems are necessary for understanding the scaling of Z_t . It is calculated by

$$\langle Z_t \rangle = \sum_{s=1}^t \langle \delta_s^2 \rangle = \sum_{s=1}^t \int_0^1 d|\delta_s| \delta_s^2 P(|\delta_s|). \quad (25)$$

The sum adds a '+1' to the exponent describing the scaling behavior of $\langle \delta_s^2 \rangle$, which was calculated in [161]. For $z < 2$, the scaling is trivial because $P(\delta)$ is stationary and integrable. For $2 < z < 4$, it can be found using the infinite invariant density in Eq. (22). For $z > 4$ the integral over $\delta^2 P_{\text{inv}}(|\delta|)$ diverges, but the Thaler-Dynkin limit theorem can be applied using Eq. (23). From these considerations Z_t scales as:

$$\langle Z_t \rangle \propto \begin{cases} t & \text{if } z < 2 \\ t^{\frac{1}{z-1}} & \text{if } 2 < z < 4 \\ t^{\frac{z-3}{z-1}} & \text{if } 4 < z \end{cases} . \quad (26)$$

Similar methods can be used to find the scaling behavior of Y_t . Again, we use the ensemble average

$$\langle Y_t \rangle = \sum_{s=1}^t \langle |\delta_s| \rangle = \sum_{s=1}^t \int_0^1 d|\delta_s| |\delta_s| P(|\delta_s|). \quad (27)$$

Here the expression is integrable with respect to the infinite invariant density for $z < 3$ and with respect to the Thaler-Dynkin limit theorem for $z > 3$. Therefore, $\langle Y_t \rangle$ scales as

$$\langle Y_t \rangle \propto \begin{cases} t & \text{if } z < 2 \\ t^{\frac{1}{z-1}} & \text{if } 2 < z < 3 \\ t^{\frac{z-2}{z-1}} & \text{if } 3 < z \end{cases} . \quad (28)$$

Note that the scaling of the mean is equivalent to the scaling of the median for both Y_t and Z_t .

No more information is needed to calculate the exponents J , L and M . Using Eqs.(17), (18), (27) and (28), one obtains for the Moses exponent

$$M = \begin{cases} 0.5 & \text{if } z < 2 \\ (1.5 - 0.5z)/(z - 1) & \text{if } 2 < z < 3 \\ (0.5z - 1.5)/(z - 1) & \text{if } 3 < z \end{cases} , \quad (29)$$

and for the latent exponent

$$L = \begin{cases} 0.5 & \text{if } z < 2 \\ (z - 1.5)/(z - 1) & \text{if } 2 < z < 3 \\ 1.5/(z - 1) & \text{if } 3 < z < 4 \\ 0.5 & \text{if } 4 < z \end{cases} . \quad (30)$$

Since the Hurst exponent H is given by Eq. (14), the Joseph exponent J can be determined using the scaling relation Eq. (4),

$$J = \begin{cases} 0.5 & \text{if } z < 2.5 \\ (1.5z - 3)/(z - 1) & \text{if } 2.5 < z < 4 \\ 1 & \text{if } 4 < z \end{cases} . \quad (31)$$

At the end of this subsection we want to add a short remark about the parameter J . Throughout this subsection followed a similar path of reasoning as in [161], where the ensemble averaged time averaged mean squared displacement (EATAMSD) of the PM map was shown to be

$$\langle \overline{X^2} \rangle \equiv \sum_{s=0}^{t-\Delta} \frac{(X_{s+\Delta} - X_s)^2}{t - \Delta} \propto t^\beta \Delta^{2H-\beta}, \quad (32)$$

for $z > 2.5$. Here t is the total measurement time. This is the result of the scale-invariant Green-Kubo relation for time-averaged diffusivity. The scaling of the EATAMSD is the difference between

the scaling of the ensemble-averaged mean squared displacement ($= 2H$) and the scaling of the “velocity displacement” $\langle \delta_t^2 \rangle \propto t^\beta$, which is, in fact, the derivative of Z_t . So Z_t scales like $t^{\beta+1}$. Then considering Eq. (18), the scaling exponent of the EATAMSD in fact is $2H - 2L - 2M + 2$. This result from the scale-invariant Green-Kubo relation for time averaged diffusivity looks very much like our scaling relation Eq. (4) and therefore implies that the EATAMSD scales as $\sim t^{2J}$. This equivalence is true, at least, for systems with scale invariant increment correlation functions

$$\langle \delta_t \delta_{t+\Delta} \rangle \propto t^{2H-2} \Phi\left(\frac{\Delta}{t}\right) \quad (33)$$

in the parameter range $J > 0.5$ and $L + M > 0.5$.

2.3 Simulation Results

To verify our analytic predictions for the exponents, we performed numerical simulations of the PM map. For each value of z from 1.5 to 4.5 in steps of 0.1, we generated an ensemble of 10^5 realizations of the process X_t for $t = 10^6$ map iterations. We then measured $w[X_t]$, $m[Y_t]$, $m[Z_t]$, and $E[R_t/S_t]$ for the ensemble. Example results for $z = 2.5$ are shown in Fig. 2. In the figure, the scaling of the functions quantified by the exponents corresponding to the slope of the function at large t , determine the exponents quantifying diffusion and the constitutive effects that cause anomalous diffusion. Here the PM map parameter is $z = 2.5$. Lines connecting the data points are shown as guides to the eye. The statistical error of the data points is smaller than the symbol size. The scaling exponents describe the asymptotic, large t scaling behavior of these functions.

We fit each of the four functions over the two-decade range from $t = 10^4$ to 10^6 to the form

$$f(t) = at^\Omega \quad (34)$$

where a and Ω are fitting parameters, and Ω is the asymptotic scaling exponent. Finding Ω for each function, we then determined the values of H , M , L and J using Eqs. 8, 17, 18 and 19. The result of the fitting for each exponent as a function of z is shown by the filled circles in Fig. 3. Circles

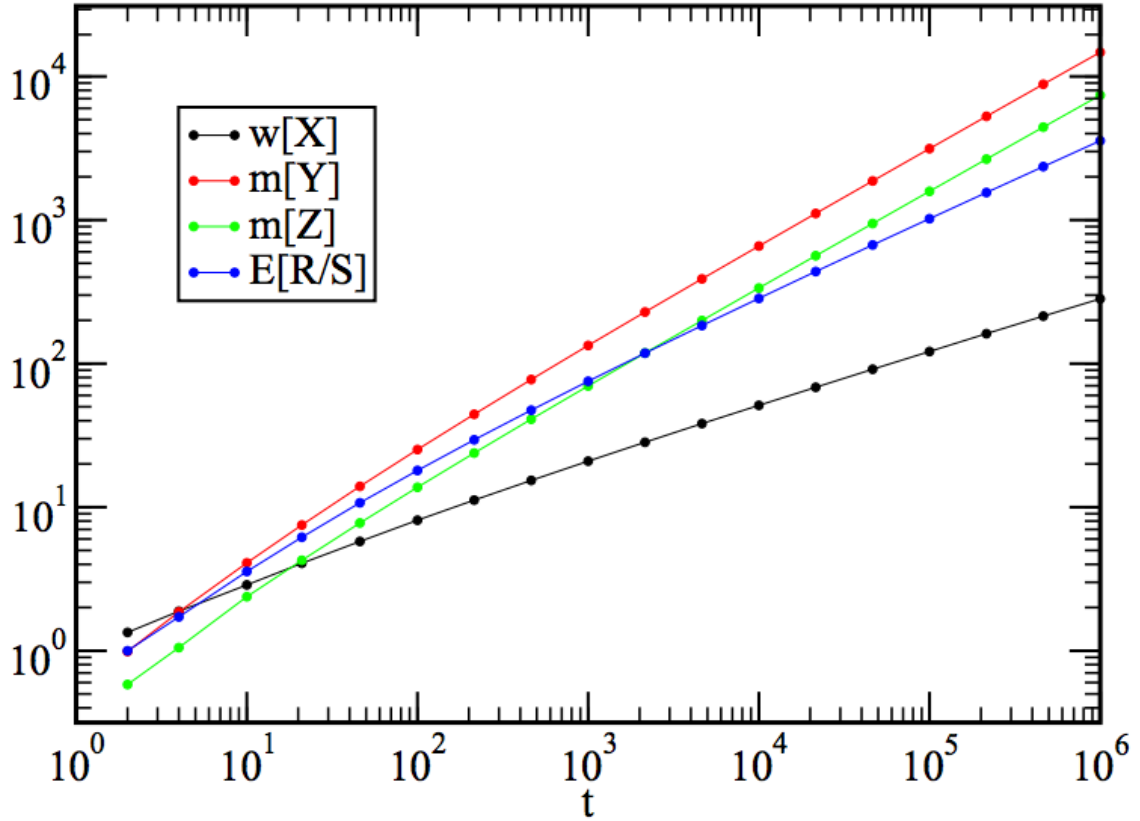


Figure 2: Log-log plot of the width of X , median of Y and of Z , and mean of R/S as a function of time t .

show the values resulting from numerical simulation and the solid lines the analytic predictions. As $z \rightarrow \infty$, $H \rightarrow 1$ and $M \rightarrow \frac{1}{2}$. The analytic predictions are shown by the solid lines in the figure. Fig. 4 confirms the scaling relation between the exponents, Eq. 4. It shows the theoretically predicted value of H , versus the fitted value of H from simulations and the result of the fitting for $J + L + M - 1$ as a function of z .

The simulation results roughly follow our theoretical predictions, but there are deviations. Upon close examination of Fig. 2, one can see that the functions are still curving on a log-log plot at $t = 10^6$. Thus the deviations between simulation results and their predictions in Figs. 3 and 4 are presumably due to finite-time corrections to scaling. The corrections are especially

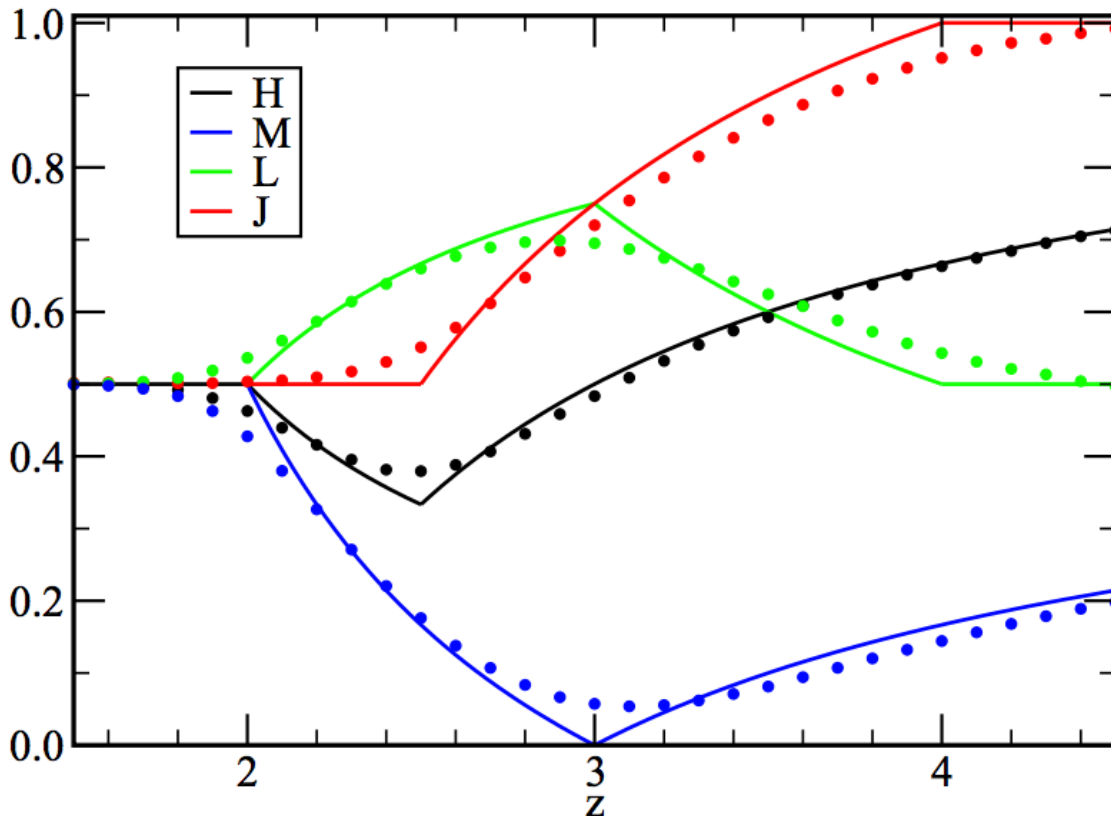


Figure 3: Values of the scaling exponents quantifying diffusion and the constitutive effects that cause anomalous diffusion in the PM map as a function of parameter z .

evident near crossover points where they have a logarithmic form [13]. To obtain more accurate numerical results, either corrections to scaling must be included in the fit or longer simulations must be run. The general form of the corrections, however, is not known, and the accuracy of long simulations is limited by the phenomenon of “round-off periodicity” [28, 85]. With double-precision calculations, the map can accurately be iterated only about 10^6 times. Longer simulations would require computationally expensive quadruple precision calculations.

2.4 Discussion

The root causes of anomalous diffusion can be decomposed into the Joseph, Noah, and Moses effects. To our knowledge, this is true for all systems, and there are no other causes; however,

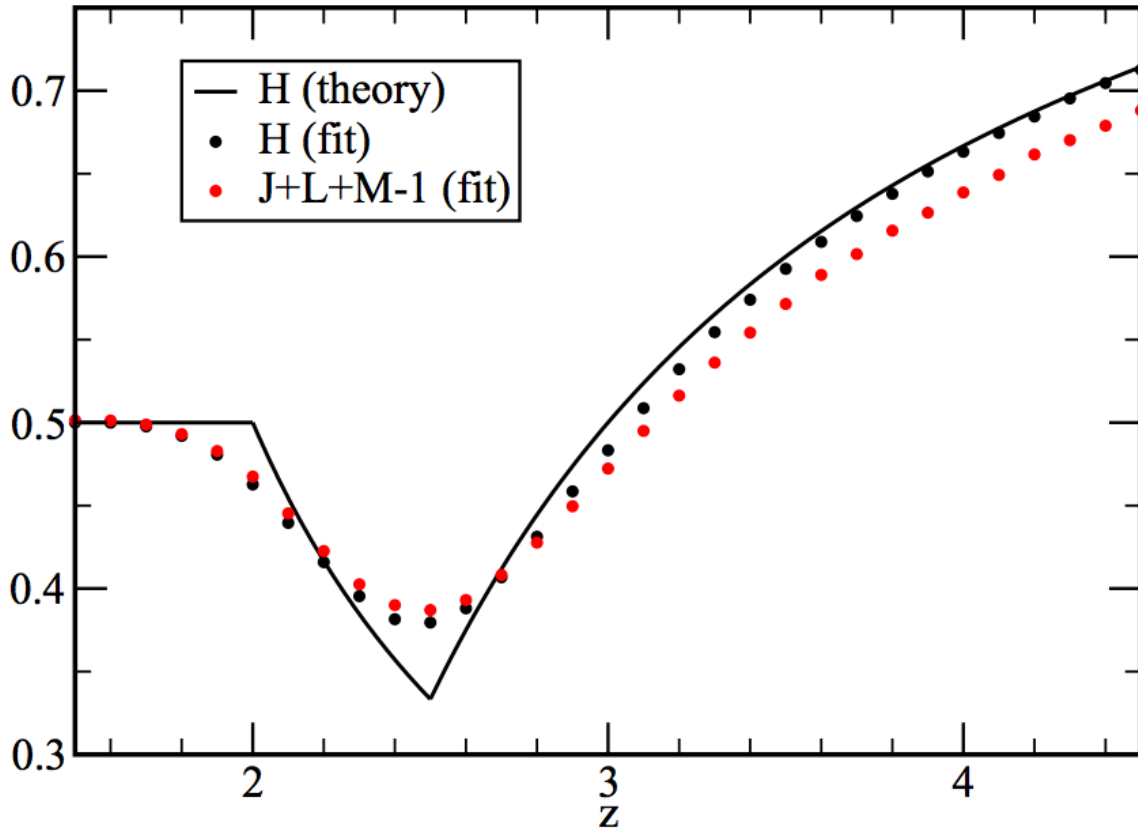


Figure 4: Verification of the scaling relation (Eq. 4) for the exponents quantifying diffusion in the PM map as a function of parameter z .

all effects might also exist in a way that does not allow us to define the scaling exponents J , L , and M properly, e.g., for systems that exhibit multiscaling the theory might have to be extended. Non-stationary increments, such as what occurs in aging processes, can cause anomalous diffusion through the Moses effect. Previous studies have found that the anomalous diffusion in intra-day financial market prices is solely due to the Moses effect [26, 27, 54, 151, 152, 194]. Here, however, we have found that the anomalous diffusion in a simple model of aging is due to a complex combination of the Joseph, Noah, and Moses effects.

It is perhaps surprising that a process consisting of increments that are iterates of the PM map can have such a rich set of behaviors. The PM map is, after all, a deterministic map from the interval $[-1, 1]$ onto itself. The value of increments, thus, is bounded. However, the dynamics

of the map consist of an intermittent mixture of regular and chaotic motion, which can produce anomalous diffusion. For $z \leq 2$, nothing surprising happens. The diffusion of the system is normal, the increments are stationary, and there is no Joseph, Noah, or Moses effect. But for $z > 2$, the system ages with time because the mean waiting time in the regular region diverges. This causes the increment distribution to become time-dependent and a sub-diffusive Moses effect to occur.

Remarkably, a Noah effect occurs despite the fact that the tails of the increment distribution are bounded. However, for $z > 2$, where the increment distribution is time-dependent, rescaling of δ using Eq. (23) results in a stationary increment distribution that has fat tails. The second moment of this stationary distribution Eq. (24) diverges for $2 < z < 4$, causing the Noah effect. For larger values of z , although the distribution still has power law tails, they decay fast enough to keep its variance finite.

For $z < 2$, the density $P(|\delta|)$ is stationary and has a well-defined mean. For $2 < z < 3$, the density becomes non-stationary and moves towards zero. However, since it has fat tails, the mean goes to zero more slowly than the density itself. For $z > 3$, the distribution (Eq. (24)) is steeper. Here the mean goes to zero with the same scaling as the distribution itself, causing a decrease of the Moses effect. As a consequence, the Noah effect also decreases because it is directly linked to the Moses effect, as stated before.

For $z < 2.5$, there are no long-time increment correlations, as they are disrupted by the frequent intermittent periods of chaotic motion. However, for $z > 2.5$, increment correlations do exist and contribute to the anomalous diffusive behavior through the Joseph effect, which increases with z and becomes maximal at $z = 4$. Both the Noah and the Joseph effects only lead to super-diffusive behavior in the system, as both L and $J \geq 0.5$ for all z , while the Moses effect only leads to sub-diffusive behavior, as $M \leq 0.5$ for all z . The three effects combine to produce sub-diffusive behavior in the model for $2 < z < 3$. In this range of z , the Moses effect dominates over the other two effects. For $z > 3$, super-diffusive behavior occurs instead as the Noah and Joseph dominate the Moses effect.

In empirical time-series analyses, it is often assumed that the increments of the process are

stationary [135, 142]. This assumption is made to justify “sliding-window” statistical analyses that combine different increments. This can lead, however, to spurious results if the increments are non-stationary, such as falsely determining that the process has a fat-tailed distribution [27]. If there are non-stationary increments, a proper statistical analysis requires studying an ensemble of processes. This can be difficult to acquire such data, especially if the data is a historical time series. For some systems, there may be periodic or intermittent triggering events that can be thought of as beginning a new process [27, 54]. For others, experiments must be repeated. Here we repeated the numerical simulations to acquire the data for the ensemble analysis.

We have shown that decomposing anomalous diffusive behavior into its fundamental constitutive causes can contribute to understanding the nature of the system’s dynamics. It would be interesting to similarly decompose the anomalous diffusive behavior found in other systems, especially experimental systems. For other aging systems, which by definition have non-stationary increments, such as blinking quantum dots [103, 143, 186], it can be expected that the Moses effect contributes to anomalous diffusive behavior, but do the Joseph and Noah effects also contribute to the observed behavior? In other systems that diffuse anomalously, which are not necessarily known as aging systems, will a decomposition of the diffusion into constitutive effects reveal that a Moses effect contributes to the observed behavior?

3 Time Series Analysis of Lévy Walks

This chapter has been published [8].

Diffusive processes that scale anomalously with time, such that the Mean-Squared Displacement (MSD) of the expanding particle packet is

$$\langle x^2(t) \rangle \sim t^{2H}, \quad (35)$$

and the Hurst exponent $H \neq 1/2$, are widely observed. This behavior is found both in theoretical models as well as in many experiments, see, e.g., [94, 157, 158, 173, 185]. Of course, if we know the exact underlying process responsible for the dynamics, H can be determined precisely, and the various features of the system that lead to the deviation from the standard linear scaling of the MSD, expected by the Gaussian Central Limit Theorem (CLT), can be understood. However, when anomalous diffusive scaling is detected in measurements, it is not always clear what is responsible for the observed behavior of the system. Imagine, for example, that we obtain an ensemble of data-series describing intra-day trades in financial markets [27, 54, 194], or experimental data obtained from observation of molecules diffusing inside cells, e.g., [37, 115, 185, 218, 227, 233]. Here, the proper characterization of the exact root causes of this phenomenon is essential, since it can have implications on how we understand the underlying functioning of the system. If, for example, we observe that the MSD grows faster than linearly with time, is this due to temporal correlations in the data that cause large random fluctuations to be followed by similar or even greater ones? Is it the result of a fat-tailed increment distribution, or is it because there is an actual trend of inflation in the system? Our analysis below allows us to answer these questions, even though we cannot completely restore the underlying process just from the data.

To make this more precise: Consider a continuous-time stochastic process $x(t')$ defined in the time interval $t' \in [0, t]$. We can choose a number Q of observation windows of duration $\Delta = t/Q$, and then, represent this process by a discrete time-series composed of consecutive *increments*, starting at times $\{0, \Delta, 2\Delta, \dots, (Q-1)\Delta\}$. The increments are $\{\delta x_1, \delta x_2, \dots, \delta x_Q\} =$

$\{x(\Delta) - x(0), x(2\Delta) - x(\Delta), \dots, x(t) - x(t - \Delta)\}$. According to the Gaussian CLT, in the limit of large Q , if the increments are independent, identically distributed (IID) random variables chosen from a distribution with finite variance, then the MSD will grow linearly with Q and thus with time. Each of the three ways that the CLT can be violated corresponds to a *constitutive effect* that can produce anomalous scaling [54].

For processes with stationary increments, where the probability distribution of δx_j is independent of time, anomalous diffusive scaling can occur because of long-time increment correlations. This is called the *Joseph effect* [54, 139, 163]. A paradigmatic process that exhibits this effect is fractional Brownian motion [54, 128]. Another cause of anomalous scaling may be that the increment distribution is fat-tailed, in the sense that its second moment is divergent. This is the *Noah effect* [54, 139, 163]. A Lévy flight process where the increments are power-law distributed, independent random variables [158, 199], but with infinite variance, is one example of a model with this effect. When the increment distribution is non-stationary, anomalous diffusive scaling can also arise due to the *Moses effect* [54, 163]. A paradigmatic model in this case is scaled Brownian motion [101, 187, 217]. Each of the three effects can appear individually in a system or in various combinations. Importantly, the three effects can be interconnected with each other. For example, in [163], it was shown that statistical aging in the process could be associated not only with a *Moses*, but *Noah effect*.

In this chapter, we investigate these three constitutive effects in a well-studied stochastic process called coupled Lévy walk [237]. This model is known to have a rich spectrum of statistical behaviors found by tuning a few well-defined handles. We explore the emergence of the three effects in different parameter regimes of the model using simulations and methods of time-series analysis of single Lévy walk trajectories and compare our findings with analytical results based on the well-developed theory for this process. This example shows that the analysis based on the three constitutive effects is a valuable tool that can be applied to study other systems.

In a two-state Lévy walk [71, 199, 237], a particle starts at $x = 0$ at time $t' = 0$ and then moves in independent steps. Each step has a random duration τ , chosen from a Probability Density

Function (PDF) of the form

$$g(\tau) \sim \frac{c}{|\Gamma(-\gamma)|} \tau^{-1-\gamma} \quad (36)$$

at long τ , where $c, \gamma > 0$ are constants. During each step, the particle travels at a constant velocity V , whose magnitude $|V|$ can be either ± 1 (sometimes referred to as “genuine Lévy walk” [237]), or a deterministic function of τ , but whose direction is chosen randomly to be either toward the right, along the positive \hat{x} - *axis* (+), or left (−) along the negative axis. The latter, generalized model, is the case studied in detail in this chapter (see also e.g., [6, 11, 12, 14, 198]), and the results include also the constant-velocity case. The probability of the direction being to the right or the left is equal, so the motion is unbiased, and the velocity has a symmetric PDF $\phi(V)$. At time $t' = t$, the process stops. Up to this point, the particle has made $N - 1$ complete steps, and one, final “partial” step of duration

$$\tau^* = t - \sum_{i=1}^{N-1} \tau_i \quad (37)$$

The properties of the final step have been shown to have a dramatic effect on the overall behavior of the system [237], as the velocity V_N during this step does not necessarily have to be distributed like all its predecessors, see, e.g., [71]. For more on this point, see subsection 3.2. The number of steps in the process $N \in [1, \infty)$, in the time interval $[0, t]$ is random, and the particle’s position at time t is given by the sum

$$x(t) = \sum_{i=0}^{N-1} \chi_i + \chi^* \quad (38)$$

where $\chi_i = V_i \tau_i$, and $\chi^* = V_N \tau^*$.

Table 1 summarizes the main notations we use throughout the paper, by order of their appearance in the main text. Note that the instantaneous velocity $v(t)$ is not always defined, for example in the case of Brownian motion. This does not matter for the general analysis of the three effects, which are defined via \mathbf{v} , see subsection 3.1. In the example that we use to demonstrate our analysis,

Notation	Definition
V, τ, χ	Lévy walk: step- velocity, duration, displacement
M, L, J, H	Exponents: Moses, Noah, Joseph, Hurst
$\Delta, \delta x$	Time series: increment- duration, size
v	Time series: Mean velocity during an increment
α, β	Exponents describing the shape of the distribution of v
z_β	v/t^β
$v(t)$	Instantaneous velocity of the Lévy walker at time t
\tilde{v}	$v/t^{\nu-1}$

Table 1: The main notations used in this chapter, by order of their appearance in the main text.

namely Lévy walk, $v(t)$ exists, and $\lim_{\Delta \rightarrow 0} v \rightarrow v(t)$, see also subsection 3.4. The chapter's structure is as follows: In subsection 3.1, we define the three exponents that quantify the Moses, Noah, and Joseph effects. We discuss the relation between them and their role in determining the scaling shape of the increment PDF. In subsection 3.2, we extend the details on the Lévy walk model. In subsection 3.3, we summarize our main results, obtained from time-series analysis of numerical simulations, and a brief comparison of these results with the theoretical predictions. In subsection 3.4 we get analytic results for the Moses and Noah effects, and in subsection 3.5 for the Joseph. We generalize the model in subsection 3.6, and the discussion is provided in subsection 3.7.

3.1 Story of Three Exponents: M , L And J

The complete decomposition of the origin of anomalous diffusion presented in the introduction, was originally derived for discrete-time processes [54]. In this case, the process starts at $\xi_0 = 0$, at $n = 0$, and evolves in discrete jumps $n = 1 \dots N$ with duration Δ , until time $t = N\Delta$. The particle's position after n steps is denoted $\xi_{n\Delta}$. The Moses effect is quantified by the exponent M , given by the median of the sum, of the absolute value of the time-series increments [54]

$$m \left[\sum_{n=1}^{t/\Delta} |\delta \xi_n| \right] \equiv m \left[\sum_{n=1}^{t/\Delta} |\xi_{n\Delta} - \xi_{(n-1)\Delta}| \right] \propto t^{M+1/2} \quad (39)$$

Here, $M = 1/2$ yields a linear relation which is similar to normal diffusion. The Noah effect is defined by the scaling of the median of the sum of square-increments, and quantified by the Latent exponent L :

$$m \left[\sum_{n=1}^{\lceil t/\Delta \rceil} (\delta\xi_n)^2 \right] \propto t^{2L+2M-1} \quad (40)$$

Here again, normal diffusion leads to linear scaling, where $M = L = 1/2$. If there is no Moses effect, namely $M = 1/2$, the deviation from this scaling is quantified only by the exponent L , and it arises if the increment PDF is fat-tailed. Finally, the Joseph exponent can be defined via the sum over the auto-correlation function [163]

$$\sum_{\Delta'=0}^{\tilde{\Delta}} \langle \delta\xi_n \delta\xi_{n+\Delta'} \rangle / \langle (\delta\xi_n)^2 \rangle \propto \tilde{\Delta}^{2J-1} \quad (41)$$

where $0 \leq J \leq 1$. Here, starting from an arbitrary time point n , we sum over a discrete lag time Δ' , up to e.g., $\tilde{\Delta} \sim \mathcal{O}(t/10)$ ($\tilde{\Delta}$ is not related to Δ , defined above), and the scaling shape is valid when $\tilde{\Delta}, t \gg 1$. When $J > 1/2$, the correlations decay very slowly with $\tilde{\Delta}$, which leads to a divergent sum when $\tilde{\Delta} \rightarrow \infty$, and superdiffusion (see discussion on “long-ranged correlations” e.g., in [30]). When $J \leq 1/2$, the correlation function decays at least as fast as $1/\tilde{\Delta}$, which may lead either to normal diffusion, or in some particular cases to sub-diffusion, see Appen. A.1.

For a process $x(t)$ in continuous time, we divide the time series into Q non-overlapping observation windows of duration $\Delta = t/Q$ as mentioned above, and define the average velocity in each time interval $v(t') \equiv |\delta x_j|/\Delta$, where $\delta x_j = x(j\Delta) - x[(j-1)\Delta]$, and $(j-1)\Delta < t' < j\Delta$. Fig. 5 illustrates the decomposition of a continuous-time random trajectory, into a time-series of N increments of equal duration $\Delta \ll t$. In the figure, at the total measurement time t , the last step is incomplete. Two red dash-dot lines mark the start and end points of one completed Lévy walk step, whose duration τ was selected from the PDF Eq. (62), and the step-velocity is $V \sim \tau^{\nu-1}$. Here $\gamma = 0.52, \nu = 0.5$. As explained in subsection 3.1, the trajectory is decomposed into a series of consecutive increments $n = 1, 2, \dots$, of equal duration Δ , the start and end points of one such

increment are marked e.g. by two green dash-dot lines. The size of the average velocity $|\mathbf{v}|$ in that increment is also presented.

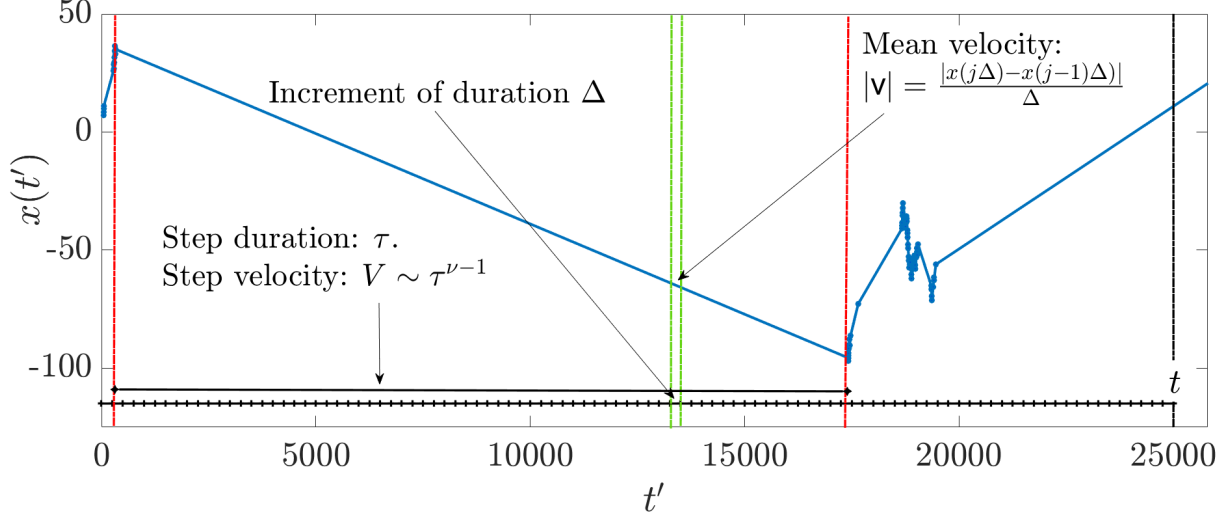


Figure 5: An example of a Lévy walk path $x(t')$ (blue) versus time, generated by the model in subsection 3.2.

Now, we can re-write the definition of the Moses effect in terms of the ensemble-time averaged absolute-velocity (when $\Delta \ll t$)

$$\langle |\overline{\mathbf{v}}| \rangle \equiv \left\langle \frac{1}{t - \Delta} \sum_{j=1}^{t/\Delta} \frac{|\delta x_j|}{\Delta} \right\rangle \propto t^{M-1/2} \quad (42)$$

We use here the ensemble mean, instead of the median, since it is a more convenient property to study analytically and numerically, hence we assume by this definition that this mean does not diverge. In the same spirit, the Noah effect is defined via the ensemble-time average of the squared velocity, when $\Delta \ll t$

$$\langle \overline{\mathbf{v}^2} \rangle \equiv \left\langle \frac{1}{t - \Delta} \sum_{j=1}^{t/\Delta} \frac{(\delta x_j)^2}{\Delta^2} \right\rangle \propto t^{2L+2M-2}, \quad (43)$$

where

$$1/2 \leq L \leq 1 \tag{44}$$

In this definition, one can notice that the Noah effect manifestation is somewhat different from the case of, e.g., a Lévy flight, since the mean of the squared increments is not divergent. As we explain in detail below, what leads to $L \neq 1/2$ in this case, is that the increment PDF has a regime where its shape is fat-tailed, but this regime has a time-dependent cutoff which is pushed towards $\pm\infty$ as time increases. The resemblance between this observation, and the source of the Noah effect in its original definition on P. 1, is the reason that we can make the association between the two cases and refer to L in Eq. (43,44) throughout this chapter as the Latent exponent. The upper bound on L , in Eq. (44), is true because $\langle \overline{v^2} \rangle \leq \langle \overline{|v|} \rangle^2$. Intuitively, tuning the parameter that leads to a Noah effect beyond $L = 1$ would automatically increase the scaling exponent of the first moment and, therefore, lead to aging and a Moses effect instead of Noah. The lower bound exists because fat tails of the increment distribution, which are described by a Noah effect, can never lead to a slowing down of the process.

In this work, we will assume that also

$$\langle |v| \rangle \propto t^{M-1/2} \tag{45}$$

and

$$\langle v^2 \rangle \propto t^{2L+2M-2} \tag{46}$$

We address the relation between our definitions and the original time-averaged definitions of these effects, which were derived when the ensemble means could be divergent, below (subsection 3.1.2). Since the ensemble and time averaging procedures are commutative, if we know the first we can

immediately obtain the latter via

$$\begin{aligned}
\langle \overline{|\mathbf{v}|} \rangle &\rightarrow \overline{\langle |\mathbf{v}| \rangle} = (1/t) \int_0^t \langle |\mathbf{v}|(t') \rangle dt' \\
&= (Const./t) \int_0^t t'^{M-1/2} dt' \\
&= [1/(M + 1/2)] \langle |\mathbf{v}| \rangle
\end{aligned} \tag{47}$$

Since we can find $\langle \overline{v^2} \rangle$ in a similar way from its ensemble mean, this yields

$$\langle \overline{|\mathbf{v}|} \rangle = \frac{\langle |\mathbf{v}| \rangle}{M + 1/2} \quad \text{and} \quad \langle \overline{v^2} \rangle = \frac{\langle v^2 \rangle}{2L + 2M - 1}. \tag{48}$$

Note that Eq. (48) introduces additional limits on the possible values of M and L , for processes with finite $\langle |\mathbf{v}| \rangle$ and $\langle v^2 \rangle$, since the ratio between the time and ensemble averages here has to be positive. These limits are consistent with our results for the Lévy walk model.

We define the Joseph exponent also in the spirit of the discrete case, via the scaling of the integral

$$\int_0^{\tilde{\Delta}} d\Delta' \langle \mathbf{v}(t) \mathbf{v}(t + \Delta') \rangle / \langle v^2 \rangle \propto \tilde{\Delta}^{2J-1} \tag{49}$$

for large $\tilde{\Delta}$. Here again, $\tilde{\Delta}$ should not be confused with Δ , which is the time duration from which we defined \mathbf{v} . In this project we only focus on the case where

$$1/2 \leq J \leq 1, \tag{50}$$

see Appen. A.1 for more explanation. Taking the derivative of the integral with respect to $\tilde{\Delta}$, the autocorrelation function is

$$f(\tilde{\Delta}) \equiv \frac{\langle \mathbf{v}(t) \mathbf{v}(t + \tilde{\Delta}) \rangle}{\langle v^2(t) \rangle} \propto \tilde{\Delta}^{2J-2}, \tag{51}$$

at $\tilde{\Delta} \gg 1$. For small $\tilde{\Delta}$, we define $f(\tilde{\Delta}) \equiv f_<(\tilde{\Delta})$, where $f_<$ insures that the autocorrelation function is regularized at $\tilde{\Delta} \rightarrow 0$. Note that in data analysis there are several known methods

to obtain the Joseph exponent without directly calculating the autocorrelation function. These methods have various advantages and disadvantages in practice, see subsection 3.5 and Appen. A.2 and A.3.

We note that by dividing δx_j by Δ and defining the three effects via the mean increment velocity v , we did not limit the generality of the definitions at all. We did not at this point take the limit $\Delta \rightarrow 0$; hence, we do not require the instantaneous velocity to be defined. In any process, one can discuss average velocities and increments of a finite-time duration interchangeably.

3.1.1 Relation between M, L, J and H

Let $v \equiv 0$, using Eq. (51) and the Green-Kubo relation [161], the MSD of the process can be written as

$$\begin{aligned}
\langle x^2 \rangle &= 2 \int_0^t d\tilde{\Delta} \int_0^{t-\tilde{\Delta}} dt' \langle v(t') v(t' + \tilde{\Delta}) \rangle \\
&\propto 2 \int_1^t d\tilde{\Delta} \int_0^{t-\tilde{\Delta}} dt' \langle v^2(t') \rangle \tilde{\Delta}^{2J-2} + 2 \int_0^1 d\tilde{\Delta} f_{<}(\tilde{\Delta}) \int_0^t \langle v^2(t') \rangle dt' \\
&\propto 2 \int_1^t d\tilde{\Delta} \tilde{\Delta}^{2J-2} \int_0^{t-\tilde{\Delta}} dt' t'^{2L+2M-2} + c_{<} t^{2L+2M-1} \\
&\propto \frac{2}{2L+2M-1} \int_1^t d\tilde{\Delta} \tilde{\Delta}^{2J-2} (t-\tilde{\Delta})^{2L+2M-1} + c_{<} t^{2L+2M-1} \\
&\quad \underbrace{\sim}_{u \leftrightarrow \tilde{\Delta}/t} \frac{2t^{2L+2M+2J-2}}{2L+2M-1} \int_0^1 du u^{2J-2} (1-u)^{2L+2M-1} \\
&\quad t \rightarrow \infty \\
&\propto t^{2L+2M+2J-2}, \quad \text{when } J > 1/2.
\end{aligned}$$

In Eq. (52), $c_{<}$ is a constant, and in the last step note that since the term $\propto t^{2M+2L-1}$ is subdominant with respect to the other when $J > 1/2$, we neglected it in the long-time limit. Using Eq. (35), this yields

$$H = J + L + M - 1. \quad (52)$$

The relation in Eq. (52) was previously shown to hold empirically in several models in [54, 163]. It was conjectured to be broadly valid, even for systems beyond the case we study here, particularly when ensemble averages diverge and the Moses and Noah effects are only quantified via their original time-averaged definitions. However, a rigorous derivation in other cases is still needed. For more details see Appen. A.1.

3.1.2 Scaling Shapes of the Increment Distribution

Considering ensemble averages allows us to obtain additional insight about the meaning of the Moses and Noah effects. Assume that $\langle |v| \rangle$ and $\langle v^2 \rangle$ are not divergent. Let $P_t(v)$ be the PDF of finding an increment velocity v at time t , given that the process started at rest at $t = 0$. This increment PDF is said to have a single scaling shape, if for any x and t it can be described by a time-independent function $W(z_\beta)$, such $W(z_\beta) = t^\beta P(v/t^\beta)$ and $z_\beta = v/t^\beta$. In our case, we do not restrict $P_t(v)$ to only one such scaling regime, and it can have two different scaling shapes in its bulk and the tails, a situation not uncommon in anomalous diffusion which is associated with multifractality, see e.g., [6, 51, 83, 109, 179, 197]. If both the mean of $|v|$ and v^2 are taken from the same scaling regime of $P_t(v)$, then in this regime

$$\lim_{t \rightarrow \infty} t^{\alpha+\beta} P_t(v/t^\beta) \rightarrow W(z_\beta), \quad \text{where } z_\beta = v/t^\beta, \quad (53)$$

and

$$L = \alpha/2 + 1/2, \quad M = \beta - \alpha + 1/2$$

(equivalently: $\alpha = 2L - 1, \quad \beta = M + 2L - 3/2$).

(54)

Notice that since $1/2 \leq L \leq 1$, Eq. (44), then $0 \leq \alpha \leq 1$. The limit function $W(z_\beta)$ is responsible for the mean of $|v|$ and $\langle v^2 \rangle$ via

$$\langle |v|^q \rangle = 2 \int_0^\infty dv |v|^q P_t(v) \underbrace{\approx}_{t \gg 1} 2t^{q\beta-\alpha} \int_0^\infty dz_\beta |z_\beta|^q W(z_\beta), \quad (55)$$

for $q = 1, 2$.

When M, L are such that both α and β are zero, the increment PDF has a stationary asymptotic (equilibrium) state. Coincidentally, this occurs only when $M = L = 1/2$, which, as mentioned, means that the time-series satisfies at least two of the Gaussian CLT conditions. Curiously, M can also be half if $\alpha = \beta \neq 0$. When $P_t(v)$ is non-stationary, we always have a Moses effect. The PDF has a normalized scaling shape, when $\alpha = 0$ but $\beta \neq 0$, namely $L = 1/2, M \neq 1/2$. This is the onset of a “pure” Moses effect. Now, the exponent M tells us how to re-scale the PDF in order to find the invariant limit, since

$$P_t(v) \sim t^{1/2-M} W(v/t^{-1/2+M}) \quad (56)$$

According to Eqs. (53,55), if we define $\langle |z_\beta|^q \rangle_W \equiv \int_0^\infty |z_\beta|^q W(z_\beta) dz_\beta$ for $q = 1, 2$, then $\langle |v|^q \rangle = 2t^{q(1/2-M)} \langle |z_\beta|^q \rangle_W$. Note that usually, based on intuition taken from Gaussian processes, there is a tendency to vaguely associate the Hurst exponent H , with the “self-similarity” property of the process. However in anomalous diffusion that is not necessarily the case; one example is when the MSD is diverging, e.g., in Lévy flight, another example is the case of multifractality [51]. In our case, it is β , not H , that may describe this property, from the point of view of the increment PDF.

The onset of a Noah effect means that v^2 becomes non-integrable with respect to the scaling function which gives the shape of the $P_t(v)$ in the bulk. In the paradigmatic example for this effect, Lévy flight [139], the PDF $P_t(v)$ can be e.g., a stationary symmetric Lévy distribution $l_{\xi,1,0}(v)$, with $0 < \xi < 2$, defined as the inverse-Laplace transform of $\exp(-|u|^\xi)$, from $u \rightarrow v$ [111]. In this case, by definition, there is no Moses effect, and the Noah effect rises since $\int_{-\infty}^\infty v^2 l_{\xi,1,0}(v) dv \rightarrow \infty$, though of-course, here it can only be quantified by the original definition of L , namely via the time-average of the squared increments of single time-series [139]. If the increment PDF would

have e.g., the scaling shape

$$P_t(v) \sim t^{-1/\xi} l_{\xi,1,0}(v/t^{1/\xi}) \quad (57)$$

we would find both a Moses effect, and a Noah effect which is still characterized via the time average.

A more involved scenario that can occur, is when the large fluctuations of the system are reduced such that $\langle v^2 \rangle$ is not strictly infinity, but is increasing with time as in Eq. (43), because at its tails the PDF $P_t(v)$ is scaled differently in time with respect to the bulk. Now, the definitions in Eqs. (42,43) are valid. The Noah effect will now appear if the function which describes the asymptotic shape of $P_t(v)$ at the bulk is fat-tailed (in the sense that its variance is infinite), but the mean $\langle v^2 \rangle$ will be given by a second scaling function to which $P_t(v)$ convergence at the tails. If it happens that the mean of $|v|$ and v^2 are obtained from different scaling regimes, then again Eq. (53) and Eq. (54) are not valid, but one can use methods such as estimating fractional moments [6, 83, 179] to find the various scaling shapes of $P_t(v)$. If both $\langle |v| \rangle$ and $\langle v^2 \rangle$ correspond to the second scaling function (that describes the large fluctuations), and are proportional to $t^{M-1/2}$ and $t^{2M+2L-2}$ respectively, then Eq. (53) is valid. But in this case, $W(z_\beta)$ which denotes these moments might not be normalizable, namely $\int_0^\infty W(z_\beta) dz_\beta \rightarrow \infty$. Here, α and the Latent exponent L serves as a measure of *how far* the increment PDF is from having a normalized limit shape. When $\alpha > 0$ and $\beta = 0$, equivalently $L > 1/2$ and

$$M = \frac{3}{2} - 2L, \quad (58)$$

$W(z_\beta)$ is an infinite-invariant density, a type of quasi-equilibrium state, see e.g., [3, 7, 10, 113, 123, 188]. The relation in Eq. (58), if observed in data, can in-fact be used to indicate that the underlying process has an infinite-invariant density in this regime, and it was also observed in the Pommeau-Manneville map [162]. If $\alpha > 0$ and $\beta \neq 0$, or equivalently $L > 1/2$ and $M \neq$ [Eq. (58)], the limit shape of the increment PDF is given by an infinite-covariant density, see e.g., [2, 5, 6, 97, 109, 133, 179, 225].

α	β	L, M	$\lim_{t \rightarrow \infty} t^{\alpha+\beta} P(\mathbf{v}/t^\beta)$
0	0	$\frac{1}{2}, \frac{1}{2}$	steady-state
0	$\beta \neq 0$	$\frac{1}{2}, M > \frac{1}{2}$	normalized scaling limit
$\alpha > 0$	0	$L > \frac{1}{2}, M < \frac{1}{2}$	infinite-invariant density
$\alpha > 0$	$\beta \neq 0$	$L > \frac{1}{2}, (all)$	infinite-covariant density

Table 2: Summary of the different scaling limit of $P_t(\mathbf{v})$, that can be found from the Moses M and Latent L exponents.

Note that, in both the invariant and the covariant case, and also in the case when the mean-absolute and mean-squared increments are non-divergent, but they correspond to different scaling regimes of the PDF, a Noah effect cannot appear without a Moses effect. The different cases for M, L and α, β are summarized in Table 2. The table gives a summary of the different scaling limit of $P_t(\mathbf{v})$, that can be found from the Moses M and Latent L exponents, via α, β Eqs. (53,54), if both $\langle |v| \rangle$ and $\langle v^2 \rangle$ correspond to the same scaling regimes of the PDF. Note that α, β set the restrictions for M, L in the various regimes, not the other way around.

3.2 The Lévy Walk Model

As mentioned in the introduction, in this work we analyse a two-state Lévy walk model. Particularly, here, we consider a continuous range of IID random step velocities, whose distribution is $\phi(V)$. In addition, we assume a nonlinear coupling between the i th step duration and the step velocity, namely

$$V_i = \pm \tilde{c}_1 \tau_i^{\nu-1}, \quad (59)$$

where

$$\nu > 0. \quad (60)$$

The sign of the step velocity is randomly chosen to be positive or negative with equal probability (the motion is unbiased). The constant \tilde{c}_1 has units of $distance/(time)^\nu$, but throughout this

manuscript we set $\tilde{c}_1 = 1$ for convenience. Eq. (59) means that

$$\phi(V) = \frac{1}{2} \int_0^\infty d\tau g(\tau) [\delta(V - \tau^{\nu-1}) + \delta(V + \tau^{\nu-1})]. \quad (61)$$

Below, in our numerical simulations, we will use a specific example where the IID random step durations are obtained from the distribution

$$g(\tau) = \gamma \tau_0^\gamma \tau^{-1-\gamma} \Theta(\tau \geq \tau_0), \quad (62)$$

though our results are more general (see the discussion, subsection 3.7). Here, $\tau_0 > 0$ can be as small as we wish, and $\Theta(\cdot) \equiv 1$ when the condition inside the brackets is satisfied and zero otherwise. For any $g(\tau)$ in Eq. (36), from Eqs. (59,61), when $|V| < 1$ one finds that

$$\phi(V) \sim \frac{c}{2(1-\nu)|\Gamma(-\gamma)|} |V|^{-1-\gamma/(\nu-1)}. \quad (63)$$

For our example, from Eq. (62) it follows that the step velocity distribution in the first $N - 1$ complete steps, when $\nu < 1$, is

$$\phi(V) = \frac{\gamma \tau_0^\gamma}{2(1-\nu)} |V|^{-\frac{\gamma}{\nu-1}-1} \Theta(|V| \leq \tau_0^{\nu-1}), \quad (64)$$

and it has a similar shape but with $\Theta(|V| \geq \tau_0^{\nu-1})$ replacing the original one when $\nu > 1$, hence $c = \gamma \tau_0^\gamma |\Gamma(-\gamma)|$. In this chapter we focus on the parameter regime

$$0 < \gamma < 1, \quad (65)$$

where $\langle \tau \rangle$ is divergent. In various models of non-linearly coupled Lévy walk, some of them are summarized in the review [237], it was shown that in addition to the various scaling exponents, the statistical properties of the process depend strongly on the treatment given to the last, incomplete, step in the sequence. We choose to correspond with the model studied in [15, 10, 35], where V_N

is determined from the time interval straddling t [224]. With this choice, all the velocities V_i , with $i = 1..N$ are IID, though the duration of the last step is given by Eq. (37). As usual, the displacement at each step (complete and incomplete) is the linear product of the step velocity and its duration.

Instantaneous velocity PDF. Akimoto et al. [10], studied the instantaneous velocity PDF $P_t(v)$ of the Lévy walker in the process described above, at time $t \gg 1$ and the regime where $0 < \nu < 1$. We can apply their results to our analysis, since in this model we can associate \mathbf{v} and v via $v = \lim_{\Delta \rightarrow 0} \mathbf{v}$, see subsection 3.4. The following analytic results are brought from that referenced paper. At long but finite times, $P_t(v)$ assumes different shapes in two separate ranges of v : Let $v_c = t^{\nu-1}$, then [10]

$$P_t(v) \approx \begin{cases} \frac{t^\gamma}{2(1-\nu)|\Gamma(-\gamma)|\Gamma(1+\gamma)} |v|^{-1-\gamma/(\nu-1)}, & |v|/v_c \leq 1 \\ \frac{1-[1-(v/v_c)^{1/(\nu-1)}]^\gamma}{c\Gamma(\gamma+1)} t^\gamma \phi(v), & |v|/v_c > 1. \end{cases} \quad (66)$$

In the fig. 6, the red dots correspond to the total time $t = 10^4$, the green for $t = 10^5$, the blue for $t = 10^6$ and the black $t = 10^8$ (a) gives the result in the integrable regime, subsection 3.4.2, with $\gamma = 0.5$ and $\nu = 0.875$, (b) the middle regime, subsection 3.4.3, with $\gamma = 0.5$ and $\nu = 0.625$, and (c) the non-integrable regime, subsection 3.4.4, with $\gamma = 0.5$ and $\nu = 0.375$. The simulation results were generated with 10^8 realizations and $\tau_0 = 0.01$. The figure shows that the transition point for increasing values of t shifts to the left which means that the support of the region when $v < v_c$ which is denoted by the horizontal straight lines drops to zero. The region when $v > v_c$ does not disappear for times $t \rightarrow \infty$ which is denoted in the figure by slant lines.

Due to the asymptotic shape of $\phi(v)$, when v itself is smaller than unity (regardless of t), $P_t(v/t^{\nu-1})$ corresponds in this regime to the scaling function $\sim t^{(\nu-1)}\rho(\tilde{v})$, where $\tilde{v} = v/t^{\nu-1}$ and

$$\rho(\tilde{v}) \approx \begin{cases} \frac{1}{2(1-\nu)|\Gamma(-\gamma)|\Gamma(1+\gamma)} |\tilde{v}|^{-1-\gamma/(\nu-1)}, & |\tilde{v}| \leq 1 \\ \frac{1-[1-(\tilde{v})^{1/(\nu-1)}]^\gamma}{2(1-\nu)|\Gamma(-\gamma)|\Gamma(\gamma+1)} |\tilde{v}|^{-1-\gamma/(\nu-1)}, & |\tilde{v}| > 1. \end{cases} \quad (67)$$

The scaling function $\rho(\tilde{v})$ is normalized to unity. On the other hand, at long times $P_t(v)$ has a second scaling shape valid in the region $v > v_c$, since in the limit $t \rightarrow \infty$ the support of the region $v/v_c < 1$ in Eq. (66) goes to zero, and at $v/v_c \gg 1$, we can expand $[1 - (v/v_c)^{1/(\nu-1)}]^\gamma$ as a Taylor series for the small parameter $(v/v_c)^{1/(\nu-1)}$. This yields, to leading order in time,

$$P_t(v) \approx \phi(v)|v|^{\frac{1}{\nu-1}} \frac{t^{\gamma-1}}{c\Gamma(\gamma)}. \quad (68)$$

Asymptotically [10] eq. (68) can be written as,

$$\lim_{t \rightarrow \infty} t^{1-\gamma} P_t(v) \rightarrow \mathcal{I}(v), \text{ where } \mathcal{I}(v) \equiv \phi(v)|v|^{\frac{1}{\nu-1}} \frac{1}{c\Gamma(\gamma)}, \quad (69)$$

and $\phi(v)$ is in Eq. (64). The time-invariant asymptotic limit given by $\mathcal{I}(v)$ in Eq. (69) is non-integrable around $v = 0$, hence it is non-normalizable:

$$\int_{-\infty}^{\infty} \mathcal{I}(v) dv \rightarrow \infty. \quad (70)$$

As such, this function is the infinite-invariant density of the process [10]. Note that when $\nu > 1$, the two regimes of the PDF, Eq. (66) simply switch places, but their functional shape remains the same.

3.3 Summary of Main Results

This summary brings the main results of our analysis of Lévy walk trajectories generated by the process described in subsection 3.2, and the detailed derivations appear below. For further discussion about the generality of the three-effect decomposition, also see below. Our simulations generated an ensemble of 10^8 realizations of the process $x(t)$ for different values of γ and ν . We observed the increments δx_j of the paths at different times ranging from $t = 10^4$ to 10^8 . We then measured the ensemble averages of $|\delta x_j|$, δx_j^2 (namely, we used v with observation windows of duration $\Delta = 1$), as well as x^2 , to calculate the values of M , L and H respectively. To obtain the

value of the exponent J , we used a method based on the time-averaged MSD δ^2 , as explained in detail in subsection 3.5 and Appen. A.2. This method's results correspond to those of a direct measurement of the correlation function, but it is numerically more convenient (see Appen. A.2).

What the data analysis says: **Without** relying on prior knowledge about the underlying process, we found that in the range defined by Eqs. (60,65), the Lévy walk data exhibits five separate dynamical phases. These phases are summed up above and in Fig. 7. The three solid lines in the figure 7, separating regions *A-B*, *B-C* and *C-D* are respectively: $\nu = \gamma/2 + 1/2$, $\nu = \gamma$ and $\nu = \gamma/2$. The dashed-line is $\nu = \gamma/2 + 1$. The results for the three-effect decomposition in the various regimes are discussed in subsection 3.3. Region A: $H = \nu$, $J = 1$, $L = 1/2$, $M = \nu - 1/2$ (“maximal” Joseph effect, namely the autocorrelation function Eq. (51) does not decay at large values of Δ , no Noah, $P_t(\mathbf{v})$ has a normalized scaling shape corresponding to M). Region B: $H = \nu$, $J = (1 + 2\nu - \gamma)/2$, $L = 1 - \nu + \gamma/2$, $M = \nu - 1/2$ (onset of a Noah effect). Region C: $H = \nu$, $J = (1 + 2\nu - \gamma)/2$, $L = 1 - \gamma/2$, $M = \gamma - 1/2$ ($P_t(\mathbf{v}) \rightarrow$ infinite-invariant density). Region D: $H = \gamma/2$, $J = 1/2$, $L = 1 - \gamma/2$, $M = \gamma - 1/2$ (infinite-invariant density, no Joseph effect). In the “ ∞ ” regime, $H \rightarrow \infty$, and M, L, J are not well defined. The summation formula, Eq. (52) is confirmed in all but the “ ∞ ” regime.

- In regime A, when $\gamma/2 + 1/2 < \nu < \gamma/2 + 1$: $H = \nu$, $J = 1$, $L = 1/2$, $M = \nu - 1/2$. Here, the auto-correlation function does not decay with $\tilde{\Delta}$, in Eq. (51), namely the increments are essentially completely correlated. In this situation, we say that the Joseph effect is maximal, since by definition J can never be bigger than its value here. There is no freedom left in the increment distribution for any Noah effect to be present. There can be, however, a Moses effect as the increment distribution does “age” with time. The existence of a Moses effect without a Noah effect means that in this regime, we expect a single scaling function in the form of $t^{\nu-1}P_t(\mathbf{v}/t^{\nu-1})$ to describe the regime of the PDF, which gives rise to the first and second moments of $|\mathbf{v}|$ (which is, therefore, no-fat tailed). Our numerics show that this regime extends also to the range $1 < \nu < \gamma/2 + 1$ (and $\gamma < 1$).

- In regime B, $\gamma < \nu < \gamma/2 + 1/2$: $H = \nu$, $J = (1 + 2\nu - \gamma)/2$, $L = 1 - \nu + \gamma/2$, $M = \nu - 1/2$. In this regime all the three effects contribute to the anomalous diffusion. Here, the Joseph effect is present but is not maximal, as the auto-correlation function decays as a power-law function of $\tilde{\Delta}$. This allows for a Noah effect to be present too. Here, the Noah effect means that the scaling shape at the bulk of $P_t(v)$ is fat-tailed, in the sense that its second moment is divergent. But the mean of $|v|$ remains unchanged from regime A, so it is expected to still be given by the same scaling regime of the increment PDF as before, namely $\langle |v| \rangle$ and $\langle v^2 \rangle$ correspond to different regimes of $P_t(v)$. Accordingly, our numerical analysis shows that Eq. (53) is not valid in this case. The Moses effect occurs here in a similar way as it does in regime A, namely also in this regime, the increment PDF is not time-invariant.
- In regime C, $\gamma/2 < \nu < \gamma$: $H = \nu$, $J = (1 + 2\nu - \gamma)/2$, $L = 1 - \gamma/2$, $M = \gamma - 1/2$. Still, all three effects contribute to the anomalous diffusion. Here, just as in regime B, the Joseph effect is present, but is not maximal. In this regime, the Moses and Noah effects are coupled, with the Moses and the Latent exponents obeying Eq. (58). This suggests that the large fluctuations of the system are described by an infinite-invariant density, Eq. (53) with $\alpha = 1 - \gamma, \beta = 0$.
- In regime D, $\nu < \gamma/2$: $H = \gamma/2$, $J = 1/2$, $L = 1 - \gamma/2$, $M = \gamma - 1/2$. Here, M, L remain coupled as in region C. Hence we expect the same infinite-invariant density to be valid in this regime too. Interestingly, now there are no long-range increment correlations and, thus, there is no Joseph effect. At this stage anomalous diffusion occurs due to the non-stationarity of $P_t(v)$ and the fat tails of the scaling-shape describing this PDF at the bulk.
- When $\nu > \gamma/2 + 1$, the MSD is divergent. The scaling relations in Eqs. (43-51) don't hold, and in this regime the decomposition is not valid. We call this the “ ∞ ” regime. See Appen. A.5.

The figure 9 shows the phase diagrams of the scaling exponents where (a) gives the Moses exponent M that quantifies the Moses effect, (b) gives the Latent exponent L that quantifies the Noah effect, (c) gives the Joseph exponent J that quantifies the Joseph effect, and (d) gives the

Hurst exponent H . These results were obtained with for $\eta = 1$ (see subsection 3.6). In the “ ∞ ” regime, the Hurst exponent is divergent and the other exponents are not well defined, see subsection 3.6 and Appen.A.5

What we know from the model, in comparison with the data analysis: When $\gamma, \nu < 1$, Eq. (67) and Eq. (69) describe two different ways to obtain a time-invariant scaling-shape of the instantaneous velocity PDF $P_t(v)$, the first is valid for small v and the second for large. We can associate this velocity PDF with the distribution of the increment velocity (see subsection 3.4). As expected from the numerics, the analytic results presented in subsection 3.4 show that the bulk function and the infinite-invariant density describe the shape of the increment PDF in regimes A and C, D respectively, in the range of v which is responsible for the various moments. In regime B, $\langle |v| \rangle, \langle v^2 \rangle$, (hence $\langle |v| \rangle, \langle v^2 \rangle$) are obtained separately from the two scaling regimes. The fact that the Joseph effect, studied in subsection 3.5, is “maximal” in regime A matches the fact that the bulk limit-function describing the PDF is thin-tailed, for the same reason that in regime D, it is “minimal”: if the increments are long- (short-) ranged correlated; their size is more (less) predictable from the first step. Therefore, large fluctuations are less (more) possible.

In regime A, when $\nu > 1$, it is easy to show that one can find similar results for $\langle |v| \rangle$ and $\langle v^2 \rangle$ as in the case when $\nu < 1$ since as mentioned, the shape of $P_t(v)$ is similar to Eq. (66), but with the two regimes for $v \leq 1$ and $v > 1$ switching roles. In addition, here $\tau_0^{\nu-1}$ becomes a lower, instead of an upper cutoff for the step velocity PDF in Eq. (64). The divergence of the MSD in the “ ∞ ” regime, was shown analytically in [15, 35], further details in subsection 3.6 and Appen. A.5.

3.4 Calculation of Latent exponent L and Moses exponent M

As explained in subsection 3.1, in order to obtain M and L , we need to examine the temporal behavior of the ensemble-time averages $\langle |\bar{v}| \rangle$ and $\langle \bar{v}^2 \rangle$, where \bar{v} is the mean velocity obtained at increments δx , whose duration Δ is defined independently from step duration of the underlying Lévy walk (namely $\Delta \neq \tau$). Choosing $\Delta \ll 1$, the mean velocity \bar{v} can be exchanged with the instantaneous velocity v of the random walker at various points in time, and then we can replace

$v \leftrightarrow v$ in Eqs.(42-43). Accordingly, this means that we can obtain the exponents of the time series from $\langle |v| \rangle$ and $\langle |v|^2 \rangle$, where we now use the following definition for the time average of an observable f : $\bar{f} = (1/t) \int_0^t f(t') dt'$. We note that here one should use a bit of care, since during an increment of duration Δ , the particle might have ended one step of the underlying random walk, and started another, and in this interval of the motion the mean velocity is different from the instantaneous value before/ after the transition. However we assume that if Δ is small enough, the effect of these occurrences is negligible in the context of the results in this manuscript. This is also confirmed by our numerics.

3.4.1 Three Regimes for M and L

One can obtain the long-time asymptotic behavior of the ensemble mean of any symmetric observable $\mathcal{O}(v)$ in the system, as follows:

$$\begin{aligned} \langle \mathcal{O}(v) \rangle &= 2 \int_0^\infty \mathcal{O}(v) P_t(v) dv \\ &= 2 \int_0^{v_c} \mathcal{O}(v) P_t(v) dv + 2 \int_{v_c}^\infty \mathcal{O}(v) P_t(v) dv. \end{aligned} \quad (71)$$

Given Eqs. (64,66), for the mean of $|v|$, we get

$$\begin{aligned} \langle |v| \rangle &\approx 2 \int_0^{v_c} \frac{1}{2(1-\nu)|\Gamma(-\gamma)|\Gamma(1+\gamma)} t^\gamma |v|^{-\frac{\gamma}{\nu-1}} dv \\ &\quad + 2 \int_{v_c}^{\tau_0^{\nu-1}} \frac{1 - [1 - (v/v_c)^{1/(\nu-1)}]^\gamma}{2(1-\nu)|\Gamma(-\gamma)|\Gamma(\gamma+1)} t^\gamma |v|^{-\frac{\gamma}{\nu-1}} dv \\ &\approx -\frac{\Gamma(-\gamma + \nu - 1)t^{\nu-1}}{|\Gamma(-\gamma)|\Gamma(\nu)} + \frac{\tau_0^{\nu-\gamma} t^{\gamma-1}}{|\Gamma(-\gamma)|\Gamma(\gamma)(\gamma - \nu)}. \end{aligned} \quad (72)$$

Similarly, for the mean of v^2 , we get

$$\begin{aligned}
\langle v^2 \rangle &\approx 2 \int_0^{v_c} \frac{t^\gamma}{2(1-\nu)|\Gamma(-\gamma)|\Gamma(1+\gamma)} |v|^{1-\frac{\gamma}{\nu-1}} dv \\
&+ 2 \int_{v_c}^{\tau_0^{\nu-1}} \frac{1 - [1 - (v/v_c)^{1/(\nu-1)}]^\gamma}{2(1-\nu)|\Gamma(-\gamma)|\Gamma(\gamma+1)} t^\gamma |v|^{1-\frac{\gamma}{\nu-1}} dv \\
&\approx -\frac{\Gamma(-\gamma+2\nu-2)t^{2\nu-2}}{\Gamma(2\nu-1)|\Gamma(-\gamma)|} + \frac{\tau_0^{-\gamma+2\nu-1}t^{\gamma-1}}{(\gamma-2\nu+1)\Gamma(\gamma)|\Gamma(-\gamma)|}.
\end{aligned} \tag{73}$$

To determine the leading behavior of these two means in the long time limit, note that Eqs. (67,69) create a distinction between two different cases, depending on whether $\mathcal{O}(v) = |v|$ or v^2 is integrable with respect to $\rho(v)$, Eq. (67), or it is integrable with respect to the infinite-invariant density $\mathcal{I}(v)$, Eq. (69). In the first case, the leading order is obtained by first changing variables: $v/t^{\nu-1} \rightarrow \tilde{v}$

$$\langle \mathcal{O}(v) \rangle = 2t^{q(\nu-1)} \int_0^{1/t^{\nu-1}} \mathcal{O}(\tilde{v})\rho(\tilde{v}) d\tilde{v} + 2t^{q(\nu-1)} \int_{1/t^{\nu-1}}^\infty \mathcal{O}(\tilde{v})P_t(\tilde{v}t^{\nu-1}) d\tilde{v}, \tag{74}$$

and then in the range $t \gg 1$ the first term is $\approx 2t^{q(\nu-1)} \int_0^\infty \mathcal{O}(\tilde{v})\rho(\tilde{v}) d\tilde{v}$ and the second term approaches zero since its support vanishes. So, in this case

$$\langle \mathcal{O}(v) \rangle \approx 2t^{q(\nu-1)} \int_0^\infty \mathcal{O}(\tilde{v})\rho(\tilde{v}) d\tilde{v}. \tag{75}$$

In the second case, when $\langle \mathcal{O}(v) \rangle_I \equiv \int_0^\infty \mathcal{O}(v)\mathcal{I}(v)v < \infty$, $\mathcal{O}(v)$ is integrable with respect to the infinite-invariant density, the contribution to its mean from the region $v < v_c$ can be neglected in Eq. (71) in the limit $t \rightarrow \infty$, to leading order, hence using Eq. (69) we get

$$\langle \mathcal{O}(v) \rangle \approx 2 \int_{v_c \rightarrow 0}^\infty \mathcal{O}(v)P_t(v) dv \xrightarrow[t \rightarrow \infty]{} 2t^{\gamma-1} \langle \mathcal{O}(v) \rangle_I. \tag{76}$$

Notice that in this case, the temporal scaling of $\langle \mathcal{O}(v) \rangle$ is similar for all the integrable observables since it is determined only by the scaling of the infinite-density. For $\mathcal{O}(v) = \langle |v| \rangle$ and $\langle v^2 \rangle$ together, there are three regimes of behavior, included within the range $\gamma, \nu < 1$: The integrable regime, where both $\langle |v| \rangle$ and $\langle v^2 \rangle$ are integrable with respect to $\rho(v)$; the middle regime, where only the

mean-absolute velocity is integrable; and the non-integrable regime, where neither observable is integrable (details below). In the figures 8, red dots and the blue diamonds represent the values of $\langle |v| \rangle$ and $\langle v^2 \rangle$, obtained from simulated data for different values of t , respectively. The solid green and black lines correspond to Eq. (72) and Eq. (73) respectively. The yellow and the magenta dashed lines represent the leading order terms in these equations, in the long time limit. (a) gives the result in the integrable regime, Sec. 3.4.2, with $\gamma = 0.5$ and $\nu = 0.875$, (b) the middle regime, Sec. 3.4.3, with $\gamma = 0.5$ and $\nu = 0.625$, and (c) the non-integrable regime, Sec. 3.4.4, with $\gamma = 0.5$ and $\nu = 0.375$. The simulation results were generated with 10^8 realizations and $\tau_c = 0.01$. Figs. 8 a-c display simulation results for the temporal behaviour of $\langle |v| \rangle$ and $\langle v^2 \rangle$ in the integrable, the middle and the non-integrable regimes, respectively. The simulations match perfectly at long times with the exact expressions in Eqs. (72,73), which denote both the leading order behavior of $\langle |v| \rangle$ and $\langle v^2 \rangle$ in time and the next-to-leading order. They also confirm the approach to the leading order asymptotic results, though this approach is slow. The results for the exponents M and L in the various regimes are shown in the lower two panels of Fig. 9.

In figures 10, 11 and 12, we use the results for these exponents in the three regimes to seek for a time-invariant asymptotic shape of $P_t(v)$, based on Eqs. (53,54). The quantification of the Moses and Noah effects based on Eqs. (53,55) are seen in these figures. From Eq. (55): $\alpha = 2L - 1$ and $\beta = M + \alpha - 0.5$. The log-log plots in figures 10, 11 and 12, in symbols, we see the rescaled PDF $t^{\alpha+\beta} P_t(v)$, obtained from simulation results of $3 * 10^8$ paths, in regimes A, B and D respectively (in regime C the shape of the PDF behaves similar to the last, at increasing times). The measurements were performed at times $t = 10^4$ (red dots), 10^5 (green dots), 10^6 (blue dots) and 10^7 (black dots). In figure 10, $\gamma = 0.5$, $\nu = 0.875$, leading to $L = 0.5$, and $M = 0.375$. The figure shows that the simulation results converge at increasing times to the normalized scaling shape given in Eq. (67) (solid mustard line). In figure 11, $\gamma = 0.5$, $\nu = 0.625$, and $L = 0.625$, $M = 0.125$. Attempting to find an asymptotic scaling shape in this regime, which corresponds to Eq. (53), does not work, since $\langle |v| \rangle$ and $\langle v^2 \rangle$ do not correspond to a single scaling regime of $P_t(v)$. In figure 12, $\gamma = 0.5$, $\nu = 0.375$, and $L = 0.75$, $M = 0$. M and L here obey the scaling relation in Eq. (58), hence we expect to

find that the increment PDF approaches the shape of a non-normalizable infinite-invariant density. This is confirmed by the solid mustard line, that represents Eq. (69). The insets for figures 10, 11 and 12 show the same results, but in semi-log plots.

3.4.2 The Integrable Regime, $1/2 + \gamma/2 < \nu < 1$

In this regime, the leading behavior in time of $\langle |v| \rangle$ and $\langle v^2 \rangle$ is given by the $\sim t^{\nu-1}$ and $\sim t^{2\nu-2}$ terms in Eq. (72) and Eq. (73), respectively. The second term in both equations gives the next-to-leading order behavior. This result agrees with the calculation based on Eq. (75). Similar to the argument in Eq. (48), the ensemble-time averages $\langle \overline{|v|} \rangle \propto t^{\nu-1}$ and $\langle \overline{v^2} \rangle \propto t^{2\nu-2}$, like their corresponding ensemble averages, and since we associate v with \mathfrak{v} , we now obtain the Latent and Moses exponents using Eqs. (42,43):

$$M = \nu - \frac{1}{2}, \quad \text{and} \quad L = \frac{1}{2}. \quad (77)$$

Since here both means are obtained from the same scaling limit of $P_t(v)$, we can now associate $\rho(\tilde{v})$ in this regime with $W(z_\beta)$, Eq. (53), and here $z_\beta = \tilde{v} = v/t^{\nu-1}$, so $\beta = \nu - 1$ and $\alpha = 0$, in agreement with Eqs. (54,77). Fig. 10 displays the convergence of simulation results of $P_t(v)$ at increasing times, rescaled according to Eq. (53), as function of z_β , to the scaling limit Eq. (67). Note that the Moses effect originates from the diverging mean duration of the Lévy walk steps, namely because $\langle \tau \rangle \rightarrow \infty$ in $g(\tau)$, Eq. (62), which leads to statistical aging [79].

3.4.3 Middle Regime, $\gamma < \nu < 1/2 + \gamma/2$

In this regime, v^2 is no longer integrable with respect to the scaling function $\rho(v)$. $|v|$, however, still is. Therefore, the leading-order behavior of $\langle |v| \rangle$ and $\langle \overline{|v|} \rangle$, remains proportional to $\sim t^{\nu-1}$, similar to the previous, integrable region. However since $\langle v^2 \rangle$ is now integrable with respect to the infinite-density $\mathcal{I}(v)$ instead of $\rho(v)$, its leading behavior is now obtained from Eq. (76). The result is equal to the term $\propto t^{\gamma-1}$ in Eq. (73) (and the second term there is now the next-to-leading order

behaviour). Therefore, also $\langle \overline{v^2} \rangle \sim t^{\gamma-1}$. Note that in this regime we can obtain the time average of $v^2(t)$ also using arguments based on infinite-ergodic theory [10]. Using Eqs. (42,43), this yields

$$M = \nu - \frac{1}{2}, \quad \text{and} \quad L = \frac{\gamma - 2\nu + 2}{2}. \quad (78)$$

This regime continuously extends the one introduced in Eq. (77). The scaling shape of the PDF can still describe the first moment at the bulk. However, since the second moment of this PDF diverges with respect to $\rho(v)$, here we see for the first time the emergence of a Noah effect, in addition to Moses. Since the mean of $|v|$ and v^2 are obtained from two different scaling regimes of $P_t(v)$, Eqs. (53-55) are not valid, and α and β are not defined. Fig. 11 shows that, if we did not know the model, and try to obtain α, β from Eq. (54) in this regime from the data, we would find $\alpha = \gamma - 2\nu + 1, \beta = \gamma - \nu$, but with this rescaling, $P_t(v)$ does not converge to a time-invariant shape.

3.4.4 The Non-Integrable Regime, $\nu < \gamma$

In this regime neither the first, nor the second moment of $|v|$ are integrable with respect to $\rho(v)$, Eq. (67). Instead, both the mean velocity, and the mean squared velocity are integrable with respect to the infinite-density. Here, using Eqs. (64,69,76) we get $\langle |v| \rangle, \langle \overline{|v|} \rangle \propto t^{\gamma-1}$, as well as $\langle v^2 \rangle, \langle \overline{v^2} \rangle \propto t^{\gamma-1}$, so from Eqs. (42,43), we find

$$M = \gamma - \frac{1}{2}, \quad \text{and} \quad L = 1 - \frac{\gamma}{2}. \quad (79)$$

In this case, we associate $W(z_\beta)$, Eq. (53), now with the infinite-invariant density $\mathcal{I}(v)$, Eq. (69), and $\alpha = 2L - 1, \beta = 0$, so $z_\beta = v$. The Noah effect tells us that the asymptotic shape of the increment PDF is given by a non-normalizable function, and the relation between M and L here also agrees with Eq. (58), as it should. Fig. 12 shows how simulation results of $t^\alpha P_t(v)$ at converge increasing times to $\mathcal{I}(v)$, the infinite invariant density. As in the other regimes, here the mean duration of the Lévy walk steps in $g(\tau)$, Eq. (62) is divergent, however since ν is small, the step

velocity decays very quickly with the duration. Therefore the step displacement $\chi \sim \tau^\nu$, is almost decoupled from τ . This implies two things: First, the MSD of the process now mainly depends on how many steps the walker can have between $t' = 0$ and t , which is determined only by the value of γ . So the Hurst exponent in this regime depends only on γ . Second, by a hand-waving argument, we can see why M and L depend only γ ; because if the step displacement depends only on this parameter, the average velocity v in all the time-series increments within those steps will depend only on this parameter too.

3.5 Calculation of Joseph exponent J

The Joseph exponent depends on the shape of the auto-correlation function. However, this quantity is difficult to obtain for many systems, analytically and numerically. In practice, the Joseph effect is often quantified by designated methods, such as the so-called rescaled range statistic (R/S) [98], wavelet decomposition [4] or detrended fluctuations analysis [177]. Additional information on the correspondence between our definition of J and the latter method is given in appendix A.3.

Here, for the Lévy process, we use a measure which is easier to handle analytically; the ensemble averaged time-averaged MSD $\langle \overline{\delta^2} \rangle$, defined as

$$\langle \overline{\delta^2} \rangle \equiv \left\langle \frac{1}{t - \Delta} \int_0^{t-\Delta} [x(t_0 + \Delta) - x(t_0)]^2 dt_0 \right\rangle. \quad (80)$$

Note that Eq. (80) should not be confused with $\langle \overline{v^2} \rangle$ in Eq. (43), since in the latter the increments are strictly non-overlapping, whereas in $\langle \overline{\delta^2} \rangle$ they are. This quantity is related to the auto-correlation function, via [161]

$$\langle \overline{\delta^2} \rangle \approx \frac{2}{t} \int_0^t dt_0 \int_0^\Delta dt_2 \int_0^{t_2} dt_1 \langle v(t_1 + t_0)v(t_2 + t_0) \rangle, \quad (81)$$

when $t \gg \Delta$. The scaling of this function for different types of auto-correlations is discussed in Appen. A.2, where we also show the correspondence between $\langle \overline{\delta^2} \rangle$, the autocorrelation function, and our definition in Eq. (51). In all the cases considered in the appendix (even for $J \leq 1/2$), the

asymptotic scaling is

$$\langle \overline{\delta^2} \rangle \sim t^{2L+2M-2} \Delta^{2J}. \quad (82)$$

Our model is described by type (II) in the appendix. This means that the Joseph exponent is given by the scaling of $\langle \overline{\delta^2} \rangle$ with the lag time Δ (note, that this observation was already made in [163], however, due to a typo it was read 't' instead of '\Delta').

To obtain the Joseph exponent in various regimes, we use the results of the calculation of the ensemble-time averaged MSD, obtained for this model in Ref. [15]. Notably, in that Ref., the scaling of $\langle \overline{\delta^2} \rangle$ with respect to time and Δ was calculated for a general shape of $g(\tau)$, with an asymptotic fall-off as in Eq. (62), at large τ , and it was shown to not depend on the exact behavior at small τ s. Given this knowledge, the time-averaged MSD (for $0 < \{\gamma, \nu\} < 1$) for the Lévy walk model we study here, has the following scaling [15]

$$\langle \overline{\delta^2} \rangle \propto \begin{cases} t^{2\nu-2} \Delta^2, & \gamma/2 + 1/2 < \nu \\ t^{\gamma-1} \Delta^{1+2\nu-\gamma}, & \gamma/2 < \nu < \gamma/2 + 1/2 \\ t^{\gamma-1} \Delta, & \nu < \gamma/2 \end{cases} \quad (83)$$

Using Eq. (83) and Eq. (82), we find that

$$J = \begin{cases} 1, & \gamma/2 + 1/2 < \nu \\ (1 + 2\nu - \gamma)/2, & \gamma/2 < \nu < \gamma/2 + 1/2 \\ 1/2, & \nu < \gamma/2 \end{cases} \quad (84)$$

Note that since $\gamma < 1$, the mean step duration in all these regimes diverges. This implies that the random walker essentially walks in the same direction for almost all of the time t , regardless of how long it is. In turn, this means the process is correlated in the whole parameter regime that we study. But when $\nu < \gamma/2$, the average correlations decay rather quickly with Δ because the step velocity changes only minimal with the step duration, hence in this regime, we do not see a

Joseph effect (the difference between the mean velocity at increments belonging to the same steps of the Lévy walk, versus increments of other steps, is small). The onset of the effect is above the line $\nu = \gamma/2$. It is maximal when $J = 1$, at $\gamma + 1 < 2\nu$.

Fig. 9 c shows a phase diagram summarizing the different regimes of the Joseph effect, shown in Eq. (84). Fig. 9 d shows the different regimes of the Hurst exponents, which results from the combined effect of the various effects leading to the anomalous diffusion and calculated using Eq. (52). Our simulation results for several arbitrary samples of values of ν and γ in these regimes agree with the analytic expectation.

3.6 A Generalized Model

In this subsection, following [15, 35] we extend the model displayed above by introducing a new parameter η . This parameter generalize Eq. (59) by modifying the relation between the i th step velocity V_i , its duration τ_i and the actual time in motion t' , as follows

$$V_{\nu,\eta} = \pm \tilde{c}_1 \tau^{\nu-\eta} t'^{\eta-1}. \quad (85)$$

Some values of η correspond to special cases: The Lévy walk we studied above corresponds to $\eta = 1$, when $\eta = \nu$ we get a Drude-like model [193, 24], and when $\eta \rightarrow 0$ or $\eta \rightarrow \infty$ we approach either a jump-then-wait type of coupled continuous-time random walk, or a wait-then-jump model, respectively [35]. As we will now show, modifying this parameter changes the onset of the “ ∞ ” regime. Our simulation results suggest that when η is within the open range $(0, \infty)$, the behavior of all the effects in regimes A,B,C,D in Fig. 7 does not change, however the regimes themselves may expand or shrink and disappear.

Let’s look again at the PDF $P_t(x)$, of the particles’ displacement x at time t . Here,

$$P_t(x) = \int_{-\infty}^{\infty} dx' \int_0^t dt' A(x', t') r(x - x' | t - t'). \quad (86)$$

where $A(x', t')$ is the joint probability density to land on x' between x and $x + dx$ in a complete

step ending at $t' < t$, and $r(x - x'|t - t')$ is the conditional probability density of the displacement in the last, incomplete step given the duration of the walk is t . The following calculation of the MSD for this model is adapted from Ref. [35]. Let $\hat{f}(k, t) = \int_{-\infty}^{\infty} f(x, t) \exp(-ikx) dx$, be the Fourier transform of some function $f(x, t)$, from $x \rightarrow k$. Eqs. (87,88) and Eq. (89) below, represent the characteristic functions of the probability densities P, r and A , respectively. All the functions except for P lack normalization on unity; the zero terms of the expansions are denoted as $r_0(t) = \int r(x|t)dx \neq 1$ and $A_0(t) = \int A(x, t)dx \neq 1$. Let $x_2(t) \equiv \langle x^2(t) \rangle$ be MSD at time t , $A_2(\tau) = \int \chi^2 A(\chi, \tau) d\chi$ is the marginal second moment of displacement χ in a single complete step of duration τ and $r_2(\tau^*) \equiv \int \chi^{*2} r(\chi^*|\tau^*) d\chi^*$ is the MSD of the displacement χ^* in the last, incomplete step. The duration τ^* of the latter is defined in Eq. (37). After Fourier transform, we get

$$\hat{P}(k|t) = 1 - \frac{1}{2}k^2 x_2(t) + o(k^2) \quad (87)$$

$$\hat{r}(k|t) = r_0(t) - \frac{1}{2}k^2 r_2(t) + o(k^2) \quad (88)$$

$$\hat{A}(k|t) = A_0(t) - \frac{1}{2}k^2 A_2(t) + o(k^2) \quad (89)$$

Let $\hat{f}(k, s) = \int_0^{\infty} \hat{f}(k, t) \exp(-st) dt$ be the Laplace transform of $\hat{f}(k, t)$. In Fourier and Laplace space, from Eq. (86) we obtain

$$\hat{P}(k, s) = A_0(s)r_0(s) - \frac{k^2}{2} [A_0(s)r_2(s) + A_2(s)r_0(s)] + o(k^2) \quad (90)$$

On comparing Eq. (87) and Eq. (90), we can now obtain the MSD using

$$\langle x^2(s) \rangle = A_0(s)r_2(s) + A_2(s)r_0(s) \quad (91)$$

Calculating the values on the right-hand side of Eq. (91), and taking the inverse Laplace transform, one can now derive the MSD. Part of this calculation, performed in [35], was to obtain the second

marginal moment of the function $r(x|t)$:

$$r_2(t) \simeq \gamma \tilde{c}_1^2 \tau_0^\gamma t^{2\eta} \int_t^\infty t'^{2(\nu-\eta)-1-\gamma} dt'. \quad (92)$$

From here, we can see that r_2 , and therefore also $\langle x^2 \rangle$, can only obtain a finite value when $\gamma > 2(\nu - \eta)$. This explains the crossover to the “ ∞ ” regime, which occurs when $\nu > \gamma/2 + \eta$.

When $\nu < \gamma/2 + \eta$ and $\gamma < 1$, $2\nu < \gamma$, the MSD is [35]

$$\langle x^2(t) \rangle \approx \gamma \left[\frac{\Gamma(2\nu + 1 - \gamma)}{\Gamma(1 - \gamma)(2(\nu - \eta) - \gamma)\Gamma(2\nu + 1)} t^{2\nu} + \frac{B(2\nu + 1, \gamma - 2\nu)}{\Gamma(1 - \gamma)\Gamma(1 + \gamma)} \tilde{c}_1^2 t^\gamma \right], \quad (93)$$

where $B(a, b)$ is the Beta-function. This is dominated by the second term, since $2\nu < \gamma$, and therefore $\langle x^2(t) \rangle \propto t^\gamma$, which gives the value of the Hurst Exponent as $H = \gamma/2$, similar to what is seen in Fig. 9d. When $\nu < \gamma/2 + \eta$, but $\gamma < 1$, $2\nu > \gamma$, the MSD reads [35]

$$\langle x^2(t) \rangle \simeq \gamma \frac{\Gamma(2\nu - \gamma)}{\Gamma(2\nu + 1)\Gamma(1 - \gamma)} \frac{4\nu - 2\eta - 2\gamma}{2(\nu - \eta) - \gamma} \tilde{c}_1^2 t^{2\nu}, \quad (94)$$

which gives the value of the Hurst Exponent as $H = \nu$ also similar to Fig. 9(d). The results shown in Fig. 9 are for $\eta = 1$, whereas Eqs. (90,91) are calculated for any value of η . This shows that the power-law dependence of the mean squared displacement is independent of the exponent η and the particular value of η only enters in the prefactors, when $\langle x^2 \rangle$ is finite. When η is very small, only regime D in Fig. 7 survives, and beyond it we have the non-scaling “ ∞ ” regime. When η is very large, regime A extends higher into the realm of $\nu > 1$.

3.7 Discussion

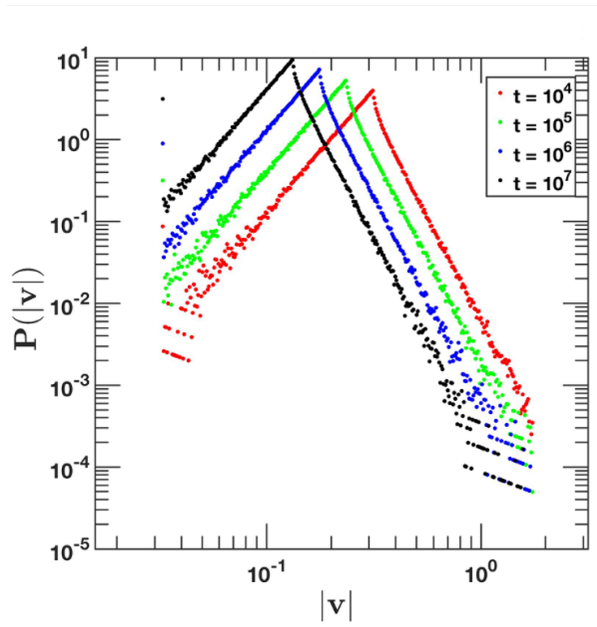
Imagine that you get hold of a “blind” set of data series, containing the positions of an ensemble of random walkers at various times in the interval $[0, t]$. A Lévy walk model generated this data, but you do not have this prior knowledge. Our analysis allows us to uncover the main features of the hidden process that cause its behavior to scale anomalously with time, even though we

do not know what process generated the data. Elucidating the origins of anomalous diffusion observed in experimental data is crucial to understand the system's underlying functioning, and it is studied therefore these days, e.g., using new advanced methods for single-particle tracing [107, 185, 222, 227]. We encourage the verification of our results, for example, in (but not limited to) future such experiments, in particular, e.g., the scaling relation in Eq. (52) and Eq. (53), and consequently its application.

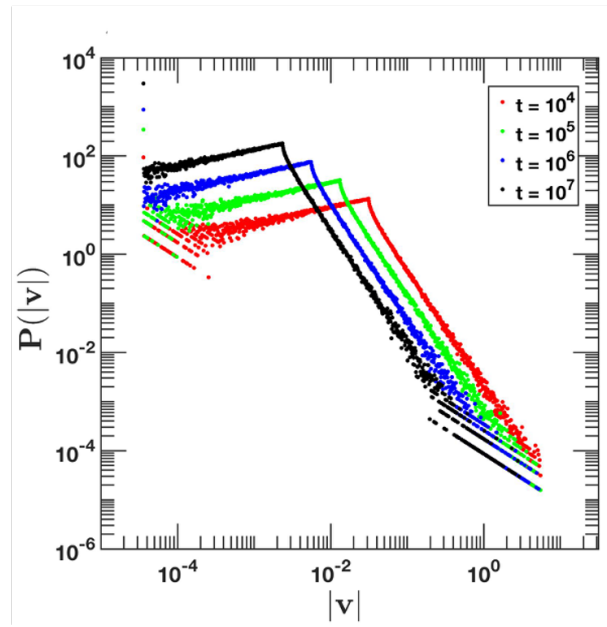
In addition to learning about the origins of the anomalous diffusion, one may use the knowledge about the Moses, Noah, and Joseph effects to extrapolate which processes can and cannot be good candidates to represent the underlying dynamics. These days, many studies use techniques such as machine learning [34, 100, 167], Bayesian statistics [215], and more, e.g., [108, 216], to try to infer the Hurst exponent or distinguish between various known models such as continuous-time random walk, fractional Brownian motion, and others, which lead to anomalous scaling of the MSD, based only on the analysis of data obtained from single trajectories. This issue is even being studied today as part of a multi-group competition to characterize the properties of anomalous diffusion in data, called the ANDI challenge [168]. Though we cannot fully and uniquely restore the underlying dynamics just by discerning the scaling properties of the process from the data, the characterization of anomalous diffusion using three additional exponents M , L , and J , in addition to the Hurst, does bring different tools which can be helpful for modeling it. In this sense, this decomposition should also be beneficial, for example, for the modeling of diffusion in the membranes of living cells done in [227], where a Moses and a Joseph effect seem to have been observed. Another interesting example is found in [211], where the authors observed intercellular transport of insulin granules in eukaryotic cells and then used information from the time-averaged MSD (Joseph) and the evolution of the absolute mean of the increments (Moses) to model it. The authors compared two candidate models to describe their dynamics: fractional Brownian motion and continuous-time random walk, and concluded that non is sufficiently good for a full description of the system. They therefore continued by proposing a different, 'hybrid' model based on the previous two [211]. Since the first model leads only a Joseph effect, but the second leads to both Moses and Noah, a full three-effect

decomposition here, which also considers the inherent relation between them, Eq. (52), might shed more light on the unified model. Of course, in any case, if one seeks to reconstruct the underlying process from the data entirely, complete knowledge of the entire correlation structure would be required, including two-point and all the higher-order correlations.

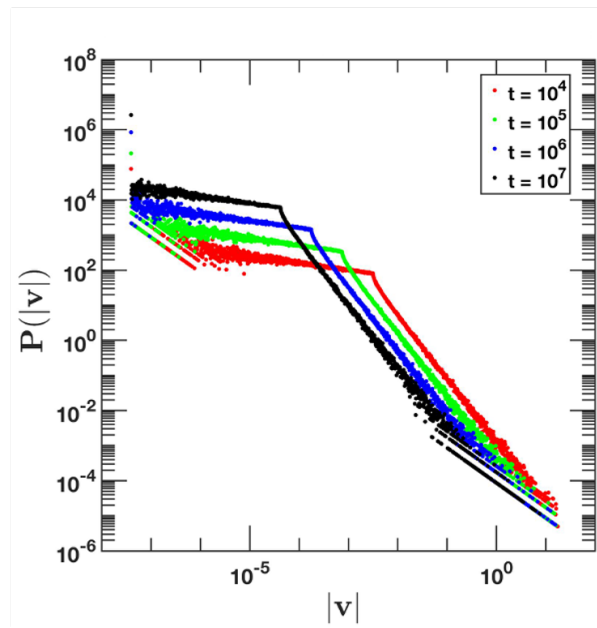
The Lévy walk model that we studied in this paper is a prototypical example that shows how the three effects analysis can be used for many other processes. The results in Fig. 7 and Fig. 9 eventually only depend on two inputs: the shape of the step durations PDF at large τ s, and the coupling between the step durations and the velocity, which can also be translated to the coupling between the step duration and displacement, since the step-displacement $\chi = V\tau$. Therefore, a class of process that can be mapped into a coupled step-duration and step-displacement process, which also includes other processes such as the Pommeau-Manneville map [163] and ATTM [150], will display similar properties as in the various regimes in Fig. 7 and Fig. 9. These phase diagrams describe their dynamics as well, after the change of variables (see, e.g., [163]).



(a)



(b)



(c)

Figure 6: Log-log plots for probability distribution as defined in eq. (66) versus $|v|$.

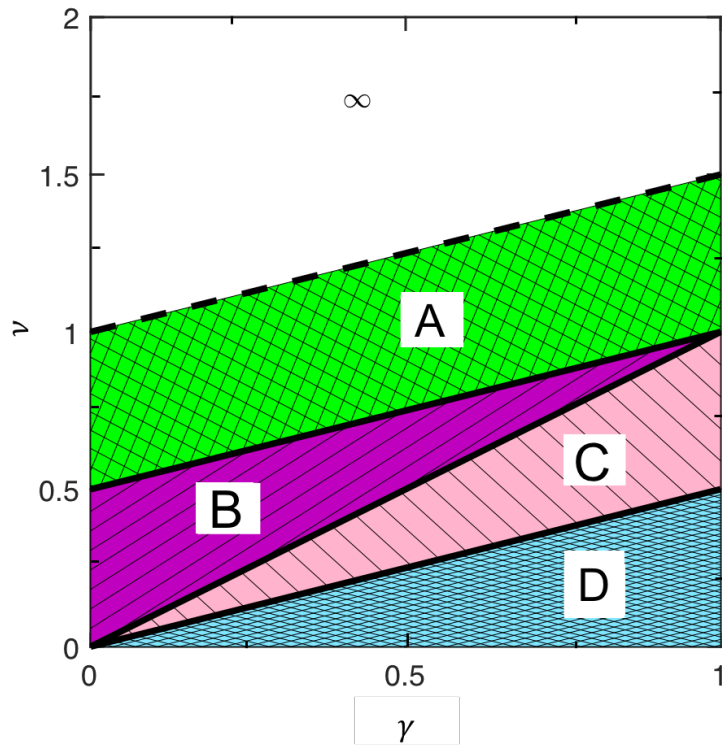
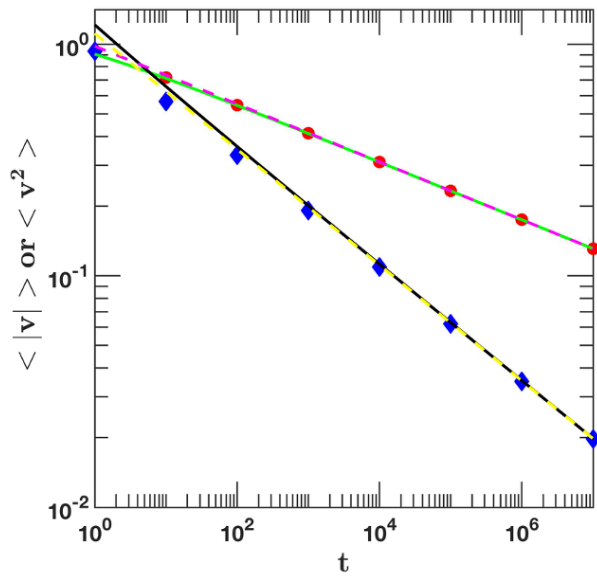
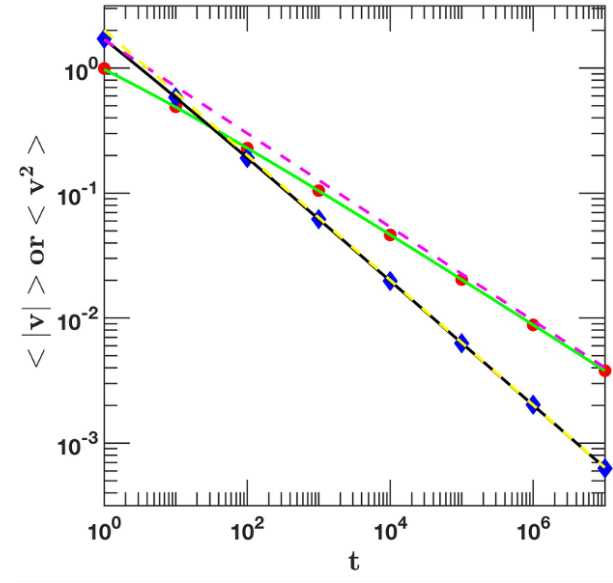


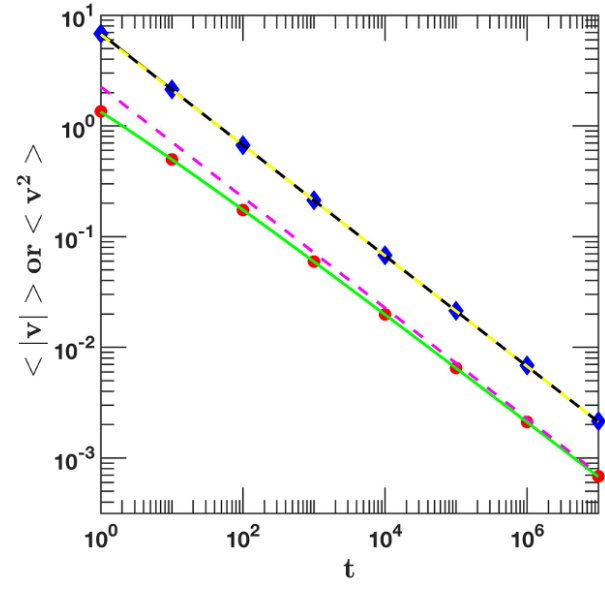
Figure 7: Phase diagram of the scaling exponents describing the decomposition of the anomalous diffusion.



(a)



(b)



(c)

Figure 8: Log-log plots for the averages of $|v|$ and v^2 , as function of time.

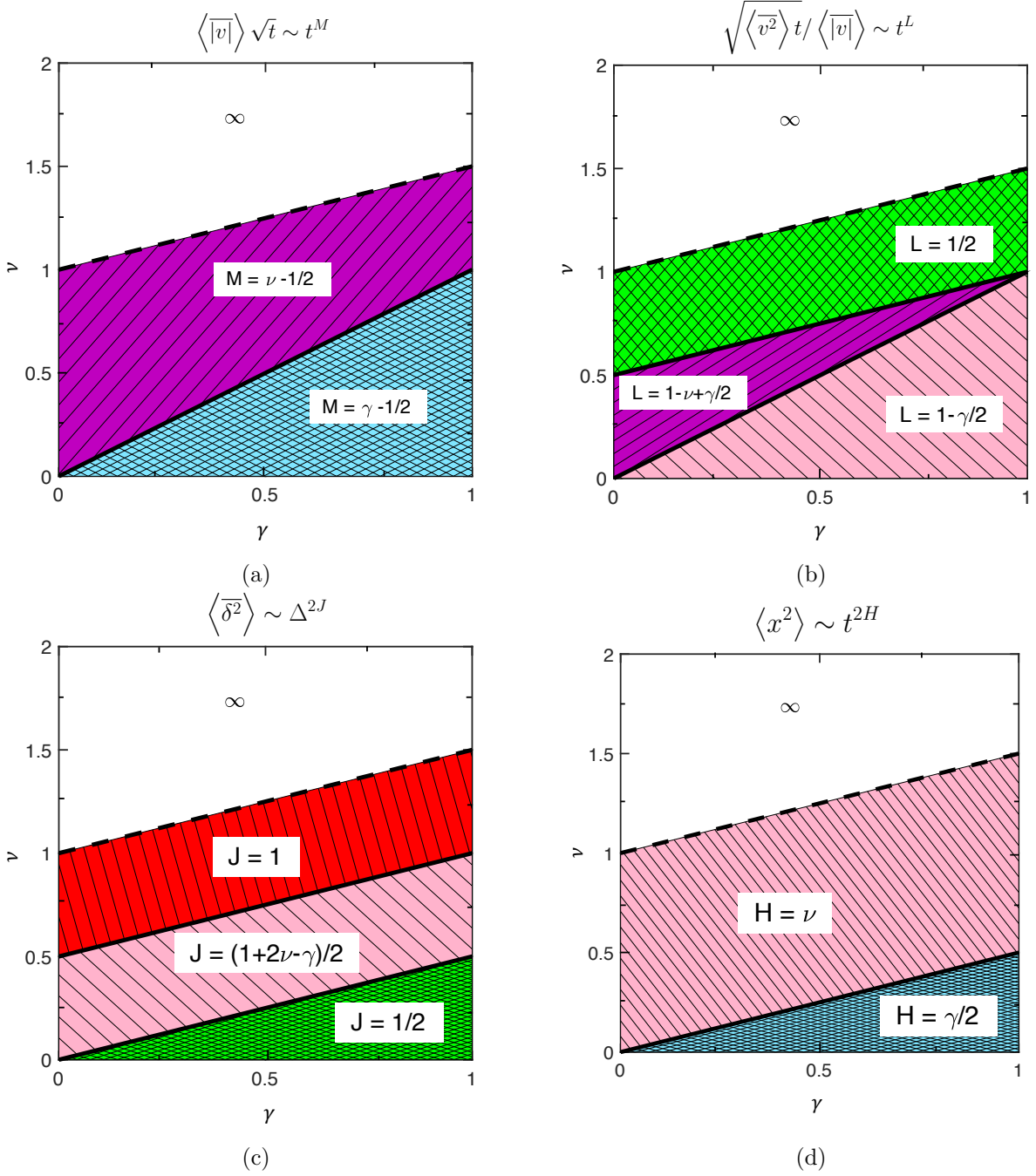


Figure 9: Phase diagrams of the scaling exponents describing the decomposition of the anomalous diffusion of Lévy walks into three constitutive effects, and their various magnitudes.

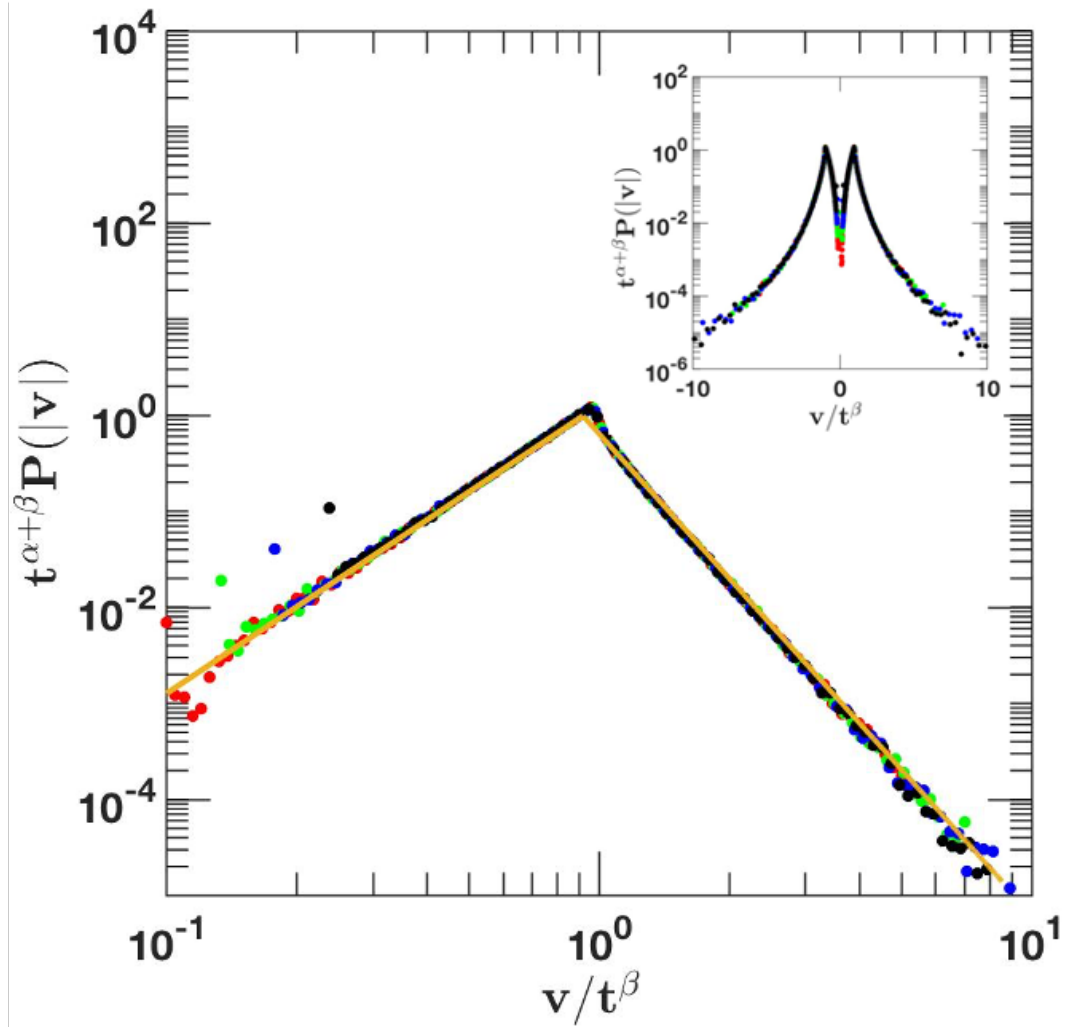


Figure 10: Numerical examination of the convergence of the increment PDF $P_t(v)$ to a time-invariant shape, here we used $\gamma = 0.5$, $\nu = 0.875$, leading to $L = 0.5$, and $M = 0.375$.

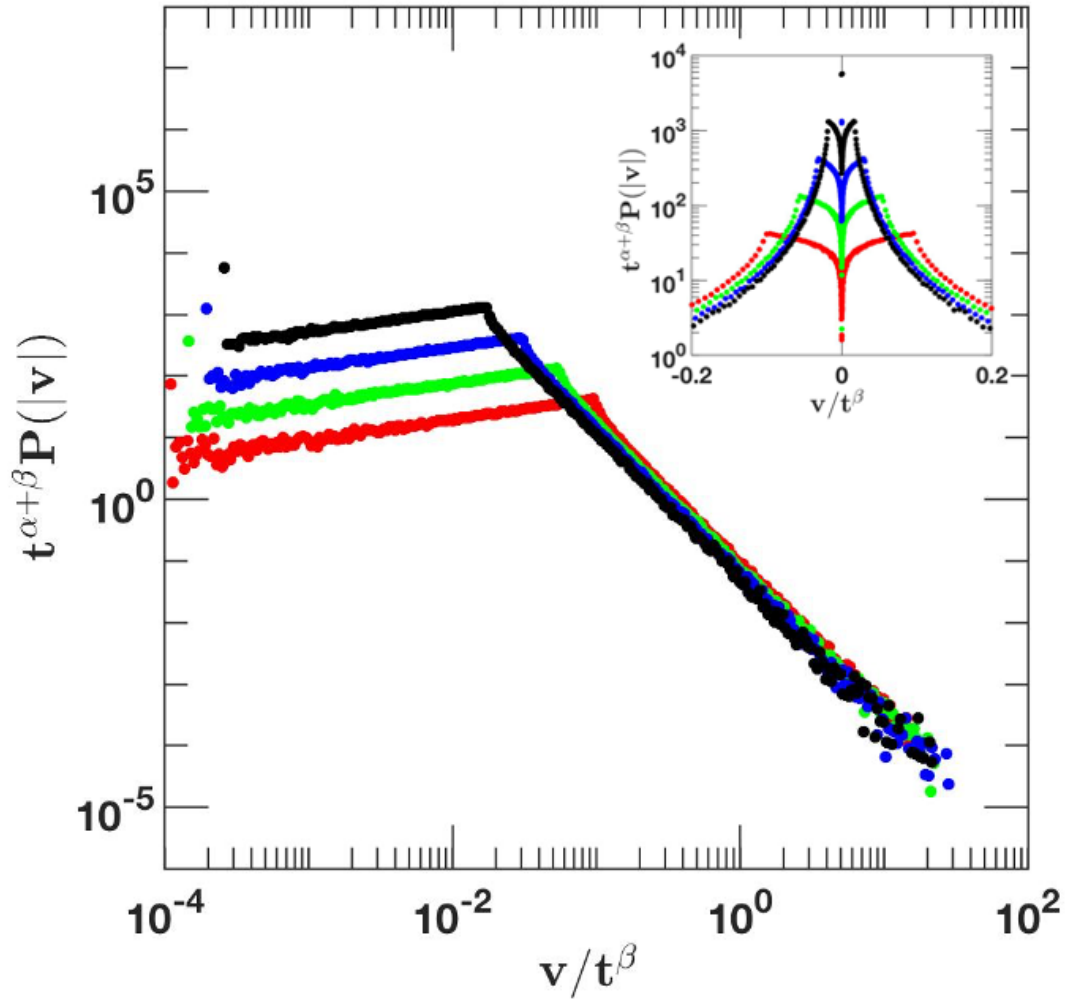


Figure 11: Numerical examination of the convergence of the increment PDF $P_t(v)$ to a time-invariant shape, here we used $\gamma = 0.5$, $\nu = 0.625$, leading to $L = 0.625$, $M = 0.125$.

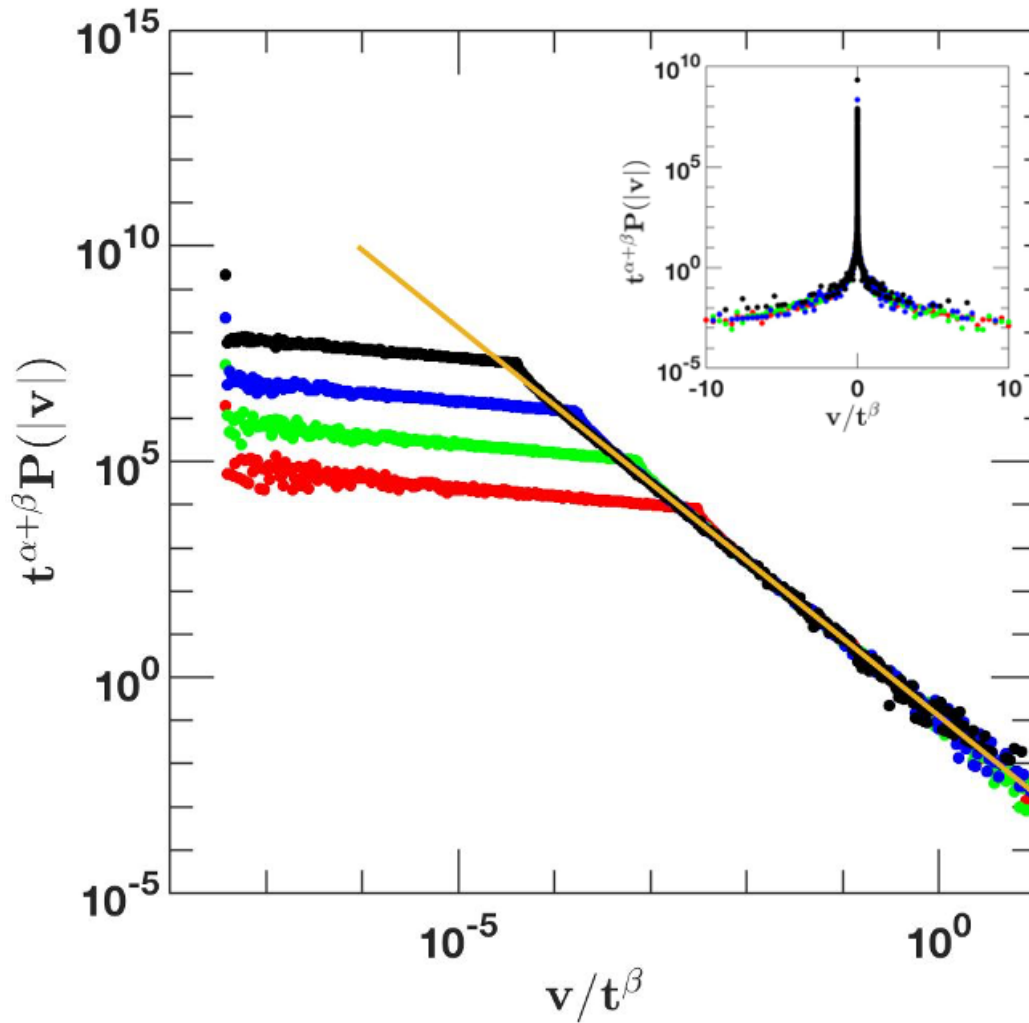


Figure 12: Numerical examination of the convergence of the increment PDF $P_t(v)$ to a time-invariant shape, here we used $\gamma = 0.5$, $\nu = 0.375$, leading to $L = 0.75$, $M = 0$.

4 Anomalous Diffusion in Heterogeneous Diffusion Processes

In a wide range of systems, anomalous diffusion of the power-law [36, 159, 160] form

$$\langle x^2(t) \rangle \simeq t^\beta \quad (95)$$

of the mean squared displacement (MSD) has been observed. Subdiffusion ($0 < \beta < 1$) and superdiffusion ($\beta > 1$) are distinguished based on the value of the anomalous diffusion exponent β . The special cases are of normal Brownian motion ($\beta = 1$) and wave-like, ballistic motion ($\beta = 2$).

The anomalous motion of charge carriers in amorphous semiconductors [190], the motion of tracer beads in polymer melts [18] and actin networks [232], the dynamics of sticky particles along a surface [234], and the spreading of tracer chemicals in subsurface hydrology [234] are all examples of subdiffusion. In weakly chaotic systems [204], bulk-surface exchange controlled dynamics in porous glasses [207], and the motion of tracer beads in wormlike micellar solutions [175], superdiffusion is observed.

Following significant developments in single-particle tracking and spectroscopic methods [23, 39, 47, 94] over the last decade or so, multiple anomalous diffusion cases have been identified for the motion of endogenous and artificial submicron tracers in living biological cells. As a result, techniques like video tracking, optical tweezer tracking, and fluorescence correlation spectroscopy have become commonplace for investigating tracers' motion like larger biomolecules or microbeads *in vivo*. The anomalous diffusion of submicron-sized tracers is not only interesting for understanding biochemical processes in the cell, but it also provides insight into the mechanical properties of the intracellular fluid and cellular mechanical structures, as tracer motion is the basis for microrheology [235].

In vivo subdiffusion, examples include the movement of endogenous granules (lipids or insulin) [102, 211, 212], fluorescently labeled RNA [80, 226] molecules at the tips (telomeres) of eukaryotic DNA, and bacterial DNA loci [43, 226]. Potassium channels found in living cell plasma membranes

were found to be subdiffusive [227], as was the membrane proteins' movement in the Golgi membrane [230]. Superdiffusion is observed in living cells during the motor-driven transport of viruses [195], microbeads [48, 49], and magnetic endosomes [184].

The theoretical approaches like continuous-time random walks, fractional Brownian motion [138], and the closely related fractional Langevin equation [132] driven by Gaussian noise when used to model processes assume that the environment is homogeneous and isotropic, or that over the relevant time and length scales of the spatial measurement variations of the environment in some sense are averaged out. Nonetheless, there are clear indications that the environment significantly impacts the local diffusion constant in biological cells.

The MSD of Markovian, heterogeneous diffusion processes (HDPs) with space dependent diffusion constant $D(x) \simeq |x|^\alpha$ scales like $\langle x^2(t) \rangle \simeq t^p$ with $p = 2/(2 - \alpha)$, whereas the time averaged MSD $\bar{\delta}^2$ scales linearly in both sub- ($\alpha < 0$) and super-diffusive ($\alpha > 0$) regimes. We calculate the scaling exponents quantifying the constitutive effects causing anomalous diffusion present in HDPs.

In hydrological applications, descriptions of space-dependent diffusion coefficients $D(x)$ are widely used to describe diffusion in heterogeneous porous media mesoscopically [88]. Inhomogeneous versions of continuous-time random walk models for water permeation in absorbent ground layers have recently been developed [60].

In various stochastic models (compare [72, 73] and [53, 201, 205, 206]), mathematically, spatially, and temporally varying diffusivities cause anomalous sub- and superdiffusion. Richardson type diffusion in turbulent media was specifically modeled using heterogeneous diffusion processes (HDPs) [181]. To capture the diffusion of a particle on fractal support [174], power-law forms for $D(x)$ were proposed; however, as seen in [57], this approach results in weakly non-ergodic motion, which is inherently different from ergodic motion on fractals [155, 156, 203].

We investigate in detail the motion of a diffusing particle subjected to a space-dependent diffusion coefficient $D(x)$ for power-law x -dependency. These processes cause anomalous diffusion of the form (95) of both sub- and super-diffusive forms, as well as an ultraslow time dependence of the MSD. Furthermore, despite being described in terms of a time local diffusion equation, these

processes exhibit weak ergodicity breaking in the sense that the time and ensemble-averaged MSDs do not converge, even in the long time limit [57].

In the following subsection, we introduce the HDP process in detail. In the third subsection, we calculate and compare our analytical results with the simulations and investigate the power-law dependence of $D(x)$. Finally, in the last subsection, we draw our conclusions and present a brief outlook.

4.1 Model and its Diffusive Behavior

The stochastic Langevin equation for the displacement $x(t)$ of a particle diffusing in a medium with the position-dependent diffusivity $D(x)$ [57], namely

$$\frac{dx(t)}{dt} = \sqrt{2D(x)}\zeta(t) \quad (96)$$

where $\zeta(t)$ denotes a Gaussian white (δ -correlated) noise with unit norm $\langle \zeta(t)\zeta(t') \rangle = \delta(t-t')$ and zero mean $\langle \zeta(t) \rangle = 0$. The nonlinear stochastic equation (96) is interpreted, both in our theoretical analyses and in the simulations, with multiplicative noise in the Stratonovich sense [183]. After averaging over the noise $\zeta(t)$, the diffusion equation for the PDF $P(x, t)$ has the symmetric form as [55, 57]

$$\frac{\partial P(x, t)}{\partial t} = \frac{\partial}{\partial x} \left[\sqrt{D(x)} \frac{\partial}{\partial x} \left(\sqrt{D(x)} P(x, t) \right) \right] \quad (97)$$

The different cases for $D(x)$ for this Markovian process with multiplicative noise are depicted in Fig. 13. The exact functional dependencies are represented by the dashed lines, while the blue curves depict the regularised forms for $D(x)$ that were used in the simulations as given in eqs. (99)-(100) where $\alpha = 1$ and $\alpha = -0.25$ for (a) and (b) respectively.

The power-law shape of the diffusion coefficient is as follows

$$D(x) = D_0 |x|^\alpha \quad (98)$$

where the scaling exponent α may assume negative and positive values, effecting sub- and super-diffusion respectively. The form (98) is convenient for the analytical calculations but we employ regularised forms for simulations [55]. Thus, for positive α , the modified form

$$D_{super} = D_0 (1 + |x|^\alpha) \quad (99)$$

prevents the particle from getting trapped at the origin ($x = 0$), while for negative α the choice

$$D_{sub} = \frac{aD_0}{a + |x|^\alpha} \quad (100)$$

avoids the divergence of $D(x)$ at the origin. The power-law form (98) along with the regularization for sub- and super-diffusion are shown in Fig. 13 . From a set of stochastic trajectories $x(t)$ generated for an initial particle position $x(0) = x_0$, the ensemble and time averaged MSDs are computed [57]. In addition, we also analysed the behaviour of HDP for the exponential as well as logarithmic dependence where

$$D_{exp}(x) = \frac{A^2}{2} e^{-2\alpha x} \quad (101)$$

$$D_{log}(x) = \frac{A^2}{2} \frac{1}{2} \log\left[\left(\frac{x}{\bar{x}}\right)^2 + 1\right]. \quad (102)$$

On calculating the ensemble-averaged MSD, we obtained logarithmic scaling [57] of the ensemble-averaged MSD as seen in eq. (103),

$$\langle x^2(t) \rangle = \frac{1}{4\alpha^2} (A_1 + A_2 \log [\alpha^2 A^2 t] + \log^2 [\alpha^2 A^2 t]) \quad (103)$$

where A_1 and A_2 are constants. To keep the calculations simple, we took $A = 1$.

Inserting the power-law form (98) of the diffusion coefficient $D(x)$ into the diffusion equation

(97), we recover the PDF [55]

$$P(x, t) = \frac{|x|^{-\alpha/2}}{\sqrt{4D_0t\pi}} \exp\left(-\frac{|x|^{2-\alpha}}{(2-\alpha)^2 D_0t}\right) \quad (104)$$

for the initial $P(x, 0) = \delta(x)$. Using the (104), we calculate the ensemble averaged MSD

$$\langle x^2(t) \rangle = \Gamma\left(\frac{6-\alpha}{2(2-\alpha)}\right) \frac{(2-\alpha)^{4/(2-\alpha)}}{\pi^{1/2}} (D_0t)^{2/(2-\alpha)} \quad (105)$$

According to eqn (105), for $\alpha < 0$ the process is subdiffusive, while for $\alpha > 0$ superdiffusion occurs. The limiting cases of Brownian motion with $\langle x^2(t) \rangle = 2D_0t$ correspond to $\alpha = 0$, and that of ballistic motion to $\alpha = 1$. The diffusion becomes increasingly fast when α increases towards the limiting value 2. The PDF (104) corresponds to a compressed Gaussian in the subdiffusive case $\alpha < 0$, i.e., we obtain an exponential distribution in which the exponent of x is larger than 2. In the super-diffusive case $0 < \alpha < 2$ the PDF (104) becomes a stretched Gaussian. Fig. 14 shows excellent agreement between the theoretical PDF (104) and the numerical solution of the diffusion equation (97). The analytical results (104) for different trajectory lengths t (coloured lines) and the numerical solution of the dynamic equation (97) are represented by the dashed lines. (a) shows the PDF for $\alpha = -2$ (sub-diffusion) and (b) PDF for $\alpha = 0.25$ (super-diffusion).

4.2 Calculation of Exponents

The MSD for the HDPs does not scale linearly with time, as shown in equation (105), resulting in anomalous diffusion. Anomalous diffusion can be decomposed into effects that are the root causes of the Central Limit Theorem's premises being violated (CLT). The CLT holds for a process X_t that is the sum of random increments δ_t if the increments are (1) independent, (2) have a finite variance distribution, and (3) are identically distributed and these are referred as the (1) Joseph, (2) Noah, and (3) Moses effects, respectively.

$$X_t = \sum_{s=0}^{t-1} \delta_s \quad (106)$$

Each of these constitutive effects, or a combination of them, can cause anomalous diffusion. For self-similar processes, they can be quantified by scaling exponents, which are related to each other and the Hurst exponent by Eq. 4.

Hurst Exponent H

The Mean-Squared Displacement (MSD) of the diffusive processes that scale anomalously with time is

$$\langle x^2(t) \rangle \sim t^{2H} \quad (107)$$

where H is the *Hurst exponent*. On comparing equation (105) and (107), we get

$$H = \frac{1}{2 - \alpha} \quad (108)$$

where α is the scaling exponent as defined in equation (98). When $\alpha < 0$, the system lies in the sub-diffusive region whereas when $0 < \alpha < 2$ the system lies in the super-diffusive region. Thus by varying the values of α , we observe different regions of anomalous diffusion.

Joseph Exponent J

To analytically calculate the Joseph exponent, we use the scaling of lag time of the ensemble averaged time-averaged MSD. The time-averaged MSD is defined as:

$$\overline{\delta^2(\Delta)} = \frac{1}{t - \Delta} \int_0^{t-\Delta} (x(t_0 + \Delta) - x(t_0))^2 dt_0 \quad (109)$$

where the time average is over the time series $x(t_0)$, whose length is t . In order to calculate the ensemble averaged time-averaged MSD, we additionally average over a sufficiently large number of individual trajectories [23, 47],

$$\langle \overline{\delta^2(\Delta)} \rangle = \frac{1}{N} \sum_{i=1}^N \overline{\delta_i^2(\Delta)}. \quad (110)$$

The trajectory-to-trajectory averaged time averaged MSD (110) of the HDP process with power-law

form (98) of the diffusion coefficient takes on a linear dependence on the lag time Δ [55],

$$\langle \overline{\delta^2(\Delta)} \rangle = \Gamma\left(\frac{6-\alpha}{2(2-\alpha)}\right) \frac{(2-\alpha)^{4/(2-\alpha)}}{\pi^{1/2}} D_0^{2/(2-\alpha)} \Delta t^{\alpha/(2-\alpha)}. \quad (111)$$

The asymptotic scaling for the ensemble averaged time-averaged MSD is [163]

$$\langle \overline{\delta^2(\Delta)} \rangle \sim t^{2L+2M-2} \Delta^{2J}. \quad (112)$$

To obtain the Joseph exponent for both sub-,super-diffusive regions, we compare the scaling of lag time Δ in (111) and (112) and get

$$J = \frac{1}{2}. \quad (113)$$

The eqn. (113) implies that the increments of the heterogeneous diffusion process are independent of each other *i.e.*, there are no correlations between the increments.

Latent Exponent L

The heterogeneous diffusion processes considered here in this chapter have finite variance which shows that $E[X_t] \sim t^H$ and $E[X_t^2] \sim t^{2H}$ and thus $Var[X_t] = t^{2H} Var[X_1]$. Hence, the value of the Latent exponent is

$$L = \frac{1}{2}. \quad (114)$$

Moses Exponent M

To obtain the Moses exponent, we compare the scaling of t in equations (111) and (112) and get

$$2L + 2M - 2 = \frac{\alpha}{2 - \alpha} \quad (115)$$

and then we substitute the value of L from eq. (114) which yields

$$M = \frac{1}{2 - \alpha}. \quad (116)$$

Also, on substituting the values of exponents from equations (108), (113), (114) and (116), we

observe that the scaling relation (4) is satisfied.

4.3 Simulation Results

To verify our analytic predictions for the exponents, we performed numerical simulations for the HDPs. We calculated exponents for various α values in both the sub- and super-diffusive regions. We generated an ensemble of 10^4 realizations of the process X_t for $t = 10^6$ for different values of α . The ensemble's $w[X_t]$, $m[Y_t]$, $m[Z_t]$, and $E[R_t/S_t]$ values were then calculated using the equations 8, 17, 18, and 19. Figure 15 shows examples of results for $\alpha = 0.5$ and $\alpha = -0.5$. The scaling of these functions, quantified by the exponents corresponding to the slope of the function at large t , determine the exponents quantifying diffusion and the constitutive effects that cause anomalous diffusion. Lines connecting the data points are shown as guides to the eye. The statistical error of the data points is smaller than the symbol size. The scaling exponents describe the asymptotic, large t scaling behavior of these functions.

Over a two-decade range, from $t = 10^4$ to 10^6 , we fitted each of the four functions to the form given by equation (34). After determining Ω for each function, we use Eqs. 8, 17, 18 and 19 to calculate the values of H , M , L , and J . The scaling relationship between the exponents, Eq. 4, is confirmed in Fig. It compares the theoretically predicted value of H to the fitted value of H derived from simulations, as well as the result of fitting for $J + L + M - 1$ as a function of α . The simulation results are generally consistent with our theoretical predictions, but there are some deviations. Either scaling corrections should be included in the fit, or longer simulations should be performed to achieve more precise numerical results. However, the general form of the corrections is unknown, and the accuracy of long simulations is restricted by the phenomenon of “round-off periodicity,” as described by [28, 85]. Longer simulations would require computationally expensive calculations.

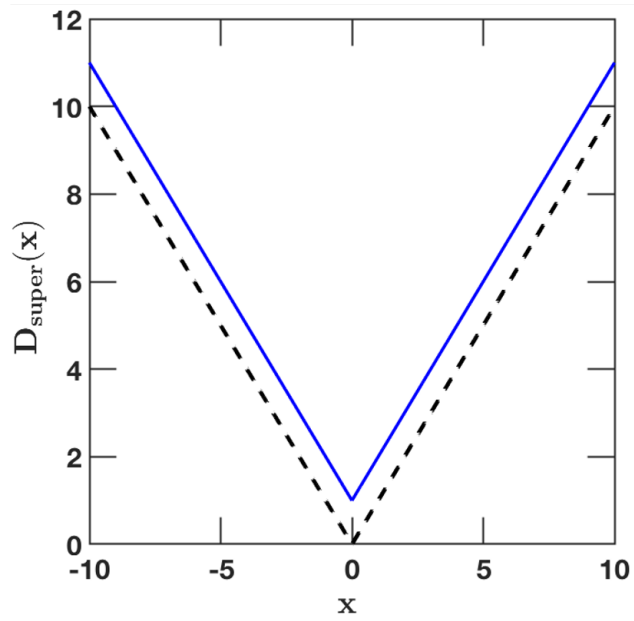
4.4 Discussion

Anomalous diffusion is a widely observed phenomenon at many scales and disciplines. With the dramatic increase in single-particle tracking studies, the question of how to physically interpret the recorded trajectories in terms of time averages of observables like the MSD arises. In particular, most available physical theories provide results for ensemble averages of physical observables. However, once a system exhibits weak ergodicity breaking, the inequivalence of ensemble from time averages prevents such ensemble theories from being applied to the measured, time-averaged quantities. The quantitative interpretation of time averages thus necessitates knowledge of whether the system is ergodic, in which case the standard results can be used to fit the data or whether the system is weakly non-ergodic. In that case, understanding the time-averaged observables is critical.

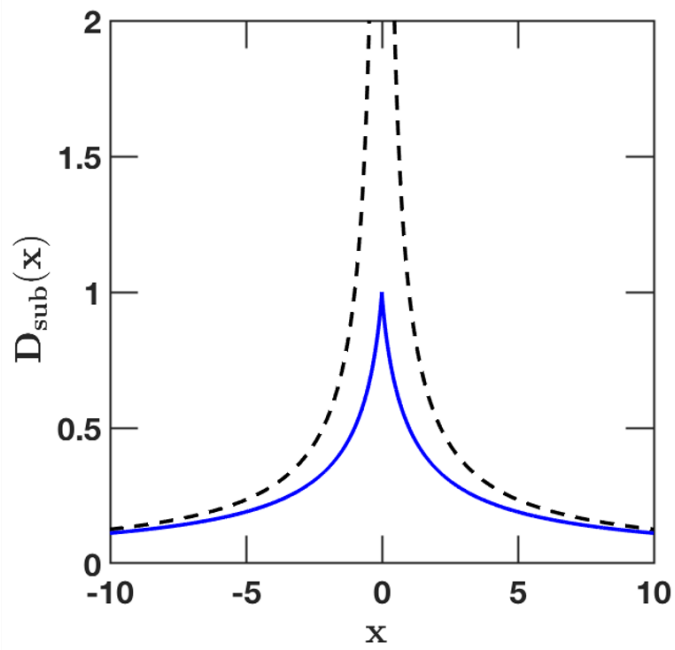
The seemingly simple Markovian HDP with power-law space-dependent diffusion coefficient, defined in terms of a Langevin equation that is fully local in both space and time, was discussed here. Despite this locality, HDPs are weakly non-ergodic: for both sub- and superdiffusion, the ensemble-averaged time-averaged MSD $\langle \overline{\delta^2(\Delta)} \rangle$ scales linearly with the lag time. Subdiffusion from more complex processes has previously shown this behavior: CTRWs with diverging characteristic waiting times [47, 89, 131], CTRWs with correlated waiting times [134, 213], non-renewal [55], aging CTRWs [129], and time-scaled Brownian motion [72, 73].

HDPs are new tools used for describing anomalous diffusion, and weakly non-ergodic dynamics [57]. The dynamic behavior of HDPs is directly related to the physical properties of the environment due to their intuitive formulation in terms of space-dependent diffusivities. Let us contrast the above observations with the subdiffusive continuous-time random walk model (compare ref. [47]). The characteristic waiting time $\langle \tau \rangle$ for this system diverges due to the underlying long-tailed distribution of trapping times τ , $\phi(\tau) \sim \tau^{-(1+\alpha)}$ with $0 < \alpha < 1$. The system remains non-stationary due to the lack of a finite microscopic time scale $\langle \tau \rangle$, which negates the existence of a long measurement time T limit. The violation of ergodicity is due solely to the spatial variation of the diffusion process for the HDPs considered here, and the anomalous diffusion is due to the multiplicative nature of the noise, which is calculated above and quantified as Moses exponent.

As modern experimental techniques produce an increasing number of long single-particle trajectories with unprecedented resolution, and anomalous diffusion is recognized as a widespread phenomenon [158], the need for more detailed stochastic models and understanding grows. We believe that this research adds to a growing body of knowledge about anomalous diffusion processes.

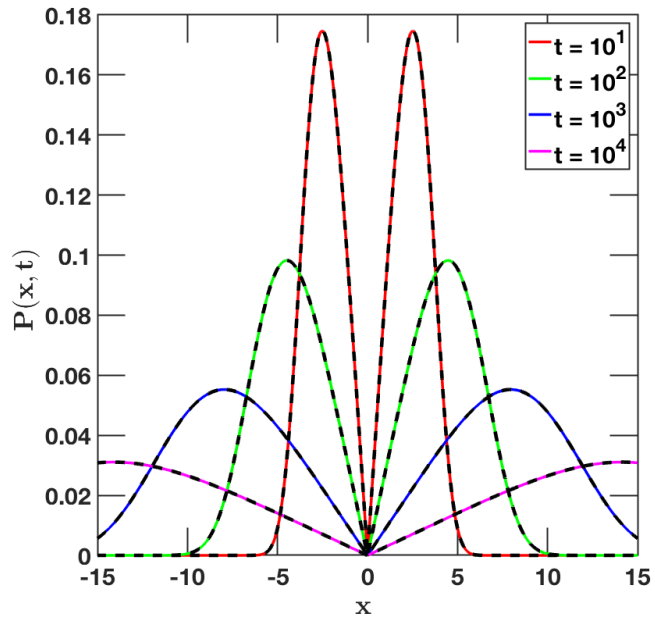


(a)

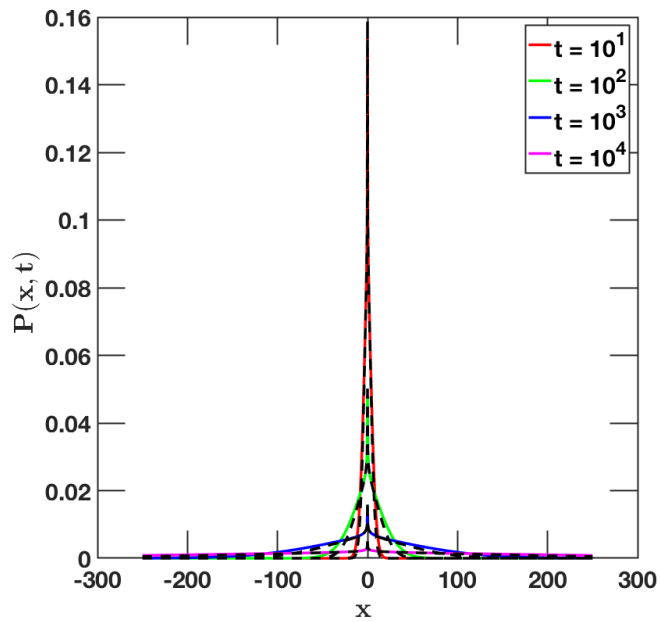


(b)

Figure 13: Functional dependencies on the position variable x of the diffusion coefficients.

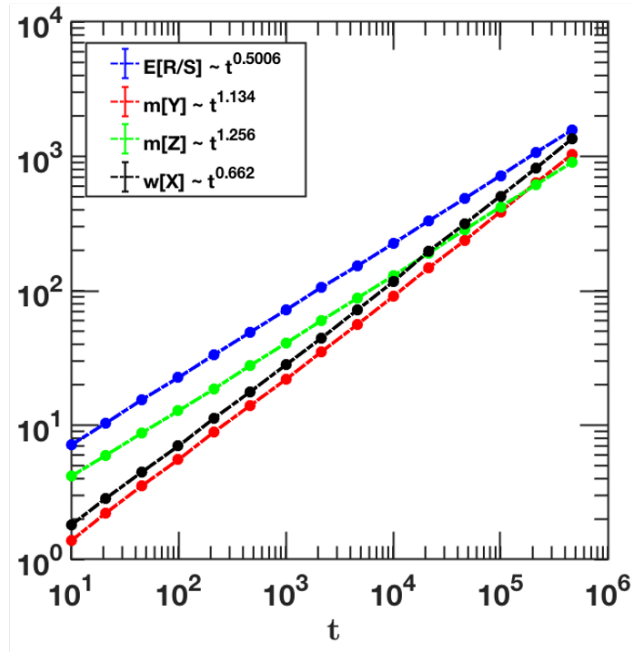


(a)

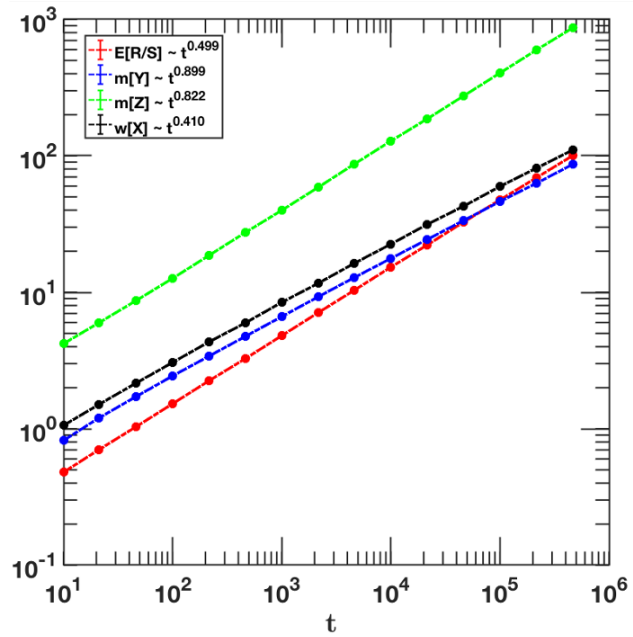


(b)

Figure 14: The PDF for sub- and superdiffusive HDPs with power-law diffusivity (98), computed for the parameters $a = 0.01$ and $D_0 = 1$.



(a)



(b)

Figure 15: Log-log plot of the width of X , median of Y and of Z , and mean of R/S as a function of time t .

5 Conclusion

The dissertation discusses causes of $H \neq 1/2$ in stochastic processes with non-stationary increments, generalizing previous work [27, 65, 136, 151] and applies the tools to better understand the anomalous diffusion in different processes. The effects, *Joseph* (correlated increments), *Noah* (fat-tailed increments), and *Moses* (nonstationary increments), can each be characterized by independent exponents, J , L , and M , respectively. Those exponents are related to the *Hurst exponent* H that characterizes the scaling of the process through the scaling relation: $H = J + L + M - 1$ [54].

The time series analysis numerical methods used to measure each of the four scaling exponents accurately are also discussed. Finite-time power-law corrections to scaling are also taken into account with these methods [54]. The fact that all four exponents can be measured independently allows the scaling relation that connects them to be verified, providing a rigorous numerical check on the accuracy of the time-series analysis. To demonstrate each of the three effects that cause $H \neq 1/2$, these numerical methods can be applied to various stochastic processes, including those with both stationary and non-stationary increments, with and without long-time auto-correlations, and with both finite and infinite increment variance.

The analysis of anomalous diffusion found in the Pomeau-Manneville (PM) map and Lévy walk models enables us to understand various processes' underlying dynamics. The results mentioned in the dissertation may find applications in a wide variety of processes. Consider the on-off blinking of a single, illuminated quantum dot as it transitions from a light-emitting to a dark state [42, 145, 209]. While such an experiment will show many rapid transitions between on and off states, there will be some instances where very long on or off periods appear. The duration of these long events typically increases with t over a sufficiently long observation period t [42, 145]. The motion of potassium channels in the plasma membrane of living cells [227] and the diffusion of submicron tracers in a cross-linked actin mesh [232] exhibit a similar effect. Glassy systems, in which the term “ageing” was first coined, are well known for such strongly non-stationary, out-of-equilibrium

behavior.[32, 46, 61, 82, 86, 165]

A model for HDPs with distance-dependent diffusivities that exhibit sub-, super-, and ultra-slow diffusion as well as weak ergodicity breaking was also investigated. Power-law variation of the diffusion coefficient was examined. This framework can be applied to other variations of the diffusion coefficient's spatial dependence $D(x)$ [57]. Our findings could be used in a wide range of spatially heterogeneous media. They could also be used to complement other approaches to anomalous diffusion, such as continuous-time random walks or diffusion in viscoelastic environments. A particular example is the viral infection dynamics, a mathematical rationale to discriminate nearly Brownian and anomalous populations of diffusing viral particles, which was observed by single-particle tracking in living bacteria [195]. An extension of the analytical and computational schemes for HDPs in higher dimensions is currently under progress [55].

These findings show that anomalous diffusion has different diffusive and ergodic properties depending on the system. The challenge is to incorporate the features of anomalous diffusion and non-ergodicity into a pluralistic range of stochastic models for the description of non-Brownian diffusion processes. Other, more physical recurrent stochastic processes with non-stationary increments could benefit from the time series analysis methods we've developed here. The amount of daily precipitation recorded at some locations [45, 104, 105, 180, 181], for example, maybe amenable to our methods. In this case, the process can be assumed to repeat itself every year, resulting in an ensemble of precipitation amounts on a given day of the year for different years that can be statistically analyzed. Our methods could also be applied to the study of hard turbulence. The temperature as a function of time at a given location can be considered as a stochastic process with non-stationary increments, in this case, [180, 181]. After a non-periodic triggering event, such as the separation of a boundary layer [50], this process repeats itself. The temperatures at a given time after a triggering event-form an ensemble in this case.

It will also be interesting to expand our study of ageing research beyond the stochastic processes we've looked at so far to more specific systems. The Lorentz gas model, with its rich behavior of cross-overs and density effects [93, 124], the motion in periodically structured environments like

elastic gels [78], or the folding dynamics of proteins [114, 236] are examples of the latter. Finally, we mention that active transportation processes may benefit from concepts similar to those discussed here. From a more practical point of view, the discussion of the extent to which anomalous diffusion may impact biological function has just begun. [23, 80, 90, 95, 99, 130, 196]

Appendices

A Proofs for Time Series Analysis of Lévy Walks

A.1 Generality of $H = L + J + M - 1$

As mentioned in the main text, the summation relation, Eq. (52), between M, L, J , and H was previously presented for several examples of processes, in [54, 163]. These studies suggest that this relation is also valid for a much larger range of systems, even though a unified proof is still required in future work. The following example shows that we can prove this relation analytically also for a widely useful system where $J \leq 1/2$ (in the derivation in Eq. (52) we assumed that $J > 1/2$), and the correlation function is negative. Consider the ARFIMA $(0, d, 0)$ process [30, 84] $x(t) = \sum_{i=0}^t X_i$, in discrete time, whose increments are defined via the transformation $(1 - \hat{B})^d X_i = \sigma^2 \eta(i)$, where η_i is Gaussian white noise with zero mean and $\langle \eta_i \eta_j \rangle = \delta_{ij}$. Here, $\hat{B}^n X_i = X_{i-n}$, $d < 0$ and

$$(1 - B)^d = \sum_{k=0}^{\infty} \frac{\prod_{a=0}^{k-1} (d - a)(-B)^k}{k!} = 1 - dB + \frac{d(d-1)}{2!} B^2 + \dots \quad (117)$$

When $-1/2 \leq d \leq 0$, this process is long-ranged anti-correlated, and the autocorrelation function of the increments of this process is [30]:

$$c(\tilde{\Delta}) = \langle X_{i+\tilde{\Delta}} X_i \rangle = \prod_{k=1}^{\tilde{\Delta}} \frac{k-1+d}{k-d} = \frac{\Gamma(\tilde{\Delta}+d)\Gamma(1-d)}{\Gamma(\tilde{\Delta}-d+1)\Gamma(d)}. \quad (118)$$

For large $\tilde{\Delta}$;

$$c(\tilde{\Delta}) \sim \frac{\Gamma(1-d)}{\Gamma(d)} \tilde{\Delta}^{2d-1} \quad (119)$$

so according to the definition in Eq. (51), the Joseph exponent is $J = d + 1/2$. The MSD is related to the correlation function via

$$\begin{aligned} \langle x^2(t) \rangle &= \langle (\sum_{i=1}^t x_i)^2 \rangle = \sum_{i,j=1}^t \langle x_i x_j \rangle \\ &= \sigma^2(t + 2 \sum_{\tilde{\Delta}=1}^t (t - \tilde{\Delta}) c(\tilde{\Delta})). \end{aligned} \quad (120)$$

Plugging Eq. (118) into Eq. (120), we find that at long t

$$\langle x^2(t) \rangle \sim \frac{t^{2d+1} |\Gamma(-d)|}{(2d+1)\Gamma(d)} + \frac{d}{2d+1} + \mathcal{O}(t^{2d-1}), \quad (121)$$

and from the leading-order term, using $J = d - 1/2$, we find $\langle x^2(t) \rangle \propto t^{2J}$, namely $H = J$. This is a well known result, and note that in the standard ARFIMA process the increment distribution is stationary and thin-tailed, hence $M = L = 1/2$ and the summation relation in the section title, and Eq. (52) is fulfilled. Now, consider the related process: $\tilde{x}(t) = \sum_{i=0}^t \tilde{X}_i$, where $(1 - \hat{B})^d X_i = \sigma^2 t^{2L+2M-2} \eta(i)$. Here we introduced the time dependence of the variance of the increments in the same way as in Eq. (43), which means that now the process can have both a Noah and a Moses effect, in addition to Joseph. A calculation in this case, which follows exactly the same lines as the above, will now yield $\langle x^2(t) \rangle \sim t^{2L+2M+2J-2}$, which again leads to Eq. (52). Further generalizations of this summation relation are discussed below, in Appen. A.2.

A.2 The ensemble-time averaged MSD and the correlation function

In this section we want to clarify the connection between the autocorrelation function and the Ensemble-Time (ensemble averaged - time averaged) Mean-Squared Displacement (EATA MSD) and thereby show the types of correlations that lead to specific values of the Joseph exponent J . The time-averaged MSD defined in Eq. (80) depends on two times, t and Δ . Here t is the measurement time and Δ is the lag time. However, for some systems, especially the ones of interest for this study, the time-averaged MSD does not converge to a single value. For an analytical approach, we

therefore consider the ensemble average of the time-averaged MSD, namely the EATA MSD

$$\langle \overline{\delta^2} \rangle \approx \frac{1}{t} \int_0^t \langle [x(t_0 + \Delta) - x(t_0)]^2 \rangle dt_0. \quad (122)$$

As discussed in [161], in the limit $t \rightarrow \infty$ only the upper bound of the integral is important and the behavior around zero is negligible. Now for the expression below the integral we have to find the MSD recorded between time t_0 and $t_0 + \Delta$ under the condition that $t_0 \gg \Delta$. It is given in equation (52). It connects the integrand in Eq. (122) to the velocity correlation function. We denote

$$\langle [x(t_0 + \Delta) - x(t_0)]^2 \rangle = 2 \int_0^\Delta dt_2 \int_0^{t_2} dt_1 \langle v(t_1 + t_0)v(t_2 + t_0) \rangle. \quad (123)$$

Now we want to discuss four different cases, i.e. three different types of correlation functions. (I) In the first step we consider correlation functions $\langle v(t_1 + t_0)v(t_2 + t_0) \rangle = C(t_2 - t_1)$, that do not depend on the measurement time t_0 . In this case the only way to violate the Gaussian CLT is with diverging correlation times, i.e. the correlation function asymptotically scales like a power law

$$\langle v(t_1 + t_0)v(t_2 + t_0) \rangle \sim (t_2 - t_1)^{2J-2}. \quad (124)$$

The equivalence of H and J can also be found by plugging the correlation function into equation (52). Now using equation (123), the exact same scaling, $\langle [x(t_0 + \Delta) - x(t_0)]^2 \rangle \sim \Delta^{2H}$, is obtained. Since this still does not depend on t , the EATA MSD exhibits the same scaling

$$\langle \overline{\delta^2} \rangle \sim \Delta^{2J}. \quad (125)$$

(II) For the second scenario we consider a correlation functions that, asymptotically, exhibits power-law scaling, both in t and Δ . Now, we can write the correlation function as

$$\langle v(t)v(t + \Delta) \rangle \sim t^{2H-2} \Phi\left(\frac{\Delta}{t}\right), \quad (126)$$

where $\Phi(q)$ (and $q = \Delta/t$), is a positive valued function describing asymptotic scaling. The scaling exponent $2H - 2$ can again be obtained using Eq. (52). This was shown in [59]. The total measurement time in this case has to be much larger than the lag time $\Delta \ll t$, then only the small- q asymptotic behavior of $\phi(q)$ is relevant

$$\phi(q) \sim q^{2J-2} \quad \text{with} \quad 2 - 2H \leq 2 - 2J < 1 \quad q \rightarrow 0. \quad (127)$$

The conditions above are necessary in order to ensure that the correlation function decays with Δ , and at the same time does not blow up with time t . Since in the $q = 0$ case, the correlation function is equal to the velocity displacement Eq. (43), continuity demands

$$2 - 2J = 2L + 2M - 2H \Leftrightarrow H = J + L + M - 1. \quad (128)$$

Now, the correlation function for $q \rightarrow 0$ can be inserted into Eq. (123)

$$\langle [x(t_0 + \Delta) - x(t_0)]^2 \rangle \sim 2 \int_0^\Delta dt_2 \int_0^{t_2} dt_1 (t_1 + t_0)^{2L+2M-2} (t_2 - t_1)^{2J-2}. \quad (129)$$

Integration yields with $t_0 \gg t_1, t_2$

$$\langle [x(t_0 + \Delta) - x(t_0)]^2 \rangle \sim \frac{2}{(2J - 1)(2J)} (t_0)^{2L+2M-2} \Delta^{2J}. \quad (130)$$

Inserting this result into Eq. (122) only yields an additional pre-factor. Therefore, the EATA MSD scales like

$$\langle \overline{\delta^2} \rangle \sim t^{2L+2M-2} \Delta^{2J}. \quad (131)$$

(III) The third case occurs for processes with correlations that do scale with the measurement time t , but decay faster with the lag time Δ . Here, we write the correlation function as

$$\langle v(t)v(t + \Delta) \rangle \sim t^{2H-2} \Phi(\Delta), \quad (132)$$

with a positive function $\Phi(\Delta)$, which decays faster than Δ^{-1} , i.e. the integral over the autocorrelation function with respect to Δ becomes finite for $\Delta \rightarrow \infty$. The dependence on H can again be verified using Eq. (52). Here, we specify the shape to be $\Phi(\Delta) = (1 + \Delta)^{2\varphi-2}$ with $\varphi < 1/2$. The calculation is as simple for the relevant cases of exponential decay or the velocity correlation function being (Dirac-) delta-distributed with $\delta(\Delta)$. Using Eqs. (123) and (132) we find for $t_0 \gg t_1, t_2$

$$\begin{aligned}
\langle [x(t_0 + \Delta) - x(t_0)]^2 \rangle &\approx \\
&2 \int_0^\Delta dt_2 \int_0^{t_2} dt_1 (t_1 + t_0)^{2-2H} (1 + t_2 - t_1)^{2\varphi-2} \\
&\approx \frac{2}{2\varphi-1} \int_0^\Delta dt_2 (t_0)^{2-2H} \left(1 - (1 + t_2)^{2\varphi-1} \right) \\
&\approx \frac{2}{2\varphi-1} (t_0)^{2-2H} \left(\Delta + \frac{1}{2\varphi} (\Delta^{2\varphi} - 1) \right). \tag{133}
\end{aligned}$$

Since $\varphi < 1/2$, for $\Delta \rightarrow \infty$, the linear term is dominant. Accordingly, the scaling of the EATA MSD for short range correlated processes is

$$\langle \overline{\delta^2} \rangle \sim t^{2-2H} \Delta. \tag{134}$$

The Hurst exponent is independent of φ and of the exact shape of the distribution as long as it decays sufficiently fast. The Joseph exponent is therefore always $J = 1/2$.

(IV) In all cases discussed so far, the Joseph exponent is $J \geq 1/2$. This is also a necessary condition for the derivation in equation (52). However, it is possible, to construct antipersistent processes with a autocorrelation functions, that lead to $J < 1/2$. Looking at the calculation (133) we see, that in order to obtain a scaling with $H < 1/2$, the constant factor after the first integration, which leads to the linear scaling, has to be eliminated. This is possible if the correlation function is not strictly positive. The most prominent example of a continuous process, which can fulfill this condition is fractional Gaussian noise, which is the continuous-time version of the discrete ARFIMA(0, d , 0) studied in Appen. A.1. This process has a correlation function similar in shape

as in case III above, but without the dependence on t , it reads

$$\langle v(t)v(t + \Delta) \rangle = \frac{1}{2} (|\Delta + 1|^{2J} - 2|\Delta|^{2J} + |\Delta - 1|^{2J}). \quad (135)$$

Putting this into equation (133) leads to $H = J < 1/2$.

In conclusion we want to point out that the exponent J is given by the scaling of the autocorrelation function with Δ^{2J-2} directly for $J > 1/2$, and by the scaling of the integral over the autocorrelation function with Δ^{2J-1} for all cases.

A.3 The Joseph effect via DFA

There are several methods that are used in practice in order to quantify long range correlations in discrete measured time series. Examples are R/S statistics, detrended moving averages [16], scaling analysis based on the wavelet transform [4] and detrended fluctuation analysis [177]. In [96] it was shown that the latter three can be expressed in the same framework. In this section we want to discuss whether or not the definition of long range correlations in DFA is different from our definition, Eq. (51) for J .

The squared fluctuation function of DFA is defined as

$$F_q^2(s) = \frac{1}{K} \sum_{k=1}^K \left(\frac{1}{s} \sum_{t=1+(k-1)s}^{ks} (x_t - p_{t,q})^2 \right). \quad (136)$$

Here $p_{t,q}$ is a polynomial that is fitted to the series x_t for segments of lengths s . The squared error $(x_t - p_{t,q})^2$ of these fits is then averaged over all the non-overlapping segments of equal length s . The index q is the order of the polynomial. DFA is not sensitive to trends with polynomial shape of order $q - 1$, i.e. the slow dynamics is filtered by the method. For the definitions used above, data with trends does not yield a meaningful exponent. So we want to concentrate on stationary data. If the detrending order is zero, in each window just the mean value is subtracted and Eq. (136) simplifies to a discrete version of the time-averaged MSD, with non-overlapping windows.

So what is difference if detrending is performed with $q > 0$? Here, for stationary systems, a

relation between the fluctuation function and the autocorrelation function was derived in [92]

$$\langle F_q^2(s) \rangle = \langle v^2 \rangle \left(L_q(0, s) + 2 \sum_{t=1}^{s-1} \frac{\langle v(t+\Delta)v(t) \rangle}{\langle v^2 \rangle} L_q(t, s) \right). \quad (137)$$

$L_q(0, s)$ is some sophisticated kernel. Its leading order is linear. So the fluctuation function is a measure of the integral (here discrete) over the autocorrelation function. Thus it measures the Joseph effect for $0 < J < 1$.

If a Noah effect is present, i.e. the variance is infinite in theory, the formula can still be used, since a measured time series always has a finite variance [164]. The Moses effect is more complicated. Even though a scaling of the increment distribution as in scaled Brownian motion (or in the parameter range A in the Lévy walk) is not visible in DFA due to the averaging over the segments, the scaling exponent DFA still might differ from J . This is true if v is diffusive as in fractional Brownian motion (DFA results shown in [91]). Here the DFA exponent is > 1 in contrast to J . In fact it is equal to H . So DFA is usually, but not always, a measure of the Joseph effect.

A.4 Calculation of $r_0(s)$ and $r_2(s)$

The generalised model of Lévy walk mentioned in section 3.6 corresponds to an ordinary Lévy walk starting at $x = 0$, where A corresponds to a set of complete stretches and r to the last, incomplete stretch starting at time t' [35]. The calculations for the last step of the walk are as follows [35]:

$$r(x | t) = \int_t^\infty \frac{1}{2} \delta(|x| - ct^\eta t'^{\nu-\eta}) g(t') dt' \quad (138)$$

where η, ν are constants and $g(t)$ is the waiting time density.

Equation 138 is normalized such that the overall probability to stay within a single step/stretch for a time longer than t

$$\int r(x | t) = \int_t^\infty g(t') dt' \quad (139)$$

Taking the Fourier transform of $r(x, t)$ for small k ,

$$\begin{aligned} r(x | t) &= \int_{-\infty}^{\infty} dx e^{ikx} \int_t^{\infty} \frac{1}{2} \delta(|x| - ct^\eta t'^{\nu-\eta}) g(t') dt' \\ &= r_0(t) - \frac{k^2}{2} r_2(t) + o(k^2) \end{aligned} \tag{140}$$

we find the marginal moments [35]

$$r_0(t) = \frac{1}{(1 + t/\tau_0)^\gamma} \tag{141}$$

$$r_2(t) = \gamma \frac{1}{\tau_0} t^{2\eta} \int_t^{\infty} \frac{t'^{2(\nu-\eta)}}{(1 + t'/\tau_0)^{\gamma+1}} dt' \tag{142}$$

where τ_0 is the cutoff. The Laplace transforms for equations 141 and 142 depend on the relationship between γ , ν and η . By varying the values of these constants, we calculate the values of $r_0(t)$ and $r_2(t)$ in different regimes.

A.5 The “ ∞ ” regime, $\nu > \gamma/2 + 1$

As explained in Sec. 3.6, the analytic results show that when $\eta = 1$ and $\nu > \gamma/2 + 1$, the Hurst exponent diverges. We expect to find a similar behaviour if we fix time and increase the ensemble size.

Bibliography

- [1] Holy bible: New king james version. *Library Journal* 107 (1982), 2102–.
- [2] AARONSON, J. The asymptotic distributional behaviour of transformations preserving infinite measures. *Journal d'analyse mathématique* 39, 1 (1981), 203–234.
- [3] AARONSON, J. “*An Introduction to Infinite Ergodic Theory*”. American Mathematical Soc., 1997.
- [4] ABRY, P., AND VEITCH, D. Wavelet analysis of long-range-dependent traffic. *IEEE Transactions on Information Theory* 44, 1 (1998), 2–15.
- [5] AGHION, E., KESSLER, D. A., AND BARKAI, E. Large fluctuations for spatial diffusion of cold atoms. *Physical Review Letters* 118, 26 (2017), 260601.
- [6] AGHION, E., KESSLER, D. A., AND BARKAI, E. Asymptotic densities from the modified montroll-weiss equation for coupled ctrws. *Eur. Phys. J. B* 91 (2018), 17.
- [7] AGHION, E., KESSLER, D. A., AND BARKAI, E. Infinite ergodic theory meets boltzmann statistics. *Chaos, Solitons & Fractals* 138 (2020), 109890.
- [8] AGHION, E., MEYER, P. G., ADLAKHA, V., KANTZ, H., AND BASSLER, K. E. Moses, noah and joseph effects in lévy walks. *New Journal of Physics* 23, 2 (2021), 023002.
- [9] AKIMOTO, T., AND BARKAI, E. Aging generates regular motion in weakly chaotic systems. *Phys. Rev. E* 87 (2013), 032915.
- [10] AKIMOTO, T., BARKAI, E., AND RADONS, G. Infinite invariant density in a semi-markov process with continuous state variables. *Physical Review E* 101, 5 (2020), 052112.
- [11] AKIMOTO, T., AND MIYAGUCHI, T. Distributional ergodicity in stored-energy-driven lévy flights. *Physical Review E* 87, 6 (2013), 062134.
- [12] AKIMOTO, T., AND MIYAGUCHI, T. Phase diagram in Stored-Energy-Driven Lévy flight. *Journal of Statistical Physics* 157, 3 (2014), 515–530.
- [13] AKIMOTO, T., SHINKAI, S., AND AIZAWA, Y. Distributional behavior of time averages of non-l1 observables in one-dimensional intermittent maps with infinite invariant measures. *J. Stat. Phys.* 158 (2014), 476.
- [14] ALBERS, T., AND RADONS, G. Weak ergodicity breaking and aging of chaotic transport in hamiltonian systems. *Physical Review Letters* 113, 18 (2014), 184101.
- [15] ALBERS, T., AND RADONS, G. Exact results for the nonergodicity of d-dimensional generalized levy walks. *Physical review letters* 120, 10 (2018), 104501.
- [16] ALESSIO, E., CARBONE, A., CASTELLI, G., AND FRAPPIETRO, V. Second-order moving average and scaling of stochastic time series. *The European Physical Journal B - Condensed Matter and Complex Systems* 27, 2 (2002), 197–200.

- [17] ALEXANDER, G. N. Comments on ‘noah, joseph, and operational hydrology’ by benoit b. mandelbrot and james r. wallis. *Water Resources Research* 5, 4 (1969), 915–916.
- [18] AMBLARD, F., MAGGS, A. C., YURKE, B., PARGELLIS, A. N., AND LEIBLER, S. Subdiffusion and anomalous local viscoelasticity in actin networks. *Phys. Rev. Lett.* 77 (1996), 4470–4473.
- [19] ARMSTEAD, D. N., HUNT, B. R., AND OTT, E. Anomalous diffusion in infinite horizon billiards. *Phys. Rev. E* 67 (2003), 021110.
- [20] BARDOU, F., BOUCHAUD, J. P., EMILE, O., ASPECT, A., AND COHEN-TANNOUJDI, C. Subrecoil laser cooling and lévy flights. *Phys. Rev. Lett.* 72 (1994), 203–206.
- [21] BARKAI, E. Aging in subdiffusion generated by a deterministic dynamical system. *Phys. Rev. Lett.* 90 (2003), 104101.
- [22] BARKAI, E., AND CHENG, Y.-C. Aging continuous time random walks. *The Journal of Chemical Physics* 118, 14 (2003), 6167–6178.
- [23] BARKAI, E., GARINI, Y., AND METZLER, R. Strange kinetics of single molecules in living cells. *Physics Today* 65, 8 (2012), 29–35.
- [24] BARKAI, E., J. KLAFTER, IN: BENKADDA, S., AND ZASLAVSKY, G. M. *Chaos, Kinetics and Nonlinear Dynamics in Fluids and Plasmas: Proceedings of a Workshop Held in Carry-Le Rouet, France, 16–21 June 1997*, vol. 511. Springer Science & Business Media, 1998.
- [25] BARON, M. *Probability and Statistics for Computer Scientists, Second Edition*. CRC Press, 2013.
- [26] BASSLER, K. E., GUNARATNE, G. H., AND MCCAULEY, J. L. Markov processes, hurst exponents, and nonlinear diffusion equations: With application to finance. *Physica A: Statistical Mechanics and its Applications* 369, 2 (2006), 343 – 353.
- [27] BASSLER, K. E., MCCAULEY, J. L., AND GUNARATNE, G. H. Nonstationary increments, scaling distributions, and variable diffusion processes in financial markets. *Proceedings of the National Academy of Sciences* 104, 44 (2007), 17287–17290.
- [28] BECK, C., AND ROEPSTORFF, G. Effects of phase space discretization on the long-time behavior of dynamical systems. *Physica D: Nonlinear Phenomena* 25, 1 (1987), 173 – 180.
- [29] BEL, G., AND BARKAI, E. Ergodicity breaking in a deterministic system. *Europhys. Lett.* 74 (2006), 15.
- [30] BERAN, J. *Statistics for long-memory processes*. Routledge, 2017.
- [31] BERG, S. V. *Annals of Economic and Social Measurement, Volume 1, number 3*. NBER, 1972.
- [32] BERTIN, E. M., AND BOUCHAUD, J.-P. Subdiffusion and localization in the one-dimensional trap model. *Phys. Rev. E* 67 (2003), 026128.

- [33] BERTSEKAS, D. P., AND SHREVE, S. E. *Stochastic Optimal Control: The Discrete-Time Case*. Athena Scientific, 1996.
- [34] BO, S., SCHMIDT, F., EICHHORN, R., AND VOLPE, G. Measurement of anomalous diffusion using recurrent neural networks. *Physical Review E* 100, 1 (2019), 010102.
- [35] BOTHE, M., SAGUES, F., AND SOKOLOV, I. Mean squared displacement in a generalized lévy walk model. *Physical Review E* 100, 1 (2019), 012117.
- [36] BOUCHAUD, J.-P., AND GEORGES, A. Anomalous diffusion in disordered media: statistical mechanisms, models and physical applications. *Physics reports* 195, 4-5 (1990), 127–293.
- [37] BRAÜCHLE, C., LAMB, D. C., AND MICHAELIS, J. *Single particle tracking and single molecule energy transfer*. Wiley Online Library, 2010.
- [38] BRESSLOFF, P. C. *Stochastic Processes in Cell Biology*. Springer, 2014.
- [39] BRESSLOFF, P. C., AND NEWBY, J. M. Stochastic models of intracellular transport. *Reviews of modern physics* 85, 1 (2013), 135–196.
- [40] BROCKMANN, D., AND HELBING, D. The hidden geometry of complex, network-driven contagion phenomena. *Science* 342, 6164 (2013), 1337–1342.
- [41] BROCKMANN, D., HUFNAGEL, L., AND GEISEL, T. The scaling laws of human travel. *Nature* 439, 7075 (2006), 462–465.
- [42] BROKMAN, X., HERMIER, J.-P., MESSIN, G., DESBIOLLES, P., BOUCHAUD, J.-P., AND DAHAN, M. Statistical aging and nonergodicity in the fluorescence of single nanocrystals. *Phys. Rev. Lett.* 90 (2003), 120601.
- [43] BRONSTEIN, I., ISRAEL, Y., KEPTEN, E., MAI, S., SHAV-TAL, Y., BARKAI, E., AND GARINI, Y. Transient anomalous diffusion of telomeres in the nucleus of mammalian cells. *Phys. Rev. Lett.* 103 (2009), 018102.
- [44] BROWN, R., F.R.S., M.R.S.E., H., AND V.P.L.S., R. A. Xxvii. a brief account of microscopical observations made in the months of june, july and august 1827, on the particles contained in the pollen of plants; and on the general existence of active molecules in organic and inorganic bodies. *The Philosophical Magazine* 4, 21 (1828), 161–173.
- [45] BRUNSELL, N. A multiscale information theory approach to assess spatial–temporal variability of daily precipitation. *Journal of Hydrology* 385, 1 (2010), 165–172.
- [46] BUROV, S., AND BARKAI, E. Occupation time statistics in the quenched trap model. *Phys. Rev. Lett.* 98 (2007), 250601.
- [47] BUROV, S., JEON, J.-H., METZLER, R., AND BARKAI, E. Single particle tracking in systems showing anomalous diffusion: the role of weak ergodicity breaking. *Physical chemistry chemical physics : PCCP* 13, 5 (2011), 18–1812.
- [48] CASPI, A., GRANEK, R., AND ELBAUM, M. Enhanced diffusion in active intracellular transport. *Phys. Rev. Lett.* 85 (2000), 5655–5658.

- [49] CASPI, A., GRANEK, R., AND ELBAUM, M. Diffusion and directed motion in cellular transport. *Phys. Rev. E* 66 (2002), 011916.
- [50] CASTAING, B., GUNARATNE, G., HESLOT, F., KADANOFF, L., LIBCHABER, A., THOMAE, S., WU, X.-Z., ZALESKI, S., AND ZANETTI, G. Scaling of hard thermal turbulence in rayleigh-bénard convection. *Journal of Fluid Mechanics* 204 (1989), 1–30.
- [51] CASTIGLIONE, P., MAZZINO, A., MURATORE-GINANNESCHI, P., AND VULPIANI, A. On strong anomalous diffusion. *Physica D: Nonlinear Phenomena* 134, 1 (1999), 75–93.
- [52] CASTIN, Y., DALIBARD, J., AND COHEN-TANNOUDJI, C. The limits of sisyphus cooling. In *Light Induced Kinetic Effects on Atoms, Ions, and Molecules* (Pisa, 1991), L. Mol, S. Gozzini, C. Gabbanini, E. Arimondo, and F. Strumia, Eds., ETS Editrice, pp. 5–24.
- [53] CHECHKIN, A. V., GORENFLO, R., AND SOKOLOV, I. M. Fractional diffusion in inhomogeneous media. *Journal of Physics A: Mathematical and General* 38, 42 (2005), L679–L684.
- [54] CHEN, L., BASSLER, K. E., MCCAULEY, J. L., AND GUNARATNE, G. H. Anomalous scaling of stochastic processes and the moes effect. *Physical Review E* 95, 4 (2017).
- [55] CHERSTVY, A. G., CHECHKIN, A. V., AND METZLER, R. Anomalous diffusion and ergodicity breaking in heterogeneous diffusion processes. *New journal of physics* 15, 8 (2013), 83039.
- [56] CHERSTVY, A. G., CHECHKIN, A. V., AND METZLER, R. Ageing and confinement in non-ergodic heterogeneous diffusion processes. *Journal of Physics A: Mathematical and Theoretical* 47, 48 (2014), 485002.
- [57] CHERSTVY, A. G., AND METZLER, R. Population splitting, trapping, and non-ergodicity in heterogeneous diffusion processes. *Physical chemistry chemical physics : PCCP* 15, 46 (2013), 222–2235.
- [58] DACOROGNA, M., MULLER, U. A., NAGLER, R. J., OLSEN, R., AND PICTET, O. V. A geographical model for the daily and weekly seasonal volatility in the foreign exchange market. *Journal of International Money and Finance* 12, 4 (1993), 413–438.
- [59] DECHANT, A., LUTZ, E., KESSLER, D., AND BARKAI, E. Scaling green-kubo relation and application to three aging systems. *Physical Review X* 4 (2014), 011022.
- [60] DENTZ, M., GOUZE, P., RUSSIAN, A., DWEIK, J., AND DELAY, F. Diffusion and trapping in heterogeneous media: An inhomogeneous continuous time random walk approach. *Advances in Water Resources* 49 (2012), 13–22.
- [61] DONTH, E.-J. *The glass transition : relaxation dynamics in liquids and disordered materials*. Springer series in materials science, 48. Springer, Berlin, 2001.
- [62] DOOB, J. L. *Stochastic Processes*. Wiley, 1990.
- [63] DOUGHERTY, E. R. *Random Processes for Image and Signal Processing*. SPIE Optical Engineering Press, 1999.

- [64] DYNKIN, E. B. *Selected Translations in Mathematical Statistics and Probability 1* (1961), 171.
- [65] ELIAZAR, I. I., AND SHLESINGER, M. F. Fractional motions. *Physics reports* 527, 2 (2013), 101–129.
- [66] EMBRECHTS, P., AND MAEJIMA, M. *Selfsimilar Processes*. Princeton University Press, 2002.
- [67] ENGLISH, B. P., HAURYLIUK, V., SANAMRAD, A., TANKOV, S., DEKKER, N. H., AND ELF, J. Single-molecule investigations of the stringent response machinery in living bacterial cells. *Proceedings of the National Academy of Sciences* 108, 31 (2011), E365–E373.
- [68] FAMA, E. F., AND ROLL, R. Some properties of symmetric stable distributions. *Journal of the American Statistical Association* 63, 323 (1968), 817–836.
- [69] FAMA, E. F., AND ROLL, R. Parameter estimates for symmetric stable distributions. *Journal of the American Statistical Association* 66, 334 (1971), 331–338.
- [70] FEIGEL'MAN, M.V., AND VINOKUR, V.M. On the stochastic transport in disordered systems. *J. Phys. France* 49, 10 (1988), 1731–1736.
- [71] FROEMBERG, D., SCHMIEDEBERG, M., BARKAI, E., AND ZABURDAEV, V. Asymptotic densities of ballistic lévy walks. *Physical Review E* 91, 2 (2015), 022131.
- [72] FULIŃSKI, A. Anomalous diffusion and weak nonergodicity. *Phys. Rev. E* 83 (2011), 061140.
- [73] FULIŃSKI, A. Communication: How to generate and measure anomalous diffusion in simple systems. *The Journal of Chemical Physics* 138, 2 (2013), 021101.
- [74] GAGNIUC, P. A. *Markov Chains: From Theory to Implementation and Experimentation*. NJ: John Wiley Sons, 2017.
- [75] GEISEL, T., AND THOMAE, S. Anomalous diffusion in intermittent chaotic systems. *Phys. Rev. Lett.* 52 (1984), 1936.
- [76] GHOSH, S. K., CHERSTVY, A. G., GREBENKOV, D. S., AND METZLER, R. Anomalous, non-gaussian tracer diffusion in crowded two-dimensional environments. *New Journal of Physics* 18, 1 (2016), 013027.
- [77] GIKHMAN, I. I., AND VLADIMIROVICH, A. *Introduction to the Theory of Random Processes*. Courier Corporation, 1969.
- [78] GODEC, A., BAUER, M., AND METZLER, R. Collective dynamics effect transient subdiffusion of inert tracers in flexible gel networks. *New journal of physics* 16, 9 (2014), 92002–.
- [79] GODRECHE, C., AND LUCK, J. Statistics of the occupation time of renewal processes. *Journal of Statistical Physics* 104, 3-4 (2001), 489–524.
- [80] GOLDING, I., AND COX, E. C. Physical nature of bacterial cytoplasm. *Physical review letters* 96, 9 (2006), 098102.

- [81] GONZÁLEZ, M. C., HIDALGO, C. A., AND BARABÁSI, A.-L. Understanding individual human mobility patterns. *Nature* 453, 7196 (2008), 779–782.
- [82] GOTZE, W. *Complex dynamics of glass-forming liquids a mode-coupling theory*. International series of monographs on physics ; 143. Oxford University Press, Oxford, 2009.
- [83] GRAHOVAC, D., JIA, M., LEONENKO, N., AND TAUFER, E. Asymptotic properties of the partition function and applications in tail index inference of heavy-tailed data. *Statistics* 49, 6 (2015), 1221–1242.
- [84] GRAVES, T., GRAMACY, R., WATKINS, N., AND FRANZKE, C. A brief history of long memory: Hurst, mandelbrot and the road to arfima, 1951-1980. *Entropy* 19(9) (2017), 437.
- [85] GREBOGI, C., OTT, E., AND YORKE, J. A. Roundoff-induced periodicity and the correlation dimension of chaotic attractors. *Phys. Rev. A* 38 (1988), 3688–3692.
- [86] GRUBER, E. L. g. e. struik: Physical aging in amorphous polymers and other materials. elsevier sci. publ. comp., amsterdam-oxford-new york 1978. 229 seiten, 141 abbildungen, preis: Us \$ 42,50, holl. gulden 97,50. *Berichte der Bunsengesellschaft für physikalische Chemie* 82, 9 (1978), 1019–1019.
- [87] GÖTZE, W. *Complex Dynamics of Glass-Forming Liquids*. Oxford University Press, Oxford, UK, 2009.
- [88] HAGGERTY, R., AND GORELICK, S. M. Multiple-rate mass transfer for modeling diffusion and surface reactions in media with pore-scale heterogeneity. *Water Resources Research* 31, 10 (1995), 2383–2400.
- [89] HE, Y., BUROV, S., METZLER, R., AND BARKAI, E. Random time-scale invariant diffusion and transport coefficients. *Phys. Rev. Lett.* 101 (2008), 058101.
- [90] HELLMANN, M., HEERMANN, D. W., AND WEISS, M. Anomalous reaction kinetics and domain formation on crowded membranes. *Europhysics letters* 94, 1 (2011), 18002–.
- [91] HENEGHAN, C., AND MCDARBY, G. Establishing the relation between detrended fluctuation analysis and power spectral density analysis for stochastic processes. *Physical review E* 62, 5 (2000), 6103.
- [92] HOELL, M., AND KANTZ, H. The relationship between the detrended fluctuation analysis and the autocorrelation function of a signal. *Eur. Phys. J. B* 88 (2015), 327.
- [93] HÖFLING, F., AND FRANOSCH, T. Crossover in the slow decay of dynamic correlations in the lorentz model. *Phys. Rev. Lett.* 98 (2007), 140601.
- [94] HÖFLING, F., AND FRANOSCH, T. Anomalous transport in the crowded world of biological cells. *Reports on Progress in Physics* 76, 4 (2013), 046602.
- [95] HOLCMAN, D., AND SCHUSS, Z. Time scale of diffusion in molecular and cellular biology. *Journal of physics. A, Mathematical and theoretical* 47, 17 (2014), 173001.

- [96] HÖLL, M., KIYONO, K., AND KANTZ, H. Theoretical foundation of detrending methods for fluctuation analysis such as detrended fluctuation analysis and detrending moving average. *Phys. Rev. E* 99 (2019), 033305.
- [97] HOLZ, P. C., DECHANT, A., AND LUTZ, E. Infinite density for cold atoms in shallow optical lattices. *EPL (Europhysics Letters)* 109, 2 (2015), 23001.
- [98] HURST, H. E. Long-term storage capacity of reservoirs. *Am. Soc. Civil Eng.* 116 (1951), 770.
- [99] HÖFLING, F., AND FRANOSCH, T. Anomalous transport in the crowded world of biological cells. *Reports on Progress in Physics* 76, 4 (2013), 046602.
- [100] JANCZURA, J., KOWALEK, P., LOCH-OLSZEWSKA, H., SZWABIŃSKI, J., AND WERON, A. Machine learning classification of particle trajectories in living cells: machine learning versus statistical testing hypothesis. *arXiv preprint arXiv:2005.06239* (2020).
- [101] JEON, J.-H., CHECHKIN, A. V., AND METZLER, R. Scaled brownian motion: a paradoxical process with a time dependent diffusivity for the description of anomalous diffusion. *Physical Chemistry Chemical Physics* 16, 30 (2014), 15811–15817.
- [102] JEON, J.-H., TEJEDOR, V., BUROV, S., BARKAI, E., SELHUBER-UNKEL, C., BERG-SØRENSEN, K., ODDERSHEDE, L., AND METZLER, R. In vivo anomalous diffusion and weak ergodicity breaking of lipid granules. *Physical review letters* 106, 4 (2011), 048103–048103.
- [103] JUNG, Y., BARKAI, E., AND SILBEY, R. J. Lineshape theory and photon counting statistics for blinking quantum dots: a lévy walk process. *Chemical Physics* 284, 1 (2002), 181 – 194. Strange Kinetics.
- [104] KANTELHARDT, J. W., KOSCIELNY-BUNDE, E., RYBSKI, D., BRAUN, P., BUNDE, A., AND HAVLIN, S. Long-term persistence and multifractality of precipitation and river runoff records. *Journal of Geophysical Research: Atmospheres* 111, D1 (2006).
- [105] KANTELHARDT, J. W., RYBSKI, D., ZSCHIEGNER, S. A., BRAUN, P., KOSCIELNY-BUNDE, E., LIVINA, V., HAVLIN, S., AND BUNDE, A. Multifractality of river runoff and precipitation: comparison of fluctuation analysis and wavelet methods. *Physica A: Statistical Mechanics and its Applications* 330, 1-2 (2003), 240–245.
- [106] KANTELHARDT, J. W., ZSCHIEGNER, S. A., KOSCIELNY-BUNDE, E., HAVLIN, S., BUNDE, A., AND STANLEY, H. E. Multifractal detrended fluctuation analysis of nonstationary time series. *Physica A* 316 (2002), 87–114.
- [107] KEPTEN, E., BRONSHTEIN, I., AND GARINI, Y. Ergodicity convergence test suggests telomere motion obeys fractional dynamics. *Physical Review E* 83, 4 (2011), 041919.
- [108] KEPTEN, E., BRONSHTEIN, I., AND GARINI, Y. Improved estimation of anomalous diffusion exponents in single-particle tracking experiments. *Physical Review E* 87, 5 (2013), 052713.
- [109] KESSLER, D. A., AND BARKAI, E. Infinite covariant density for diffusion in logarithmic potentials and optical lattices. *Phys. Rev. Lett.* 105 (2010), 120602.

- [110] KLAFTER, J., SHLESINGER, M. F., AND ZUMOFEN, G. Beyond brownian motion. *Physics today* 49, 2 (1996), 33–39.
- [111] KLAFTER, J., AND SOKOLOV, I. M. “*First steps in random walks: from tools to applications*”. Oxford University Press, 2011.
- [112] KLAFTER, J., AND ZUMOFEN, G. Lévy statistics in a hamiltonian system. *Phys. Rev. E* 49 (1994), 4873–4877.
- [113] KORABEL, N., AND BARKAI, E. Pesin-type identity for intermittent dynamics with a zero lyaponov exponent. *Physical Review Letters* 102, 5 (2009), 050601.
- [114] KOU, S. C., AND XIE, X. S. Generalized langevin equation with fractional gaussian noise: Subdiffusion within a single protein molecule. *Phys. Rev. Lett.* 93 (2004), 180603.
- [115] KRAPP, D., LUKAT, N., MARINARI, E., METZLER, R., OSHANIN, G., SELHUBER-UNKEL, C., SQUARCINI, A., STADLER, L., WEISS, M., AND XU, X. Spectral content of a single non-brownian trajectory. *Physical Review X* 9, 1 (2019), 011019.
- [116] KÜHN, T., IHALAINEN, T. O., HYVÄLUOMA, J., DROSS, N., WILLMAN, S. F., LANGOWSKI, J., VIHINEN-RANTA, M., AND TIMONEN, J. Protein diffusion in mammalian cell cytoplasm. *PloS one* 6, 8 (2011).
- [117] LAING, C., AND J LORD, G. *Stochastic Methods in Neuroscience*. OUP Oxford, 2010.
- [118] LALOUX, L., AND LE DOUSSAL, P. Aging and diffusion in low dimensional environments. *Phys. Rev. E* 57 (1998), 6296–6326.
- [119] LANDE, R., ENGEN, S., AND SÆTHER, B.-E. *Stochastic Population Dynamics in Ecology and Conservation*. Oxford University Press, 2003.
- [120] LAWALL, J., BARDOU, F., SAUBAMEA, B., SHIMIZU, K., LEDUC, M., ASPECT, A., AND COHEN-TANNOUJJI, C. Two-dimensional subrecoil laser cooling. *Phys. Rev. Lett.* 73 (1994), 1915–1918.
- [121] LE DOUSSAL, P., MONTHUS, C., AND FISHER, D. S. Random walkers in one-dimensional random environments: Exact renormalization group analysis. *Phys. Rev. E* 59 (1999), 4795–4840.
- [122] LEE, K., LEE, J., YI, Y., RHEE, I., AND CHONG, S. Mobile data offloading: How much can wifi deliver? *IEEE/ACM Transactions on Networking* 21, 2 (2013), 536–550.
- [123] LEIBOVICH, N., AND BARKAI, E. Infinite ergodic theory for heterogeneous diffusion processes. *Physical Review E* 99, 4 (2019), 042138.
- [124] LEITMANN, S., AND FRANOSCH, T. Nonlinear response in the driven lattice lorentz gas. *Phys. Rev. Lett.* 111 (2013), 190603.
- [125] LEPRETI, F., FANELLO, P., ZACCARO, F., AND CARBONE, V. Persistence of solar activity on small scales: Hurst analysis of time series coming from h flares. *Solar physics* 197, 1 (2000), 149–156.

- [126] LEPRI, S., LIVI, R., AND POLITI, A. Thermal conduction in classical low-dimensional lattices. *Physics Reports* 377, 1 (2003), 1–80.
- [127] LEVANDOWSKY, M., WHITE, B., AND SCHUSTER, F. Random movements of soil amoebas. *Acta Protozoologica* 36 (1997), 237–248.
- [128] LIM, S., AND MUNIANDY, S. Self-similar gaussian processes for modeling anomalous diffusion. *Physical Review E* 66, 2 (2002), 021114.
- [129] LOMHOLT, M. A., LIZANA, L., METZLER, R., AND AMBJÖRNSSON, T. Microscopic origin of the logarithmic time evolution of aging processes in complex systems. *Phys. Rev. Lett.* 110 (2013), 208301.
- [130] LOVERDO, C., BÉNICHOU, O., VOITURIEZ, R., BIEBRICHER, A., BONNET, I., AND DESBIOLLES, P. Quantifying hopping and jumping in facilitated diffusion of dna-binding proteins. *Phys. Rev. Lett.* 102 (2009), 188101.
- [131] LUBELSKI, A., SOKOLOV, I. M., AND KLAFTER, J. Nonergodicity mimics inhomogeneity in single particle tracking. *Phys. Rev. Lett.* 100 (2008), 250602.
- [132] LUTZ, E. Fractional langevin equation. *Phys. Rev. E* 64 (2001), 051106.
- [133] LUTZ, E., AND RENZONI, F. Beyond Boltzmann-Gibbs statistical mechanics in optical lattices. *Nature Physics* 9, 10 (2013), 615–619.
- [134] MAGDZIARZ, M., METZLER, R., SZCZOTKA, W., AND ZEBROWSKI, P. Correlated continuous-time random walks in external force fields. *Phys. Rev. E* 85 (2012), 051103.
- [135] MANDELBROT, B. The variation of certain speculative prices. *The Journal of Business* 36, 4 (1963), 394–419.
- [136] MANDELBROT, B. *Gaussian Self-Affinity and Fractals : Globality, The Earth, 1/f Noise, and R/S*, vol. 8. Springer Science Business Media, 2002.
- [137] MANDELBROT, B. B. *Statistical Methodology for Nonperiodic Cycles: From the Covariance To R/S Analysis*. NBER, 1972, pp. 259–290.
- [138] MANDELBROT, B. B., AND VAN NESS, J. W. Fractional brownian motions, fractional noises and applications. *SIAM Review* 10, 4 (1968), 422–437.
- [139] MANDELBROT, B. B., AND WALLIS, J. R. Noah, joseph, and operational hydrology. *Water Resources Research* 4, 5 (1968), 909–918.
- [140] MANDELBROT, B. B., AND WALLIS, J. R. Computer experiments with fractional gaussian noises: Part 2, rescaled ranges and spectra. *Water Resources Research* 5, 1 (1969), 242–259.
- [141] MANDELBROT, B. B., AND WALLIS, J. R. Robustness of the rescaled range r/s in the measurement of noncyclic long run statistical dependence. *Water Resources Research* 5, 5 (1969), 967–988.
- [142] MANTEGNA, R. N., AND STANLEY, H. E. Scaling behaviour in the dynamics of an economic index. *Nature* 376 (1995), 46.

- [143] MARGOLIN, G., AND BARKAI, E. Aging correlation functions for blinking nanocrystals, and other on–off stochastic processes. *The Journal of Chemical Physics* 121, 3 (2004), 1566–1577.
- [144] MARGOLIN, G., AND BARKAI, E. Nonergodicity of blinking nanocrystals and other lévy-walk processes. *Physical Review Letters* 94, 8 (2005), 080601.
- [145] MARGOLIN, G., AND BARKAI, E. Nonergodicity of a time series obeying lévy statistics. *Journal of statistical physics* 122, 1 (2006), 137–167.
- [146] MARGOLIN, G., PROTASENKO, V., KUNO, M., AND BARKAI, E. Photon counting statistics for blinking cdsezn quantum dots: a lévy walk process. *The Journal of Physical Chemistry B* 110, 38 (2006), 19053–19060.
- [147] MARINARI, E., AND PARISI, G. On toy ageing. *Journal of Physics A: Mathematical and General* 26, 22 (1993), L1149–L1156.
- [148] MARKSTEINER, S., ELLINGER, K., AND ZOLLER, P. Anomalous diffusion and lévy walks in optical lattices. *Phys. Rev. A* 53 (1996), 3409–3430.
- [149] MARTIN, R. L., JEROLMACK, D. J., AND SCHUMER, R. The physical basis for anomalous diffusion in bed load transport. *Journal of Geophysical Research: Earth Surface* 117, F1 (2012).
- [150] MASSIGNAN, P., MANZO, C., TORRENO-PINA, J., GARCÍA-PARAJO, M., LEWENSTEIN, M., AND LAPEYRE JR, G. Nonergodic subdiffusion from brownian motion in an inhomogeneous medium. *Physical review letters* 112, 15 (2014), 150603.
- [151] MCCAULEY, J. L., BASSLER, K. E., AND GUNARATNE, G. H. Martingales, detrending data, and the efficient market hypothesis. *Physica A: Statistical Mechanics and its Applications* 387, 1 (2008), 202 – 216.
- [152] MCCAULEY, J. L., GUNARATNE, G. H., AND BASSLER, K. E. Hurst exponents, markov processes, and fractional brownian motion. *Physica A: Statistical Mechanics and its Applications* 379, 1 (2007), 1 – 9.
- [153] MCCULLOCH, J. H. Simple consistent estimators of stable distribution parameters. *Communications in Statistics - Simulation and Computation* 15, 4 (1986), 1109–1136.
- [154] MEJÍA-MONASTERIO, C., METZLER, R., AND VOLLMER, J. Editorial: Anomalous transport: Applications, mathematical perspectives, and big data. *Frontiers in Physics* 8 (2020), 550.
- [155] MEROZ, Y., ELIAZAR, I., AND KLAFTER, J. Facilitated diffusion in a crowded environment: from kinetics to stochasticity. *Journal of Physics A Mathematical General* 42, 43 (2009), 434012.
- [156] MEROZ, Y., SOKOLOV, I. M., AND KLAFTER, J. Test for determining a subdiffusive model in ergodic systems from single trajectories. *Phys. Rev. Lett.* 110 (2013), 090601.

- [157] METZLER, R. Brownian motion and beyond: first-passage, power spectrum, non-gaussianity, and anomalous diffusion. *Journal of Statistical Mechanics: Theory and Experiment* 2019, 11 (2019), 114003.
- [158] METZLER, R., JEON, J.-H., CHERSTVY, A. G., AND BARKAI, E. Anomalous diffusion models and their properties: non-stationarity, non-ergodicity, and ageing at the centenary of single particle tracking. *Physical Chemistry Chemical Physics* 16, 44 (2014), 24128–24164.
- [159] METZLER, R., AND KLAFTER, J. The random walk’s guide to anomalous diffusion: a fractional dynamics approach. *Physics reports* 339, 1 (2000), 1–77.
- [160] METZLER, R., AND KLAFTER, J. The restaurant at the end of the random walk: recent developments in the description of anomalous transport by fractional dynamics. *Journal of physics. A, Mathematical and general* 37, 31 (2004), R161–R208.
- [161] MEYER, P., BARKAI, E., AND KANTZ, H. Scale-invariant green-kubo relation for time-averaged diffusivity. *Phys. Rev. E* 96 (2017), 062122.
- [162] MEYER, P., AND KANTZ, H. Infinite invariant densities due to intermittency in a nonlinear oscillator. *Physical Review E* 96, 2 (2017), 022217.
- [163] MEYER, P. G., ADLAKHA, V., KANTZ, H., AND BASSLER, K. E. Anomalous diffusion and the mooses effect in an aging deterministic model. *New Journal of Physics* 20, 11 (2018), 113033.
- [164] MEYER, P. G., AND KANTZ, H. Inferring characteristic timescales from the effect of autoregressive dynamics on detrended fluctuation analysis. *New Journal of Physics* 21, 3 (2019), 033022.
- [165] MONTHUS, C., AND BOUCHAUD, J.-P. Models of traps and glass phenomenology. *Journal of Physics A: Mathematical and General* 29, 14 (1996), 3847–3869.
- [166] MULLER, U. A., DACOROGNA, M., OLSEN, R., PICTET, O. V., SCHWARZ, M., AND MORGENEGG, C. Statistical study of foreign exchange rates, empirical evidence of a price change scaling law, and intraday analysis. *Journal of Banking Finance* 14, 6 (1990), 1189–1208.
- [167] MUÑOZ-GIL, G., GARCIA-MARCH, M. A., MANZO, C., MARTÍN-GUERRERO, J. D., AND LEWENSTEIN, M. Machine learning method for single trajectory characterization. *arXiv preprint arXiv:1903.02850* (2019).
- [168] MUÑOZ-GIL, G., VOLPE, G., GARCIA-MARCH, M. A., METZLER, R., LEWENSTEIN, M., AND MANZO, C. Andi: The anomalous diffusion challenge. *arXiv preprint arXiv:2003.12036* (2020).
- [169] MUSIELA, M., AND RUTKOWSKI, M. *Martingale Methods in Financial Modelling*. Springer Science Business Media, 2006.
- [170] MÉNDEZ, V., CAMPOS, D., AND BARTUMEUS, F. *Stochastic Foundations in Movement Ecology: Anomalous Diffusion, Front Propagation and Random Searches*. Springer, 2014.

- [171] NICOLAU, D. V., HANCOCK, J. F., AND BURRAGE, K. Sources of anomalous diffusion on cell membranes: A monte carlo study. *Biophysical Journal* 92, 6 (2007), 1975–1987.
- [172] NIEMANN, M. From anomalous deterministic diffusion to the continuous-time random walk. *Ph.D. diss.* (2009).
- [173] OLIVEIRA, F. A., FERREIRA, R., LAPAS, L. C., AND VAINSTEIN, M. H. Anomalous diffusion: A basic mechanism for the evolution of inhomogeneous systems. *Frontiers in Physics* 7 (2019), 18.
- [174] O’SHAUGHNESSY, B., AND PROCACCIA, I. Analytical solutions for diffusion on fractal objects. *Phys. Rev. Lett.* 54 (1985), 455–458.
- [175] OTT, A., BOUCHAUD, J. P., LANGEVIN, D., AND URBACH, W. Anomalous diffusion in “living polymers”: A genuine levy flight? *Phys. Rev. Lett.* 65 (1990), 2201–2204.
- [176] PARZEN, E. *Stochastic Processes*. Courier Dover Publications, 2015.
- [177] PENG, C. K., BULDYREV, S. V., HAVLIN, S., SIMONS, M., STANLEY, H. E., AND GOLDBERGER, A. L. Mosaic organization of dna nucleotides. *Phys. Rev. E* 49 (1994), 1685.
- [178] POMEAU, Y., AND MANNEVILLE, P. Intermittent transition to turbulence in dissipative dynamical systems. *Communications in Mathematical Physics* 74, 2 (1980), 189–197.
- [179] REBENSHTOK, A., DENISOV, S., HÄNGGI, P., AND BARKAI, E. Non-normalizable densities in strong anomalous diffusion: beyond the central limit theorem. *Physical Review Letters* 112, 11 (2014), 110601.
- [180] REHMAN, S. Study of saudi arabian climatic conditions using hurst exponent and climatic predictability index. *Chaos, Solitons Fractals* 39, 2 (2009), 499–509.
- [181] RICHARDSON, C. W. Stochastic simulation of daily precipitation, temperature, and solar radiation. *Water Resources Research* 17, 1 (1981), 182–190.
- [182] RICHARDSON, L. F. Atmospheric diffusion shown on a distance-neighbour graph. *Proceedings of the Royal Society of London. Series A, Containing papers of a mathematical and physical character* 110, 756 (1926), 709–737.
- [183] RISKEN, H. H. *The Fokker-Planck equation : methods of solution and applications*, second edition. ed. Springer series in synergetics ; volume 18. Springer-Verlag, Berlin, 1989.
- [184] ROBERT, D., NGUYEN, T.-H., GALLET, F., AND WILHELM, C. In vivo determination of fluctuating forces during endosome trafficking using a combination of active and passive microrheology. *PLOS ONE* 5, 4 (2010), 1–9.
- [185] SABRI, A., XU, X., KRAPF, D., AND WEISS, M. Elucidating the origin of heterogeneous anomalous diffusion in the cytoplasm of mammalian cells. *Physical Review Letters* 125, 5 (2020), 058101.
- [186] SADEGH, S., BARKAI, E., AND KRAPF, D. $1/f$ noise for intermittent quantum dots exhibits non-stationarity and critical exponents. *New Journal of Physics* 16, 11 (2014), 113054.

- [187] SAFDARI, H., CHECHKIN, A. V., JAFARI, G. R., AND METZLER, R. Aging scaled brownian motion. *Phys. Rev. E* 91, 042107.
- [188] SATO, Y., AND KLAGES, R. Anomalous diffusion in random dynamical systems. *Physical review letters* 122, 17 (2019), 174101.
- [189] SAXTON, M. J. Anomalous subdiffusion in fluorescence photobleaching recovery: A monte carlo study. *Biophysical Journal* 81, 4 (2001), 2226–2240.
- [190] SCHER, H., AND MONTROLL, E. W. Anomalous transit-time dispersion in amorphous solids. *Phys. Rev. B* 12 (1975), 2455–2477.
- [191] SCHUBERT, M., PREIS, E., BLAKESLEY, J. C., PINGEL, P., SCHERF, U., AND NEHER, D. Mobility relaxation and electron trapping in a donor/acceptor copolymer. *Phys. Rev. B* 87 (2013), 024203.
- [192] SCHULZ, J. H. P., BARKAI, E., AND METZLER, R. Aging renewal theory and application to random walks. *Phys. Rev. X* 4 (2014), 011028.
- [193] SCHULZ-BALDES, H. Anomalous drude model. *Physical review letters* 78, 11 (1997), 2176.
- [194] SEEMANN, L., HUA, J.-C., MCCAULEY, J. L., AND GUNARATNE, G. H. Ensemble vs. time averages in financial time series analysis. *Physica A: Statistical Mechanics and its Applications* 391, 23 (2012), 6024–6032.
- [195] SEISENBERGER, G., RIED, M. U., ENDRESS, T., BÜNING, H., HALLEK, M., AND BRÄUCHLE, C. Real-time single-molecule imaging of the infection pathway of an adeno-associated virus. *Science (American Association for the Advancement of Science)* 294, 5548 (2001), 1929–1932.
- [196] SERESHKI, L. E., LOMHOLT, M. A., AND METZLER, R. A solution to the subdiffusion-efficiency paradox: Inactive states enhance reaction efficiency at subdiffusion conditions in living cells. *Europhysics letters* 97, 2 (2012), 20008–.
- [197] SEURONT, L., AND STANLEY, H. E. Anomalous diffusion and multifractality enhance mating encounters in the ocean. *Proceedings of the National Academy of Sciences* 111, 6 (2014), 2206–2211.
- [198] SHLESINGER, M., WEST, B., AND KLAFTER, J. Lévy dynamics of enhanced diffusion: Application to turbulence. *Physical Review Letters* 58, 11 (1987), 1100.
- [199] SHLESINGER, M. F., AND KLAFTER, J. Lévy walks versus Lévy flights. In *On growth and form*. Springer, 1986, pp. 279–283.
- [200] SHREVE, S. E. *Stochastic Calculus for Finance II: Continuous-Time Models*. Springer Science Business Media, 2004.
- [201] SILVA, A. T., LENZI, E. K., EVANGELISTA, L. R., LENZI, M. K., RIBEIRO, H. V., AND TATEISHI, A. A. Exact propagator for a fokker-planck equation, first passage time distribution, and anomalous diffusion. *Journal of Mathematical Physics* 52, 8 (2011), 083301.

- [202] SOKOLOV, I., BLUMEN, A., AND KLAFTER, J. Linear response in complex systems: Ctrw and the fractional fokker–planck equations. *Physica A: Statistical Mechanics and its Applications* 302, 1 (2001), 268–278. Proc. Int. Workshop on Frontiers in the Physics of Complex Systems.
- [203] SOKOLOV, I. M. Models of anomalous diffusion in crowded environments. *Soft Matter* 8 (2012), 9043–9052.
- [204] SOLOMON, T. H., WEEKS, E. R., AND SWINNEY, H. L. Observation of anomalous diffusion and lévy flights in a two-dimensional rotating flow. *Phys. Rev. Lett.* 71 (1993), 3975–3978.
- [205] SROKOWSKI, T. Lévy flights in nonhomogeneous media: Distributed-order fractional equation approach. *Phys. Rev. E* 78 (2008), 031135.
- [206] SROKOWSKI, T., AND KAMIŃSKA, A. Diffusion equations for a markovian jumping process. *Phys. Rev. E* 74 (2006), 021103.
- [207] STAPF, S., KIMMICH, R., AND SEITTER, R.-O. Proton and deuteron field-cycling nmr relaxometry of liquids in porous glasses: Evidence for lévy-walk statistics. *Phys. Rev. Lett.* 75 (1995), 2855–2858.
- [208] STEELE, J. M. *Stochastic Calculus and Financial Applications*. Springer Science Business Media, 2001.
- [209] STEFANI, F. D., HOOGENBOOM, J. P., AND BARKAI, E. Beyond quantum jumps: blinking nanoscale light emitters. *Phys. today* 62, 2 (2009), 34–39.
- [210] STRALEY, J. P. The ant in the labyrinth: diffusion in random networks near the percolation threshold. *Journal of Physics C: Solid State Physics* 13, 16 (1980), 2991–3002.
- [211] TABELI, S. A., BUROV, S., KIM, H. Y., KUZNETSOV, A., HUYNH, T., JURELLER, J., PHILIPSON, L. H., DINNER, A. R., AND SCHERER, N. F. Intracellular transport of insulin granules is a subordinated random walk. *Proceedings of the National Academy of Sciences* 110, 13 (2013), 4911–4916.
- [212] TAYLOR, M. A., JANOUSEK, J., DARIA, V., KNITTEL, J., HAGE, B., BACHOR, H.-A., AND BOWEN, W. P. Biological measurement beyond the quantum limit. *Nature photonics* 7, 3 (2013), 229–233.
- [213] TEJEDOR, V., AND METZLER, R. Anomalous diffusion in correlated continuous time random walks. *Journal of Physics A: Mathematical and Theoretical* 43, 8 (2010), 082002.
- [214] THALER, M. Asymptotic distributions and large deviations for iterated maps with an indifferent fixed point. *Stoch. Dyn.* 5 (2005), 425.
- [215] THAPA, S., LOMHOLT, M. A., KROG, J., CHERSTVY, A. G., AND METZLER, R. Bayesian analysis of single-particle tracking data using the nested-sampling algorithm: maximum-likelihood model selection applied to stochastic-diffusivity data. *Physical Chemistry Chemical Physics* 20, 46 (2018), 29018–29037.

- [216] THAPA, S., WYŁOMAŃSKA, A., SIKORA, G., WAGNER, C. E., KRAPP, D., KANTZ, H., CHECHKIN, A. V., AND METZLER, R. Leveraging large-deviation statistics to decipher the stochastic properties of measured trajectories. *arXiv preprint arXiv:2005.02099* (2020).
- [217] THIEL, F., AND SOKOLOV, I. M. Scaled brownian motion as a mean-field model for continuous-time random walks. *Physical Review E* 89, 1 (2014), 012115.
- [218] TOLIĆ-NØRRELYKKE, I. M., MUNTEANU, E.-L., THON, G., ODDERSHEDE, L., AND BERG-SØRENSEN, K. Anomalous diffusion in living yeast cells. *Physical Review Letters* 93, 7 (2004), 078102.
- [219] VAN KAMPEN, N. *Stochastic Processes in Physics and Chemistry*. Elsevier, 2011.
- [220] VICENÇ, M., CAMPOS, D., AND BARTUMEUS, F. *Stochastic Foundations in Movement Ecology*. Springer Series in Synergetics, 2014.
- [221] VISWANATHAN, G. M., DA LUZ, M. G. E., RAPOSO, E. P., AND STANLEY, H. E. *The Physics of Foraging: An Introduction to Random Searches and Biological Encounters*. Cambridge University Press, 2011.
- [222] WANG, D., WU, H., AND SCHWARTZ, D. K. Three-dimensional tracking of interfacial hopping diffusion. *Physical Review E* 119, 26 (2017), 268001.
- [223] WANG, Q., SAWYER, I. A., SUNG, M.-H., STURGILL, D., SHEVTSOV, S. P., PEGORARO, G., HAKIM, O., BAEK, S., HAGER, G. L., AND DUNDR, M. Cajal bodies are linked to genome conformation. *Nature communications* 7, 1 (2016), 10966–10966.
- [224] WANG, W., SCHULZ, J. H., DENG, W., AND BARKAI, E. Renewal theory with fat-tailed distributed sojourn times: Typical versus rare. *Physical Review E* 98, 4 (2018), 042139.
- [225] WANG, W., VEZZANI, A., BURIONI, R., AND BARKAI, E. Transport in disordered systems: the single big jump approach. *Physical Review Research* 1, 3 (2019), 033172.
- [226] WEBER, S. C., SPAKOWITZ, A. J., AND THERIOT, J. A. Bacterial chromosomal loci move subdiffusively through a viscoelastic cytoplasm. *Phys. Rev. Lett.* 104 (2010), 238102.
- [227] WEIGEL, A. V., SIMON, B., TAMKUN, M. M., AND KRAPP, D. Ergodic and nonergodic processes coexist in the plasma membrane as observed by single-molecule tracking. *Proceedings of the National Academy of Sciences* 108, 16 (2011), 6438–6443.
- [228] WEISS, M. Single-particle tracking data reveal anticorrelated fractional brownian motion in crowded fluids. *Phys. Rev. E* 88 (2013), 010101.
- [229] WEISS, M., ELSNER, M., KARTBERG, F., AND NILSSON, T. Anomalous subdiffusion is a measure for cytoplasmic crowding in living cells. *Biophysical Journal* 87 (2004), 3518–3524.
- [230] WEISS, M., HASHIMOTO, H., AND NILSSON, T. Anomalous protein diffusion in living cells as seen by fluorescence correlation spectroscopy. *Biophysical journal* 84, 6 (2003), 4043–4052.
- [231] WOLFGANG, P., AND BASCHNAGEL, J. *Stochastic Processes: From Physics to Finance*. Springer Science Business Media, 2013.

- [232] WONG, I. Y., GARDEL, M. L., REICHMAN, D. R., WEEKS, E. R., VALENTINE, M. T., BAUSCH, A. R., AND WEITZ, D. A. Anomalous diffusion probes microstructure dynamics of entangled f-actin networks. *Phys. Rev. Lett.* *92* (2004), 178101.
- [233] XIE, X. S., CHOI, P. J., LI, G.-W., LEE, N. K., AND LIA, G. Single-molecule approach to molecular biology in living bacterial cells. *Annu. Rev. Biophys.* *37* (2008), 417–444.
- [234] XU, Q., FENG, L., SHA, R., SEEMAN, N. C., AND CHAIKIN, P. M. Subdiffusion of a sticky particle on a surface. *Phys. Rev. Lett.* *106* (2011), 228102.
- [235] YAMADA, S., WIRTZ, D., AND KUO, S. C. Mechanics of living cells measured by laser tracking microrheology. *Biophysical journal* *78*, 4 (2000), 1736–1747.
- [236] YANG, H., LUO, G., KARNCHANAPHANURACH, P., LOUIE, T.-M., RECH, I., COVA, S., XUN, L., AND XIE, X. S. Protein conformational dynamics probed by single-molecule electron transfer. *Science (American Association for the Advancement of Science)* *302*, 5643 (2003), 262–266.
- [237] ZABURDAEV, V., DENISOV, S., AND KLAFTER, J. Lévy walks. *Rev. Mod. Phys.* *87* (2015), 483–530.
- [238] ZUMOFEN, G., KLAFTER, J., AND SHLESINGER, M. *Lévy flights and Lévy walks revisite*. Springer, Berlin, Heidelberg, 1999.